FLORIDA INTERNATIONAL UNIVERSITY

Miami, Florida

POLY (IONIC LIQUID) BASED ELECTROLYTE FOR LITHIUM BATTERY APPLICATION

A dissertation submitted in partial fulfillment of the

requirements for the degree of

DOCTOR OF PHILOSOPHY

in

MATERIALS SCIENCE AND ENGINEERING

by

Meer N Safa

2018

To: Dean John Volakis
College of Engineering and Computing

This dissertation, written by Meer N Safa, and entitled Poly (Ionic Liquid) Based Electrolyte for Lithium Battery Application, having been approved in respect to style and intellectual content, is referred to you for judgment.

We have read this dissertation and recommend that it be approved.

Norman Munroe

Chunlei Wang

Yu Zhong

Irene Calizo

Bilal El-Zahab, Major Professor

Date of Defense: May 14, 2018

The dissertation of Meer N Safa is approved.

Dean John Volakis
College of Engineering and Computing

Andrés G. Gil
Vice President for Research and Economic Development
and Dean of the University Graduate School

Florida International University, 2018

DEDICATION

To my parents, wife, and children. You have made me stronger than I could have ever imagined. Your continuous love and support helped me to fulfill this research.

ACKNOWLEDGMENTS

I want to express my gratitude to my major professor Dr. Bilal El-Zahab for his proper guidance, encouragement, and support throughout my Ph.D. research. I would also like to thank Professor Chunlei Wang for her collaboration and insightful suggestions as my committee member during my Ph.D. work. I would also thank my other committee members Dr. Norman Munroe, Dr. Yu Zhong and Dr. Irene Calizo for their willingness to be on my committee and their invaluable support and encouragement.

I sincerely thank my past and present group members Amir, Neha, Ata, Elnaz, Kamran, and Marcus and also Ebenezer, Yong, and Amin from Dr. Wang's group for their invaluable help and support. I would also like to appreciate the help from the staff of Advanced Materials Engineering Research Institute (AMERI) at FIU especially Dr. Alexander Franco for his continuous support during my stay.

Finally, I acknowledge the Mechanical and Materials Engineering (MME) Department at FIU for supporting me through Graduate Assistantship and also the University Graduate School (UGS) at FIU for supporting me through Dissertation Year Fellowship (DYF).

ABSTRACT OF THE DISSERTATION

POLY (IONIC LIQUID) BASED ELECTROLYTE FOR LITHIUM BATTERY APPLICATION

by

Meer N Safa

Florida International University, 2018

Miami, Florida

Professor Bilal El-Zahab, Major Professor

The demand for electric vehicles is increasing rapidly as the world is preparing for a fossil fuel-free future in the automotive field. Lithium battery technologies are the most effective options to replace fossil fuels due to their higher energy densities. However, safety remains a major concern in using lithium as the anode, and the development of non-volatile, non-flammable, high conductivity electrolytes is of great importance.

In this dissertation, a gel polymer electrolyte (GPE) consisting of ionic liquid, lithium salt, and a polymer has been developed for their application in lithium batteries. A comparative study between GPE and ionic liquid electrolyte (ILE) containing batteries shows a superior cyclic performance up to 5C rate and a better rate capability for 40 cycles for cells with GPE at room temperature. The improvement is attributed to GPE's improved stability voltage window against lithium as well as higher lithium transference number.

The performance of the GPE in lithium-sulfur battery system using sulfur-CNT cathodes shows superior rate capability for the GPE versus ILE for up to 1C rates. Also, GPE containing batteries had higher capacity retention versus ILE when cycled for 500 cycles

at C/2 rate. Electrochemical impedance spectroscopy (EIS) studies reveal interfacial impedances for ILE containing batteries grew faster than in GPE batteries. The accumulation of insoluble Li_2S_2/Li_2S on the electrodes decreases the active material thus contributes to capacity fading. SEM imaging of cycled cathodes reveals cracks on the surface of cathode recovered from ILE batteries. On the other hand, the improved electrochemical performance of GPE batteries indicates better and more stable passivation layer formation on the surface of the electrodes.

Composite GPE (cGPE) containing micro glass fillers were studied to determine their electrochemical performance in Li batteries. GPE with 1 wt% micro fillers show superior rate capability for up to 7C and also cyclic stability for 300 cycles at C/2 rate. *In situ,* EIS also reveals a rapid increase in charge transfer resistance in GPE batteries, responsible for lowering the capacity during cycling. Improved ion transport properties due to ion-complex formations in the presence of the micro fillers, is evidenced by improved lithium transference number, ionic conduction, and ion-pair dissociation detected using Raman spectroscopy.

TABLE OF CONTENTS

LIST OF TABLES

TABLE PAGE

LIST OF FIGURES

1 INTRODUCTION

1.1 State of Lithium Batteries

For the past two decades, the world has seen rapid progress of lithium-ion battery (LIB) development in the electronics, transportation, and grid storage sectors. Environmental pollution caused by fossil fuel resources demands an alternative route to clean and renewable energy resources. Due to their long cycle life and high energy densities, LIBs have been used in consumer portable electronics and power tools[1]. The state-of-the-art LIBs use a negative graphite electrode and a metal oxide as a positive electrode separated by a polymeric separator soaked with an organic solvent containing a lithium salt[2]. The specific energy and energy density of the battery system are approximately 150 $Wh.kg^{-1}$ and 250 $Wh.L^{-1}$, respectively; with a capital cost of < 300 $USD/kW.h^{-1}$[3]. However, these parameters are not sufficient for electric vehicle (EV) applications. The US Department of Energy (DOE) goal is to achieve the specific energy of 250 $Wh.kg^{-1}$ and energy density of 500 $Wh.L^{-1}$ with the capital cost of less than 125 $USD/kW.h^{-1}$for EV batteries[3]. Thus, alternative electrode materials with higher energies are of great interest to go beyond lithium-ion batteries.

The introduction of lithium metal as a replacement of graphite electrode results in ~ 35% and 50% increases in specific energy and energy density, respectively[3]. Lithium metal has a high theoretical specific capacity (3860 $mAh.g^{-1}$), low density (0.59 $g.cm^{-1}$) and high negative potential (-3.04 V versus hydrogen electrode) which makes them attractive in LIB technology[4]. However, the major problem of using lithium metal anodes is the uneven plating on the surface, which results in the growth of dendrites. Continuous

deposition of dendrites with subsequent cycling can reach the cathode and results in a short-circuit which leads to a thermal runaway [5]. Furthermore, the conventional organic carbonate electrolytes which are used in the present LIBs are highly volatile and have low flash points, which raises a serious safety concern for lithium batteries[6].

To meet the above mentioned requirements, polymer electrolytes (PE), either in solid-state or gelled by a nonflammable solvent (i.e. ionic liquid), have emerged as potential candidates capable of preventing the growth of uneven dendrites and also reduce the safety concerns associated with electrolyte leakage and fire accelerated by the organic electrolyte[7].

Bolloré first introduced a lithium polymer battery in their electric car in 2011. The electric range of the car was 160 miles on a full charge with a maximum speed of 81 mph[8]. Recently, Toyota announced a solid-state lithium battery to be used in their cars in 2022[9]. Other automakers like BMW[10], Fiskers[11], Dyson[12], Byton[13] are also invested in making EVs using an all solid-state lithium battery.

1.2 Fundamentals of Lithium Batteries:

Rechargeable batteries are electrochemical energy storage devices which convert chemical energy into electrical energy during discharging or vice versa during the charging process[14]. Batteries consist of one positive electrode (cathode) and one negative electrode (anode) separated by an ionically conductive and electronically insulating electrolyte soaked with a porous polymeric separator. Figure 1-1 shows a schematic illustration of lithium batteries where $LiFePO_4$ (LFP) is a positive electrode and lithium as a negative electrode. During the electrochemical reactions, ions are shuttled between the

electrodes through the electrolyte while the electrons transfer through the external wires and form a closed circuit[15]. For a rechargeable battery, both oxidation and reduction reactions occur at the same electrode which means a cathode during discharging acts as an anode during charging. In a rechargeable battery with LFP/Li during charge, Li^+ moves from LFP to lithium anode through the electrolyte, and at discharge, the reverse reaction occurs.

$$Li \underset{\text{Charge}}{\overset{\text{Discharge}}{\rightleftharpoons}} Li^+ + \bar{e} \qquad (1)$$

The redox reaction on the positive electrode is

$$FePO_4 + Li^+ + \bar{e} \underset{\text{Charge}}{\overset{\text{Discharge}}{\rightleftharpoons}} LiFePO_4 \qquad (2)$$

So, the overall reaction is

$$Li + FePO_4 \underset{\text{Charge}}{\overset{\text{Discharge}}{\rightleftharpoons}} LiFePO_4 \qquad (3)$$

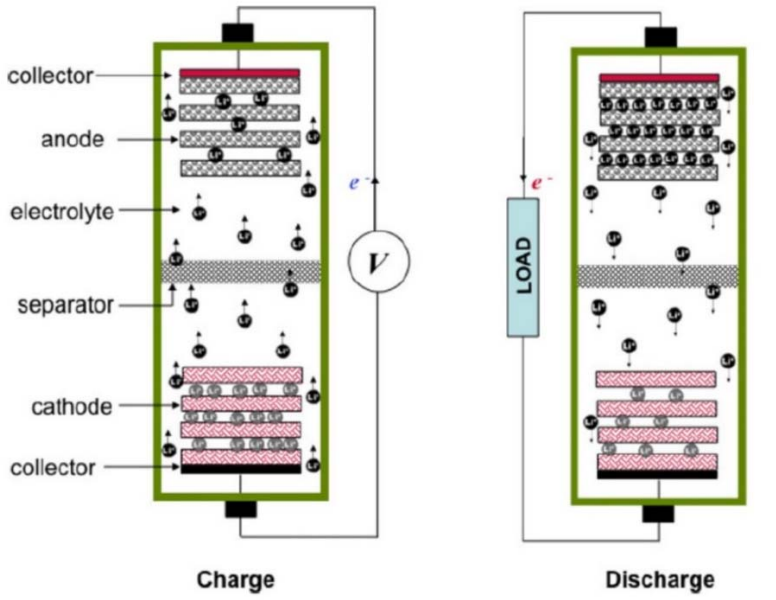

Figure 1-1 Schematic illustration of a rechargeable lithium battery[15].

1.3 Overview and Challenges of the Electrodes:

1.3.1 Cathode Materials:

Cathode materials became one of the most important areas of research since the commercialization of lithium-ion batteries by Sony Corporation in 1991. The cell consisted of $LiCoO_2$/C electrodes which have a three times higher potential of 3.6 V than alkaline systems[16]. Another advantage of this electrode system is its high gravimetric energy densities of 120-150 $Wh.kg^{-1}$ which is about 2-3 times higher than Ni-Cd batteries[17]. A number of researches are undergoing to synthesize cathode materials which have a higher energy density, specific capacity, rate capability, cyclic stability as well as being environmentally-safe and economically viable. So far, lithiated transition metal oxides and their composites such as $LiCoO_2$, $LiNiO_2$, $LiMn_2O_4$, and LFP have been explored[16]. Although $LiCoO_2$ is the most used cathode in present LIBs, there are safety concerns surrounding cobalt oxide materials due to their toxicity which makes them unsafe. Additionally, these compounds are not cost-effective, as minimizing the cost of raw materials is also in consideration to design a better battery[16]. $LiNiO_2$ is another promising electrode; however, safety concerns also limit the commercialization due to the exothermic delithiation reaction of Li_xNiO_2 with the presence of organic electrolyte[18]. The spinel $LiMn_2O_4$ is sourced from an abundant element that is environmentally safe. However, their low theoretical capacity (110 $mAh.g^{-1}$) and rapid capacity fading at a higher temperature (>55^oC) during cycling limit their usage. In addition, $LiMn_2O_4$ cathodes experience loss of active materials when cycled at higher voltages due to the transformation of an unstable two-phase structure to a stable single-phase structure via loss of MnO[19].

Padhi *et al.* for the first time proposed LFP as a potential candidate for LIB cathode. They have shown the extraction of lithium from LFP and forms iron phosphate ($FePO_4$) which is the same space group of LFP[20]. A typical cycling behavior of LFP against lithium is shown in figure 1-2. From the figure, it can be seen that one lithium can be electrochemically extracted from LFP and thus close to the theoretical capacity of 170 $mAh.g^{-1}$ can be achieved[21]. LFP has major advantages such as. modest theoretical capacity (170 $mAh.g^{-1}$), moderate operating voltage around 3.4 V against Li/Li^+ which makes it compatible with most of the electrolytes[22]. Furthermore, this compound is thermally stable, has excellent cyclability, abundant, less costly, and non-toxic. Due to these advantages, LFP is considered as promising cathode material for lithium-ion and lithium metal batteries. However, the major drawback of using LFP in an industrial application is its low electronic conductivity and ionic conductivity [23]. The electrical conductivity of bare LFP is 10^{-9} to 10^{-11} $S.cm^{-1}$, and the chemical diffusion coefficient is around 10^{-11} to 10^{-13} cm^2s^{-1} limits its application to low current rates[24].

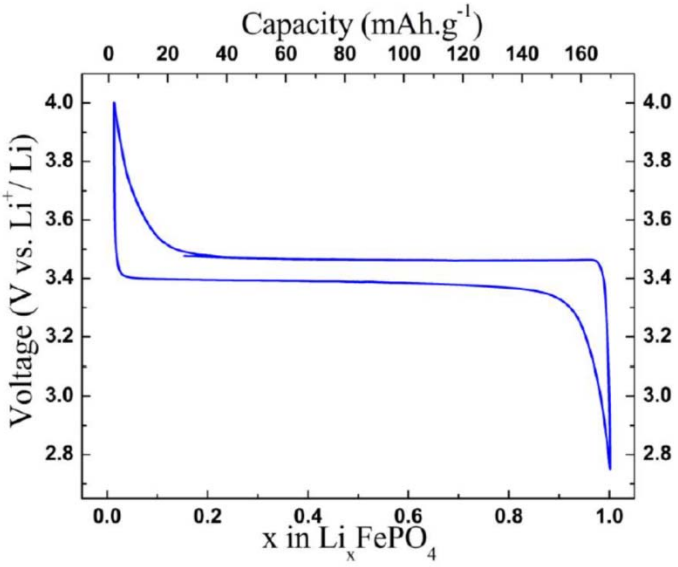

Figure 1-2 Typical charge-discharge profile of LFP cathode against lithium[25].

A number of techniques have been applied to overcome the low electronic and ionic conductivities of the electrode. Armand *et al.* suggested improved kinetics of the electrochemical reaction after coating the $LiFePO_4$ particles with carbon[26]. This coating helped achieve the theoretical capacity of 170 $mAh.g^{-1}$ at room temperature. The improvement of the performance upon carbon coating was mainly due to the following [27]: (1) carbon acts as a reducing agent which prevents the formation of trivalent Fe^{3+} during the synthesis, (2) prevents particle growth by isolating the particles from each other, (3) improves electronic conductivity, and (4) prevents the aggregation of particles thus provides pathways of Li^+. Particle size is another important parameter which plays an important role in improving LFP performance. It has been reported that minimizing the particle size improves the rate capability of LFP because of the increase in specific surface area. Pre-coating the LFP particles with carbon during synthesis decreases the particle sizes. This type of electrode material shows small charge-transfer resistances which improves electrochemical performances at higher C-rates[28]. Although the addition of carbon improves the conductivity, it lowers the volumetric energy density. Therefore, a balance of the carbon content is required to achieve improved conductivity while maintaining higher volumetric energy density[16].

1.3.2 Anode Materials:

In LIBs, graphite is the mostly used anode material. The main mechanism behind it is the intercalation of Li^+ into the vacant sites of carbon to form lithiated carbon during polarization and deintercalation occur from the lithiated carbon when a reverse polarization is applied[29]. The theoretical specific capacity of graphite is 370 $mAh.g^{-1}$ where the intercalation mechanism can be achieved by transfer of one lithium per mole of six carbon.

However, an upper limit regarding energy content has already been attained with graphite anodes because of the higher volume and the weight of the hosts into which lithium intercalates. So for EV applications, batteries of higher specific energy capacity and energy density are required[3]. Replacing the graphite anode with lithium metal can dramatically increase the energy density of the battery as it has higher theoretical specific capacity (3860 $mAh.g^{-1}$) and possess higher negative potential (3.04 V vs. standard hydrogen electrode)[6]. As seen from figure 1-3, Li metal battery outperforms LIBs, Ni-MH, Ni-Cd and lead-acid batteries regarding specific energy and power[29]. However, there are some serious drawbacks using lithium metal as an anode. Because of its high electronegativity, it reacts with the electrolyte solutions and forms solid electrolyte interphases (SEI) on its surface. Although this SEI helps to prevent further decomposition of the electrolyte, it suffers mechanical deformation during lithium plating/stripping thus leads to surface defects on the lithium surface[30]. With the subsequent cycling, lithium ions diffuse to these defects where the applied current density is locally concentrated. The continuous growth of dendrites passes through the separator and short-circuits the battery which causes a serious safety concern for the lithium metal battery[31]. In the past years, great efforts have been made to block the dendrite growth and allow the use of lithium as anode material by using new lithium salts[32], using various electrolyte additives[33], deposition of protective layers on lithium e.g. ceramics[34], and replacing liquid electrolyte with polymer electrolyte[35]. Polymer electrolytes are either solid or gelled by a nonflammable solvent and have been found to be effective in overcoming dendrite growth [36].

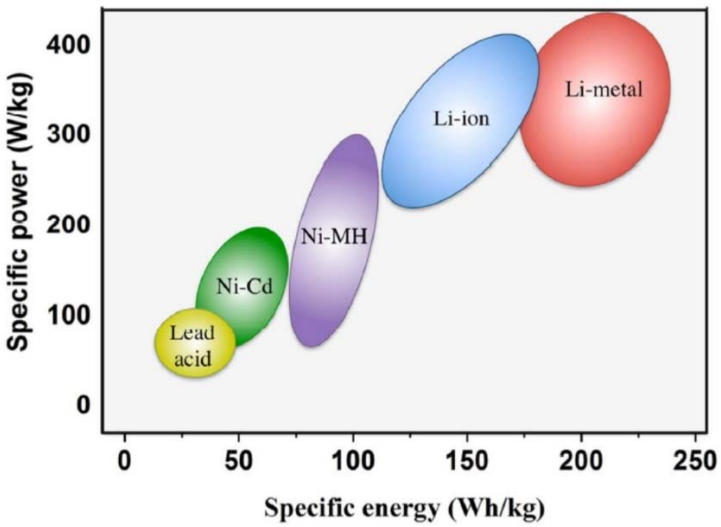

Figure 1-3 Ragone plot of different battery systems[29].

1.4 Overview of Electrolytes and their Challenges:

While most researches are focused on electrode materials, the electrolyte is another key part of the battery as it affects the overall power capability, stability, and safety. Furthermore, the carbonate electrolytes that are commonly used in lithium batteries are highly volatile and flammable which raises serious safety concerns [37]. The basic function of the electrolyte is to allow the transfer of Li^+ between the electrodes by means of diffusion during the charge-discharge process. The transfer of Li^+ between the electrodes produces an electric current and delivers the desired load to an external circuit[38]. Due to the liquid nature of the electrolyte, it cannot prevent the contact between the electrodes which will create a short circuit in the battery. For the prevention of short-circuiting, a porous polyolefin film, known as separator soaked with the liquid electrolyte placed in between the electrodes[39]. Generally, electrolytes consist of a solute which is a lithium salt dissolved in a solvent, mostly organic molecules (aprotic type) for the nonaqueous battery

system. The selection of non-aqueous electrolyte for LIBs based on some of the very important features that an electrolyte must have are mainly[15],

- The solvent of the electrolyte should have good solvability with lithium salt which means it should have high dielectric constant (ε).
- The electrolyte should be less viscous and highly fluidic. High fluidity helps achieve high ion mobility between the electrodes through the electrolyte and separator.
- The electrolyte should have high thermal stability, high flash point, and wide liquidus range to be operational for wider temperature ranges which means it should have a low melting point (T_m) and high boiling point (T_b) and also should not thermally decompose at an operational temperature to improve LIB safety.
- The electrolyte should have wide electrochemical stability window (ESW) so that the electrolyte should not electrochemically decompose in the operational voltage range of the electrodes during the charge-discharge process of LIB.
- It should be ionically conductive as well electronically insulating. Electrolytes with good ionic conduction properties help to improve lithium ion transfer between the electrodes.
- Chemical inertness is another important factor that an electrolyte should have. It should not react with any of the cell components such as electrode substrates, separator, and packaging materials.
- The electrolyte should be environmentally-friendly and nontoxic.

The separator is another important part of LIBs which is a porous membrane soaked with the electrolyte and placed in between the electrodes. The main function of a separator is to prevent short-circuiting of the batteries by impeding direct contact between the electrodes. Besides this, a separator should allow ionic flow and also act as an electronic insulator. It should be mechanically and dimensionally stable and also should have high chemical resistance towards electrode materials and electrolytes. It should also maintain a uniform thickness and impede any particle migration between the electrodes[39].

1.4.1 Solvents for Electrolytes in LIB application:

To satisfy the criteria mentioned above, solvents of different types have been used so far. A mixture of organic solvents is mostly used in state-of-the-art batteries because of the failure of fulfilling all the requirements of an electrolyte should have. More recently, ionic liquids emerged as a promising electrolyte solvents to replace organic solvents because of their prominent electrochemical, thermal, and safety features.

1.4.1.1 Organic Solvents:

State-of-the-art batteries utilize a mixture of organic carbonates as an electrolyte for LIBs. The mixture often consists of two types of aliphatic carbonates. They can be classified as cyclic carbonates and linear carbonates. Ethylene carbonate (EC) and propylene carbonate (PC) are the most used cyclic carbonates, and dimethyl carbonate (DMC), diethyl carbonate (DEC), ethyl methyl carbonates (EMC) are the mostly used linear carbonates in LIB electrolytes.

Scrosati and Pistoia *et al.* [40] for the first time reported that the addition of 9 wt% PC in EC helped form a liquid solution resulting in improved ionic conductivity and good

interfacial properties with various cathode surfaces which opened the door for the application of cyclic carbonates in LIB system. Table 1-1 lists the structure and properties of cyclic and linear carbonate solvents that were used as electrolyte solvents in LIBs. EC has a high boiling point and dielectric constant which indicates high salt dissociation ability and makes it a strong candidate for electrolyte application. However, at room temperature, EC is solid (melting temperature of 36^{o}C) which results in higher viscosity and a poor ionic conductivity. Newer types of ether-based cosolvents such as tetrahydrofuran (THF), diethoxyethane (DEE) and dimethoxyethane (DME) were mixed with EC based electrolytes. Due to the instability towards oxidation on the cathode surfaces, ether-based co-solvents were not a good candidates for LIB battery electrolyte[38]. Tarascon and Guyomard *et al.* for the first time reported the concept of adding linear carbonates as a co-solvent with EC in LIB electrolyte. They reported that addition of any mixing ratio of dimethyl carbonate (DMC) to EC could form homogenous mixture and the main advantages of adding linear carbonates are their low viscosity which yields high ionic conductivity. Adding these types carbonates also helps to widen the stability window up to 5.0 V vs. Li^{+}[41]. The mixing of cyclic and linear carbonates ensures most of the properties that an electrolyte should have. As it is mentioned earlier that EC has good solvation ability with lithium salts and good anodic stability towards the cathode, the addition of DMC helps to improve fluidity and thus improve ion transport properties. Other types of linear carbonates such as diethyl carbonate (DEC), ethyl methyl carbonate (EMC), etc were also explored with EC, and they also found to be applicable as a co-solvent for EC. At present, the state-of-the-art battery electrolytes are based on mixtures of EC with one or two mixtures of DMC and DEC as a solvent for LIB electrolyte[38].

Although carbonate solvents have low viscosity, high ionic conductivity, and good electrolyte/electrode interaction, these solvents specifically linear carbonates have low flash points (DMC: 18ºC and DEC: 31ºC), are highly volatile and possess low thermal stability in the presence of lithium salt leading to serious safety concerns[42,43]. Cyclic carbonate EC has a higher flash point (160ºC); however, mixing of EC with DMC still shows lower flash point (23ºC) and with lithium hexafluorophosphate ($LiPF_6$) (24ºC)[43].

Table 1-1 Lists of organic solvents for lithium battery electrolytes[38].

Solvent	Structure	M. Wt	T_m/ °C	T_b/ °C	η/cP 25 °C	ε 25 °C	Dipole Moment/debye	T_f/ °C	d/gcm^{-3}, 25 °C
EC		88	36.4	248	1.90, (40 °C)	89.78	4.61	160	1.321
PC		102	-48.8	242	2.53	64.92	4.81	132	1.200
BC		116	-53	240	3.2	53			
γBL		86	-43.5	204	1.73	39	4.23	97	1.199
γVL		100	-31	208	2.0	34	4.29	81	1.057
NMO		101	15	270	2.5	78	4.52	110	1.17
DMC	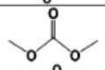	90	4.6	91	0.59 (20 °C)	3.107	0.76	18	1.063
DEC	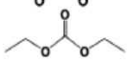	118	-74.3 [a]	126	0.75	2.805	0.96	31	0.969
EMC	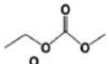	104	-53	110	0.65	2.958	0.89		1.006
EA		88	-84	77	0.45	6.02		-3	0.902
MB	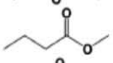	102	-84	102	0.6			11	0.898
EB	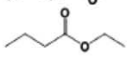	116	-93	120	0.71			19	0.878

1.4.1.2 Ionic Liquids (ILs):

Intensive research has been going on to replace state-of-the-art organic electrolytes partially or completely by introducing safer and environment-friendly solvents with comparable ionic conductivity, elevated thermal stability, good electrode/electrolyte interface properties and also shows better electrochemical stability window. Ionic liquids

have emerged as a promising electrolyte solvents regarding safety and environment-friendly for more than a decade as replacements for organic carbonates.

The first molten salt (ionic liquid) at ambient temperature was synthesized by German scientist Walden *et al.* in 1914[44]. Ionic Liquids (ILs) are salts consisting only of ions which are compounds composed of a large asymmetrical cation and a charge diffuse anion and have low melting points. ILs have by definition a melting point less than 100ºC. However, ILs which are molten at room temperature are known as room temperature ionic liquids (RTIL). RTILs mostly attracted attention to be applicable as a solvent in LIB electrolyte[45]. RTILs consist of bulky and asymmetrical ions which create a large degree of charge delocalization. Bulky cation and anions have decreased ion-ion interactions and resulted in lower efficiency of forming a crystal structure. It has been found that the increment of the size and delocalization of cations and anions decreases the melting point of the ILs. As shown in figure 1-4, NaCl with the smaller size of cation and anion have a melting point of 803ºC. However, replacing Na with the larger cation 1-butyl-3methyl imidazolium ($BMIM^+$) decreases the melting point to 65ºC. On the other hand, replacing smaller Cl^- with the larger bis(trifluoromethanesulfonyl)imide ($TFSI^-$) decreases the melting point to -22ºC[45]. Cations in RTILs used for energy storage applications are shown in table 1-2. They are mainly large organic ions of imidazolium, pyrrolidinium, and piperidinium while the anions are mainly bulky inorganic ions such as tetrafluoroborate (BF_4^-), hexafluorophosphate (PF_6^-), $TFSI^-$, and bis(fluorosulfonyl)imide (FSI^-) based.

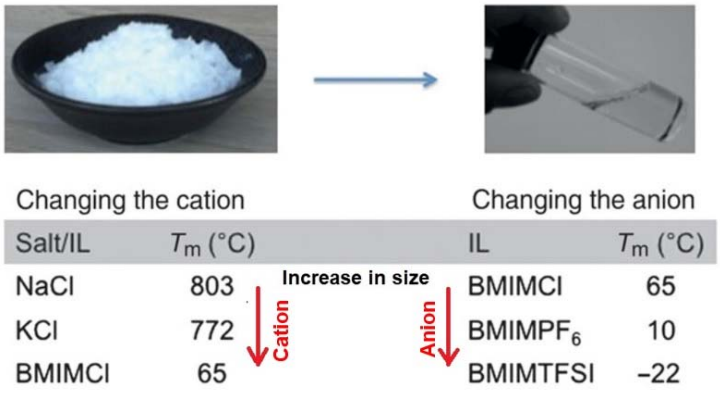

Figure 1-4 Change in melting temperature by the variation of cation and anion[45].

Table 1-2 List of cation and anion available for battery electrolyte.

Label	Abbreviation	Structure
Cation		
Alkylmethylimidazolium	$[C_nmim]^+$	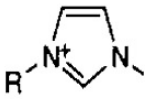
Alkylmethylpyrrolidinium	$[C_nmpyr]^+$	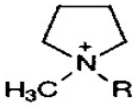
Alkylmethylpiperidinium	$[C_nmpip]^+$	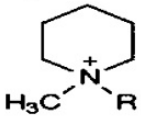
Anion		
Tetrafluoroborate	$[BF_4]^-$	
Hexafluorophosphate	$[PF_6]^-$	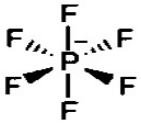
Bis(fluorosulfonyl)imide	[FSI]- or $[N(SO_2F)_2]^-$	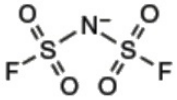
Bis(trifluoromethanesulfonyl)imide	$[TFSI]^-$	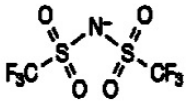

The mostly used imidazolium-based ionic liquid is 1-ethyl-3-methyl imidazolium bis(trifluoromethanesulfonylimide) (EMIMTFSI). Armand *et al.* [46] have shown that $LiCoO_2$/(EMIMTFSI 1M LiTFSI)/$Li_4Ti_5O_{12}$ shows more than 90% capacity retention after 200 cycles at 1-C rate with 106 $mAh.g^{-1}$ capacity. Lower viscosity (34 cP), lower melting point (-15ºC), higher ionic conductivity (8.8 $mS.cm^{-1}$ at 25ºC), and good electrochemical stability window (1-5.3 V) of EMIMTFSI ionic liquid makes them promising candidates for lithium-ion battery electrolytes [46,47]. However, imidazolium-based IL failed to form solid electrolyte interphase (SEI) on lithium and graphitic anode unless an SEI-forming additive (e.g., VC) was added to the IL[48]. With the addition of 5 wt%, VC yields to SEI formation on the first cycle, and the cell has shown no noticeable capacity fading after 100 cycles with graphitic anodes[49]. Although pyrrolidinium based ILs have low viscosities, they are also some of the best candidates to be used in LIB system due to their inherent SEI forming ability with graphitic anodes and also their good electrochemical properties[50].

1.4.2 Lithium Salts:

Lithium salts are used in the preparation of electrolytes to provide Li^+ content in the electrolytes. Different types of lithium salts are used in LIB electrolytes. An ideal solute for an electrolyte should fulfill some requirements to apply to LIB system. They mainly have the following characteristics[38]:

- Should have the ability to dissolve and dissociate in the solution.
- The dissociated cation (Li^+) should have high mobility so that they can move in the solution.

- The anion in the lithium salt should be stable enough towards oxidative decomposition at the cathode.
- The ions should not react with the separator, electrode, and electrolyte of the cell.

The list of salts with their structure and chemical properties are shown in table 1-3. The number of available lithium salts for battery electrolyte is very limited due to the small ionic size of lithium ions which have very low solvability with the low dielectric nonaqueous solvent. Application of soft Lewis base anion replacing the simple Cl^- and F^- ions with Br^- and I^- improves the solubility. However, these anions oxidized with the cathode materials at less than 4 V vs. Li. Introduction of complex anions with lithium cation satisfies the minimum solubility requirement for a nonaqueous solvent[38]. The complex anions which are also known as anions of superacids composed of an anion being stabilized by a Lewis, acid agent. For example, $LiPF_6$ is the mostly used lithium salt in the state-of-the-art battery where F^- is stabilized by Lewis acid PF_5 whose strong electron-withdrawing ability helps to distribute the F- anion smoothly. These types of complex salts have good solubility with low dielectric solvent and have a lower melting point. Lithium salts that are mostly used in LIB electrolyte are $LiMX_n$ (where M=Boron or Arsenic and Phosphorous, X=F and n=4 and 6 respectively). Other lithium salts are lithium perchlorate ($LiClO_4$) and imide based LiTFSI[51].

Table 1-3 Lists of lithium salt for lithium battery system[38].

Salt	Structure	M. Wt	T_m/ °C	$T_{decomp.}$, / °C in solution	Al-corrosion	σ /mScm^{-1} (1.0 M, 25 ° C) in PC	in EC/DMC
$LiBF_4$	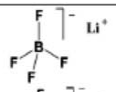	93.9	293 (d)	> 100	N	3.4 [a]	4.9 [c]
$LiPF_6$	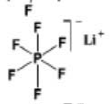	151.9	200 (d)	~ 80 (EC/DMC)	N	5.8 [a]	10.7 [d]
$LiAsF_6$	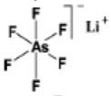	195.9	340	> 100	N	5.7 [a]	11.1 [e]
$LiClO_4$	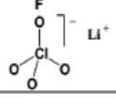	106.4	236	>100	N	5.6 [a]	8.4 [d]
Li Triflate	$Li^+ CF_3SO_3^-$	155.9	>300	>100	Y	1.7 [a]	
Li Imide	$Li^+ [N(SO_2CF_3)_2]^-$	286.9	234 [b]	>100	Y	5.1 [a]	9.0 [e]
Li Beti	$Li^+ [N(SO_2CF_2CF_3)_2]^-$				N		

Due to good solubility, high ionic conductivity with EC/DMC solvents (8.4 mS.cm^{-1} at 25ºC[38]) and also high anodic stability (5.1 V in EC/DMC solvent[41]), $LiClO_4$ became a promising candidate as a solute for lithium-ion battery. However, because of the presence of highly oxidative chlorine, this salt is a strong oxidant and reacts with the organic solvents at higher temperature and higher charge current[38]. Lithium hexafluoroarsenate ($LiAsF_6$) is another type of lithium salt which is superior to $LiClO_4$ due to its nonoxidant behavior with high ionic conductivity (11mS.cm^{-1} at 25ºC in EC/DMC) and high anodic stability up to 4.7 V[41]. However, the formation of toxic As(III) and As(0) during the reduction process of AsF_6^- anion hinders the salt to be used as a solute in LIB electrolyte[52]. $LiBF_4$ is another type of salt based on inorganic superacid anion with moderate ionic conductivity, however poor cyclic efficiency made the salt less effective to be used in LIB application[38]. $LiPF_6$ is the most commercialized salt for LIB because of its multiple well-balanced properties. It has an ionic conductivity of 10.7 mS.cm^{-1} at room

temperature with the nonaqueous carbonate solvents like EC/DMC which is enough for LIB application. Addition of $LiPF_6$ salt to carbonate solvents can resist the oxidation decomposition of the electrolyte up to 5.1 V. It has moderate ion mobility and dissociation constant comparing to the other lithium salts. These well-balanced properties made this salt the most commercialized salt for LIB. However, low thermal stability of this salt causes serious concern regarding safety. Thermogravimetric analysis shows the salt losses half of its weight >200ºC, and when dissolved in mixed carbonates it starts to deteriorate from 70ºC[53]. Lithium bis(trifluoromethanesulfonyl)imide (LiTFSI) consists of imide anion with two trifluoromethanesulfonyl (triflic) groups which acts as a stabilizer for imide anion. DesMarteau *et al.* in 1983 for the first time synthesized this salt[54]. Since its discovery, a number of extensive studies have been performed to see its applicability in lithium ion or lithium batteries. The one of the main advantages of this salt is its safety. It is thermally stable up to 360ºC and melts at 236ºC[55]. Its ionic conductivity at room temperature is 9 $mS.cm^{-1}$ at 25ºC in EC/DMC and highly stable to 1000 discharge with EC/DMC in lithium-ion cell where $LiNiO_2$ as a cathode and petroleum coke as anode[56]. Electrochemical stability results shows that the salt is stable as high as 5 V vs. Li and it dissociates to solvents even with low dielectric constants[38]. Due to the large size of imide anion, LiTFSI salt is viscous in solvents comparing to other salts which may lower the ionic conductivity, however its high dissociation properties compromise the ionic conductivity[38].

1.4.3 Polymer Electrolyte

Polymer electrolytes for solid state lithium ion batteries are very promising prospect for the next generation due to its safety and flexibility. These electrolytes are of two types

and classified as solid polymer electrolyte (SPE) and gel polymer electrolyte (GPE). The former one consists of a lithium salt dissolved in high content of polymer, and the later one consists of polymer gelled by electrolyte solutions.

1.4.3.1 Solid Polymer Electrolyte

In 1973 Wright *et al*. for the first time reported introduction of inorganic salts in polyethylene oxide (PEO) complexes and observed variation of ionic conductivity with increasing temperature[57] while Armand *et al*. investigated lithium salts in SPEs based on PEO for the first time for lithium-ion battery application[58]. Since then a number of research have been performed by using polymers mainly based on ethylene oxide and its copolymers and lithium salts as SPEs. One of the main advantages of using PEO is its ability to dissolve lithium salts due to its high dielectric constant. PEO is a semicrystalline polymer at room temperature. Its glass transition temperature (T_g) is -60ºC and melting point (T_m) is 65ºC. Ion conduction in solid occurs in amorphous phases. Due to the PEOs semicrystalline structure, room temperature ionic conductivity is very low ($<10^{-6}$ S.cm^{-1}). PEO is fully amorphous only above its melting temperature. For this reason, PEO based solid polymer electrolyte works best at or above 70ºC where ionic conductivity value goes around 1mS.cm^{-1} at 80-90ºC[59]. Extensive research on PEO based polymer electrolyte also found that lithium salt anion also has a contribution to lithium ion conduction. Smaller the anion size of the salt higher is the mobility of the anion which lowers cation mobility and decreases ionic conductivity and low lithium transference number. Both ionic conductivity and cation transference number were improved by the introduction of salts with larger anion size such as $TFSI^-$. Because of its large size it is less mobile and frees up lithium ion movement, and also it can act as a plasticizer and hence improve the flexibility

and conductivity[59,60]. Although PEO-LiTFSI SPEs have better ionic conductivity at a higher temperature with good mechanical stability, very low room temperature ionic conductivity prevents them from the application in lithium metal battery electrolyte.

1.4.3.2 Gel Polymer Electrolyte (GPE)

To overcome the drawback of poor room temperature ionic conductivity of SPEs, the introduction of liquid electrolyte in the polymer matrix showed a new hope of the application of polymer electrolyte in practical use. Addition of liquid electrolyte in the polymer forms a gel where the polymer matrix trapped the liquid. Moreover, it improved room temperature ionic conductivity while maintaining mechanical stability, flexibility, lightweight and a lower chance of leakage. They are classified as a gel polymer electrolyte (GPE). In 1975, Feuillade and Perche *et al.* for the first time reported GPEs based on PVDF/poly(vinyl formal) copolymer and organic carbonate electrolyte[61]. Later, Tarascon *et al.* reported poly(vinylidene difluoride-co-hexafluoropropylene) (PVDF-HFP) swollen in liquid electrolyte solution ($LiPF_6$ in organic carbonates)[62]. As it is mentioned earlier, in SPEs main mechanism of ion conduction depends on the amorphousness of the polymer. In GPEs based on PVDF polymers, ion conduction occurs by the liquid electrolyte only. PVDF polymers role is only to trap the liquid solvent inside the polymer network. Room temperature ionic conductivity was further improved by replacing PVDF based polymers with polymers which can also play role in ion conduction by having polar elements such as PEO, polypropylene oxide (PPO), poly(methyl methacrylate) (PMMA) where oxygen is the polar element and in polyacrylonitrile (PAN) where nitrogen is the polar element[43].

Incorporation of organic electrolytes showed promising results regarding both room temperature ionic conductivity and mechanical stability. However as it is mentioned earlier, organic carbonates are highly volatile and thermally unstable at high temperature causes safety concerns even though they are trapped inside nonflammable polymers. To overcome safety issues another new concept is the introduction of room temperature ionic liquid salt in the polymer-salt matrix. Watanabe and Noda *et al.* for the first time added room temperature ionic liquid in solid polymer electrolytes and reported an increase in ionic conductivity and lithium transport number within the polymer matrix[63]. Since then different polymer hosts such as PEO, PVDF, PMMA, PAN, etc have been reported with ionic liquids mostly of imidazolium and pyrrolidinium cation based. LiTFSI is being used mostly in PEs because of the plasticizing ability of $TFSI^-$ anion and also helps to promote amorphous phase fraction[59].

Ohno *et al.* [64] proposed another approach which is named as polymeric ionic liquid (PIL) where ionic liquid monomers are being polymerized and used as matrices for polymer electrolyte system. These type of monomers contains a double bond functional group to allow the polymerization of monomers, an aliphatic chain ($-CH_2-$) known as spacer, electric charge group (positive or negative), and the counter-ion. The spacer allows the segmental motions in the PIL matrix which lowers the glass transition temperature and thus improves ion conductivity[58]. This system exhibits very promising properties because of the chemical affinity between the polymer and ionic liquid. Due to this advantage, PILs shows low phase separation and leakage problem, very simple processability (such as solvent casting), good electrochemical and thermal properties such as ionic conductivity, stability window and thermally stable at high temperature. Marcilla

and Pont *et al.* suggested different approaches to synthesizing PILs. They synthesized imidazolium and pyrrolidinium based polymer by simple anion exchange reaction between the polymer halide with lithium salt (such as LiTFSI) in water. A scheme of the synthesis of the PIL is shown in figure 1-5. These type of polymers are hydrophobic, have high thermal stability and wide stability window[65,66]. Appetecchi *et al.* reported this type of PILs practical use in lithium metal battery and reported 140 $mAh.g^{-1}$ capacity at 40°C for 70 cycles at C/10 rate[67].

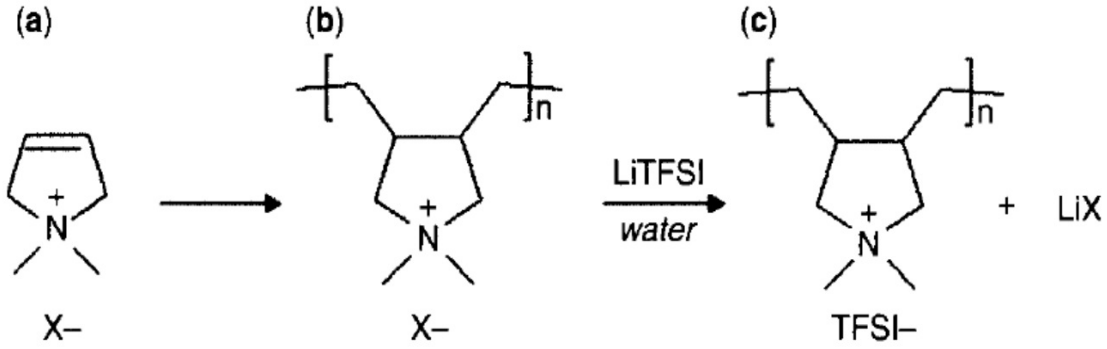

Figure 1-5 Synthesis route to prepare PIL by simple anion exchange reaction.

1.4.3.3 Composite Polymer Electrolyte

Composite polymer electrolyte is another concept where filler materials such as inorganic SiO_2, Al_2O_3, TiO_2 etc have been introduced at a certain percentages into the polymer matrices in order to improve both mechanical and electrochemical properties of the composites. Weston *et al.*[68], for the first time reported composite polymer electrolyte by adding Al_2O_3 filler particles into polymer-salt matrix and suggested improved mechanical properties with no notable changes in ionic conductivity at room temperature. Later Scrosati *et al.*, incorporated nanosize TiO_2 and Al_2O_3 fillers and reported increase in both ionic conductivity and good mechanical stability at low temperature[69]. Li *et al.*

reported the effect of filler material addition in the polymer-ionic liquid system for the first time and found 5times increase in ionic conductivity by the addition of 10 wt% methylsisesquioxane (MSQ) filler[70]. While most of the research in this field focused on adding ceramic nanoparticles, only a few number of research have been made so far with one-dimensional filler. Mesoporous silica materials (SBA15)[70], Fe_2O_3 nano rod[71], $Li_{0.33}La_{0.557}TiO_3$ (LLTO) nanowire[72], Silica fiber(SF) [73] are investigated as the effect of fiber materials in polymer electrolytes. Increase in both ionic and mechanical properties were observed in all the cases. Kimura *et al.* reported the addition of silica fiber in PIL based on polyethylene carbonate (PEC), LiTFSI salt and pyrrolidinium-based ionic liquid. Increase in both mechanical and electrochemical properties have been reported by the addition of 5 wt% silica fiber while cells based on LFP/PIL-SF/Li was cycled at 75ºC with C/15 rate and discharge capacity close to 100 $mAh.g^{-1}$ at the first two cycles then decreased to below 80 $mAh.g^{-1}$ on 4^{th} cycle[73].

1.5 Scope of the Dissertation

Based on literature studies and researches conducted so far, it can be concluded that a breakthrough in battery technology is required to achieve batteries with high energy density and specific energy as the parameters of the state-of-the-art batteries are not sufficient enough to be applicable in long-range EV vehicles as well as in grid storage sectors. Lithium metal as an anode can improve the specific energy and density of the battery. However, safety remains a major concern in using lithium as anode where the conventional electrolyte is one of the major cause due to its nature of volatility and flammability.

The goal of this research is to develop a PIL based gel electrolyte and to improve the electrochemical performances of lithium batteries over its liquid counterpart using lithium as an anode. To achieve this goal, imidazolium-based IL with a dissolved lithium based salt is used as a solvent and a pyrrolidinium based PIL used as a matrix to develop a GPE for lithium battery application. One of the major advantages of IL is its non-flammability and non-volatility in nature. Additionally, the good chemical affinity between the PIL and the IL can afford high IL content in the GPE which improves high ionic conductivity while maintaining dimensional stability. Later on, the addition of inorganic micro glass filler in GPE (composite GPE) improved electrochemical performances in lithium batteries against lithium as an anode comparing to GPE and its liquid counterpart.

In chapter 2 details of the electrochemical and characterization techniques used in this work are discussed. Furthermore, the synthesis process of PIL, IL, and GPE, as well as the preparation technique of cathode materials, are described in details. Chapter 3 discusses the application of GPE in lithium battery application at room temperature, and a comparative study of GPE and ILE based electrolytes show improved electrochemical performances of GPE than ILE. This work has been published in:

Safa, M., Chamaani, A., Chawla, N., & El-Zahab, B. (2016). Polymeric ionic liquid gel electrolyte for room temperature lithium battery applications. Electrochimica Acta, 213, 587-593.

In chapter 4, the application of GPE in high energy Li-S batteries is investigated. The performance of the cell was evaluated using various electrochemical analysis, and a possible capacity fading mechanism was discussed using impedance spectroscopy

technique. Furthermore, a comparative study of GPE and ILE shows improved interfacial contact between GPE and the electrodes. This work has been published in:

Safa, M., Hao, Y., Chamaani, A., Adelowo, E., Chawla, N., Wang, C., & El-Zahab, B. (2017). Capacity Fading Mechanism in Lithium-Sulfur Battery using Poly (ionic liquid) Gel Electrolyte. Electrochimica Acta, 258, 1284-1292.

In chapter 5, the effect of the addition of glass micro filler content in GPE was investigated by using electrochemical characterization and spectroscopic technique. The analysis revealed that at a certain optimum glass filler content the battery showed the highest performance regarding rate capability and cyclability. Later on, a possible mechanism of improved electrochemical performance has been investigated. This manuscript has been prepared to submit to the Journal of Power Sources. Chapter 6 gives a summary of the work done and also proposes future works.

2 EXPERIMENTAL METHODS AND THEORY

2.1 Chemicals and Materials

The following list of chemicals and materials were used in this thesis work: Poly(diallyldimethylammonium chloride) (PDADMAC, MW = 200,000- 350,000 Dal), bis(trifluoro methane) sulfonyl imide lithium salt (LiTFSI), 1-ethyl-3-methylimidazolium chloride (EMIMCL, ≥ 95%) and poly (vinylidene fluoride) PVDF (MW = 530,000 Dal) pellets, and vinylene carbonate (VC, $C_3H_2O_3$) were purchased from Sigma-Aldrich. Acetone and 1-methyl-2-pyrroli- dinone (NMP) were purchased from Fisher Scientific. Lithium metal chips and carbon pre-coated LFP powder were purchased from MTI Corporation. Carbon Black, acetylene (99.9+ %, bulk density 170-230 gL^{-1}) was purchased from Alfa Aesar. Celgard 2400 was purchased from Celgard LLC. Sulfur were purchased from Sigma-Aldrich. Multiwalled Carbon Nanotubes were purchased from Cheap Tubes Inc. Whatman glass microfiber filters grade GF/B were purchased from Sigma-Aldrich. Carbon black, Super P conductive, 99+% (metals basis) were purchased from Alfa Aesar.

2.2 Cell Preparation

2.2.1 Cathode Preparation

Two types of techniques were used to prepare cathode in this work. Tape casting technique was used to prepare LFP and Sulfur – Carbon composite cathode using PVDF as a binder. The binder-free LFP cathode was prepared by using electrochemical spray deposition (ESD) technique. The detail procedures are discussed below:

2.2.1.1 Tape Casting Technique

Carbon pre-coated LFP powder was used to prepare the cathode slurry where the carbon content was 1.8 wt%. Before making the slurry, the cathode powder was baked at 140ºC for 2 hours to remove moisture. Then the LFP and carbon black were mixed in a vial using homogenizer and finally were gradually added to a pre-dissolved PVDF in NMP and stirred for 3 hours. Finally, the slurry was bath sonicated for 3 more hours and after that coated on aluminum foil. The slurry was then air dried overnight and finally at 90ºC for 24 hours.

For the Li-S battery cathode, first sulfur-CNT composite was obtained by electrochemical reaction deposition method. In this technique, 0.02 mol $Na_2S_2O_3$ was dissolved in 500 ml deionized (DI) water by stirring for 30 min. Then, 0.8 g commercial short COOH functionalized MWCNT with an outer diameter of <8 nm was dispersed into the solution mentioned above. After that mixture was ultrasonicated for 1 h, 40 ml 10 M hydrochloric acid was added to the solution gradually to form sulfur precipitation. The solution was then stirred for 24 hr to allow the reaction to complete. After that, the composite was filtered and washed with DI water three times. The final product was collected by drying the composite in an air oven at 60ºC for 36 h.

2.2.1.2 Electrostatic Spray Deposition (ESD) Technique

Electrostatic spray deposition (ESD) is a unique thin film technique where no binder is used. Schooman *et al.* from Delft University of Technology for the first time developed this technique[74]. In this technique, a liquid precursor solution is atomized into an aerosol spray by the application of a high electric field between the feeding source and

a preheated substrate[75]. After reaching the substrate, the solvent of the solution evaporates, and a solid or porous film can be obtained. By varying the flow rate, the distance between the source and the substrate, dc potential, substrate temperature and the composition of the solution one can control the morphology and thickness of the deposited film[76]. This technique operates without vacuum which makes the method less costly compared to other thin film deposition techniques such as. Chemical vapor deposition (CVD), electrophoretic deposition (EPD) and layer-by-layer (LBL) deposition technique[77]. Electrodes prepared with this technique does not need any polymeric binders thus lowers resistance and dead weight to the electrode[78]. Porous, high surface area and homogenous film forming ability make ESD technique suitable for the application as electrodes in energy storage devices.

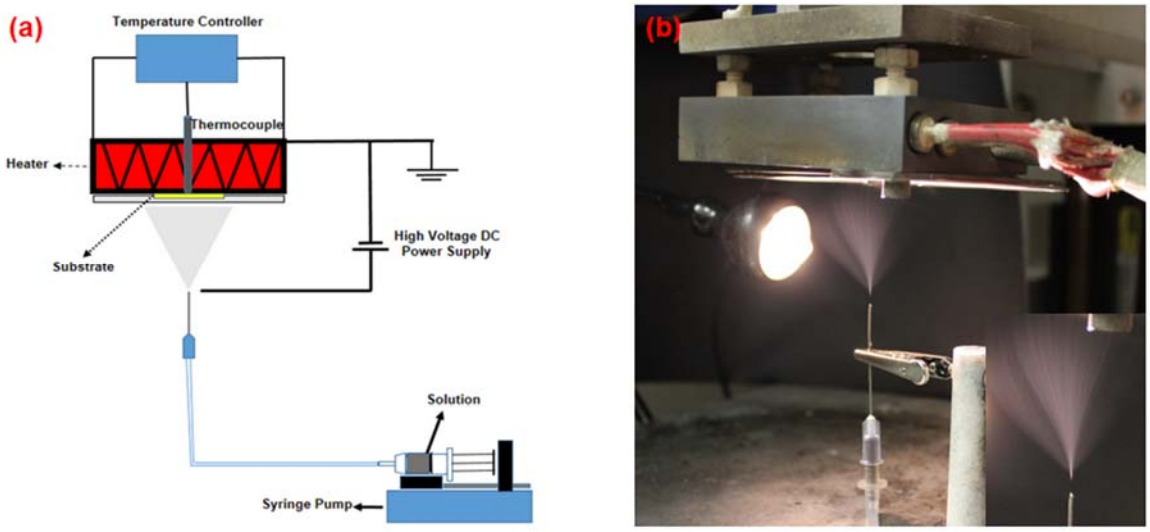

Figure 2-1 (a) Schematic illustration of ESD (b) Practical image of ESD Technique (inset: cone-shaped flow).

Figure 2-1 (a) shows the schematic drawing and an image of the experimental set-up used for ESD, respectively. The major components in the ESD set-up contain a nozzle connected with a syringe that supplies the precursor solution through a syringe pump, a

substrate which is heated up to a high temperature, and a DC high voltage power supply which is applied between the nozzle and substrate. In this technique, a high DC voltage is used to generate a high electrostatic force to accelerate the atomization of liquid droplets at the tip of a nozzle. The charged droplets formed aerosol and sequentially deposited on a heated substrate. The desired electrode material then deposits on the current collector (substrate). The structures and morphologies of the resulting film can be controlled by varying: applied DC voltage, deposition flow rate, time of the deposition, the temperature of the substrate, the distance between the needle and substrate, precursor solution concentration, etc.

2.2.2 Electrolyte Preparation

2.2.2.1 Ionic Liquid Electrolyte (ILE)

In this work, 1-Ethyl-3-Methylimidazolium Bis(trifluoromethane sulfonyl)imide ([EMIM][TFSI]) was used as an electrolyte solvent. The synthesis of the liquid was followed by the procedure suggested by Bonhote *et al.* [79]. 107 mmol of EMIMCL and 107 mmol of LiTFSI were dissolved in 50 mL and 100 mL of DI water. The solution of EMIMCL in DI water was stirred and heated at 70ºC and the solution LiTFSI was added in the EMIMCL solution gradually. Two separate phases were obtained. The bottom part was the desired IL and was extracted by using a separation funnel in 100 mL CH_2Cl_2. The solution was then heated at 60ºC overnight then finally under vacuum for 2 hrs.

For the ionic liquid electrolyte preparation, first 1M LiTFSI was dissolved in [EMIM][TFSI], and polyolefin-based Celgard 2400 separator was soaked in the electrolyte. Before soaking, both sides of the separator was plasma etched to improve the soaking ability. Later on, this electrolyte is labeled as ionic liquid electrolyte (ILE).

2.2.2.2 Poly (Ionic Liquid) (PIL)

For the preparation of gel electrolyte, poly (ionic liquid) (PIL) was used as the polymer matrix. In this work, pyrrolidinium cation based PIL was used which was synthesized by a simple anion exchange reaction between a commercially available polymer poly(diallydimethyleammonium) bis(trifluoromethane sulfonyl)imide (PDADMAC) and LiTFSI salt[66]. First, 30 mmol of LiTFSI salt in 10 ml DI water and 25 mmol monomers of PDADMAC in 100 ml of DI water was dissolved separately and finally mixed in a 250 ml beaker. After shaking the solution, thick white precipitates were formed at the bottom of the beaker. The precipitates were then washed multiple times and filtered out from the solution. The white product was then dried at 70^{o}C in a vacuum oven until a constant weight was achieved.

2.2.2.3 Gel Polymer Electrolyte (GPE)

For the preparation of GPE, first 1M LiTFSI salt was dissolved in the [EMIM][TFSI], and then the desired ratio of the ionic liquid solution and PIL was dissolved in acetone solution in separate vials. Then both the solutions were mixed and stirred for 24 hrs. The solution was then solvent cast into a 0.5” circular pre-cut PDMS template layered on a glass slide. The cast solution was dried at room temperature for 20 minutes to evaporate the acetone and finally dried in a vacuum oven at 90^{o}C for 72 hrs to completely cure the GPE. After the drying process, the PDMS layer was peeled off, and the circular GPE was stored in the glove box until further use.

2.2.2.4 Composite Gel Polymer Electrolyte (cGPE)

For the preparation of cGPE, a certain content of shredded glass micro-filler was added to the GPE solution. To prepare the glass micro-filler, Whatman glass separator grade B was shredded into pieces and fragmented using probe sonication for 3 hrs in acetone. The micro-fillers were then dried in air to remove the acetone and finally dried at 300^{o}C in a vacuum oven for 48 hrs to remove undesirable impurities. For the preparation of cGPE, various contents of glass filler were first mixed in acetone and sonicated for an hour, then the acetone solution with fillers was added to the polymer solutions, and finally, the IL solution was added to the mixture. After 24 hrs of stirring, the solution was solvent cast on the PDMS layered glass slides. For the uniform distribution of micro fillers, a syringe pump was used to cast the solution for each sample.

2.2.3 Cell Assembly

For the cell preparation, 0.5” diameter Swagelok pipe fittings were used. Figure 2-2 shows the cell parts and a full setup of the assembly. From the figure, it is seen that the electrode materials and the electrolyte are placed in between two steel rods. One rod is supported by a spring which helps to create a uniform pressure on the electrode and thus make better contact. Lithium metal foil of 0.5” in diameter was placed on the spring side and top of it the electrolyte film was placed. Finally, the cathode of 7/16” diameter was placed on top of the electrolyte, and the cell was locked tightly. A smaller cathode was used compared to the electrolyte and separator to prevent a short circuit in the cell.

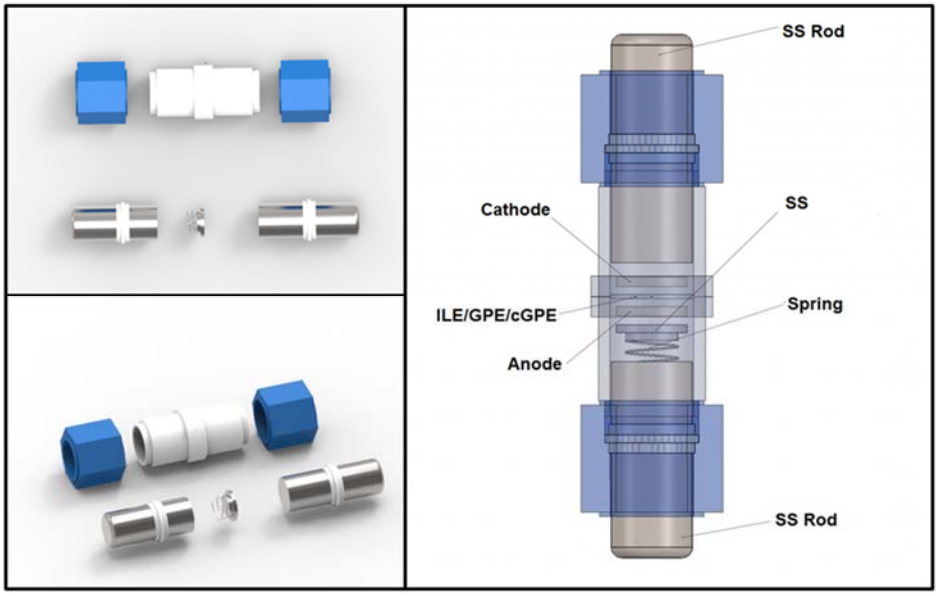

Figure 2-2 Cell parts and cross-sectional view of a Swagelok type battery.

2.3 Thermal Characterization

Thermogravimetric Analysis (TGA) is an important technique used for material characterization. In this technique, the change of mass is recorded with the change of temperature in a controlled atmosphere. One can determine the thermal and oxidative stability and composition of multi-component systems. The heating/cooling rate is programmed to the range of 2 to 20°C/minute depending on the decomposition products of the sample. For better resolution, a slower scan rate is required. Depending on the material, the weight may decrease or increase with the temperature. With the loss of weight, one can determine the types and content of volatile materials in the sample as well as the decomposition temperature of an element or compound. On the other hand, weight gain with temperature indicates oxidation of the sample with an oxidizing atmosphere. To have inert atmosphere nitrogen or argon gases are mostly used and for oxidizing atmosphere air or oxygen gas is used[80]. A typical TGA curve of CaC_2O_4 is shown in figure 2-3[81]

where step 1 indicates the evaporation of water content, step 2 indicates the decomposition of CaC_2O_4 to $CaCO_3$ and at step 3 $CaCO_3$ decomposes to CaO.

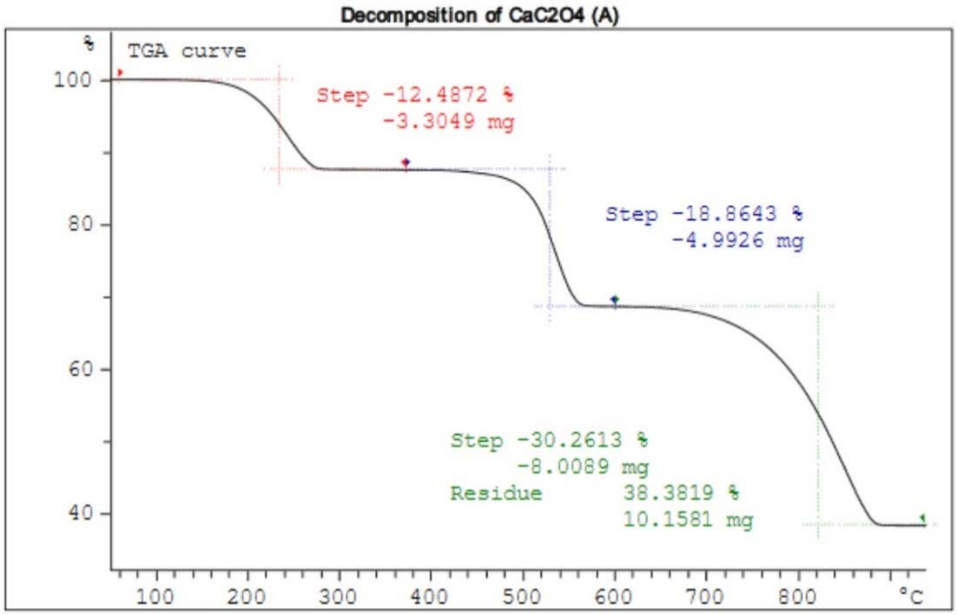

Figure 2-3 A typical TGA curve for CaC_2O_4[80].

2.4 Electrochemical Characterization

Various electrochemical characterization techniques were used to evaluate the performance of the electrolytes.

2.4.1 Voltammetry

2.4.1.1 Cyclic Voltammetry (CV)

Cyclic voltammetry (CV) is one of the most important electrochemical technique to understand the reaction mechanisms or to perform quantitative analysis. A typical cyclic voltammogram is shown in figure 2-4. This technique consists of a variation of a linear electrode potential between two limits: one is the initial electrode potential E_i and the final electrode potential E_f. Within the limit, one can understand the reactivity of the electrochemical system over the range of potentials in a single sweep. Variation of sweep

rate is another important parameter which probes the reaction kinetics and mass transfer process. The scanning starts from an open circuit voltage to more positive voltages which is known as forward scan for the oxidation reaction.

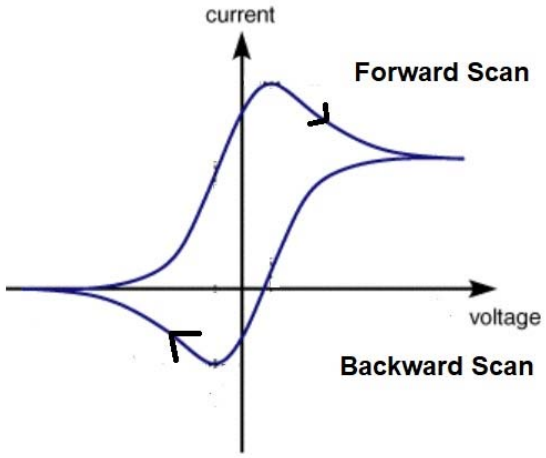

Figure 2-4 A typical Cyclic Voltammogram (CV)[82].

$$E(t) = E_i + vt \ldots\ldots\ldots (4)$$

After reaching the final value usually which is the electrode potential value just before the oxidation of the electrolyte, the electrode potential scanned to the backward direction to the initial value.

$$E(t) = E_f - vt \ldots\ldots\ldots (5)$$

On the reverse scan, the part of the product that was oxidized on the forward scan gets reduced. v is called the scan or sweep rate, and t is the time. According to the size and application of the electrode, the scan rate varies from a few millivolts per second to a few million volts per second[82].

2.4.1.2 Linear Sweep Voltammetry (LSV)

Linear Sweep Voltammetry (LSV) is an electrochemical technique to determine the electrochemical stability window (ESW) of an electrolyte. The electrolyte for batteries must be electrochemically stable up to the high voltage cutoff and also down to the lowest voltage cutoff. ESW measures the electrochemical stability of an electrolyte against oxidation and reduction processes of the electrolyte[83]. Two fresh cells are required to determine the voltage window. To determine the oxidation limit, a forward voltage is applied from the open circuit voltage of the setup where no electrochemical reaction occurs. At a certain voltage, an intense increase in current is observed which indicates the decomposition of the electrolyte, and it determines the anodic limit (oxidation) of the electrolyte.

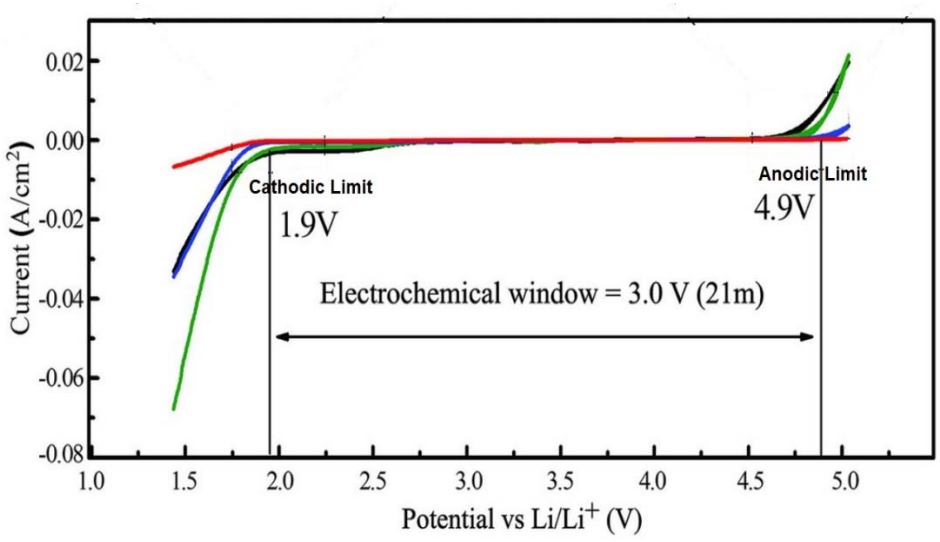

Figure 2-5 A typical linear sweep voltammogram showing the stability window[84].

To determine the reduction limit, another fresh cell is scanned in the backward direction, and at a certain voltage, the current starts to increase intensely in a negative direction. This voltage determines the cathodic limit (reduction) of the electrolyte against

the reference electrode as shown in figure 2-5. The voltage difference between the anodic and cathodic limit determines the ESW of the electrolyte. From the ESW of an electrolyte, one can understand the range of potentials available for the electrochemical study that will not be affected by the electrolytes[84].

2.4.2 Electrochemical Impedance Spectroscopy (EIS)

Electrochemical impedance is the measure of current through a cell when an AC potential is applied to the cell. Impedance refers to the frequency dependent resistance to current flow of a circuit element which consists of resistors, capacitors, etc. Impedance assumes an AC current at a specific frequency in Hertz (cycles/s) and computes the impedance by measuring the response at each frequency[85]. Impedance is represented as a complex number,

$$Z_\omega = E_\omega / I_\omega = Z_o \exp(j\varphi) = Z_o(\cos\varphi + j\sin\varphi) \ldots\ldots\ldots (6)$$

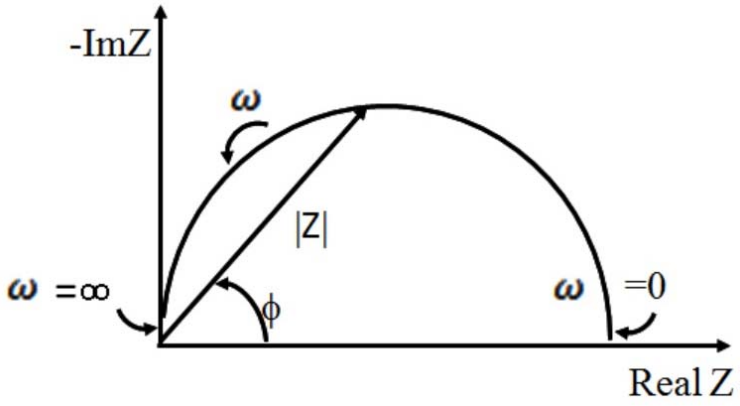

Figure 2-6 Nyquist plot of a cell[86].

where, E_ω = Frequency-dependent potential, I_ω = Frequency-dependent current. The expression for Z_ω is composed of a real and an imaginary part. The real part is plotted on the X-axis and the imaginary part on the Y-axis of a chart. Figure 2-6 shows a typical

Nyquist plot. In this plot the Y-axis is negative and that each point on the Nyquist plot is the impedance Z at a particular frequency. On the Nyquist plot, the impedance can be represented as a vector of length |Z|. The angle between this vector and the X-axis is known as phase angle f(=argZ)[86].

2.4.2.1 Electrical Circuit Elements

To analyze the EIS data, an equivalent electrical circuit model is designed to fit the Nyquist plot. For simple plots, most of the circuit elements in the model are common electrical elements such as resistors, capacitors, and inductors. EIS models usually consist of a number of elements in a network. Based on the plot the elements are connected both in serial (eq 7) and parallel (eq 8) combinations. For linear impedance elements in series, the total equivalent impedance is

$$Z_{eq} = Z_1 + Z_2 + Z_3 + \ldots (7)$$

While the linear impedance elements in parallel one can calculate the equivalent impedance as,

$$\frac{1}{Z_{eq}} = \frac{1}{Z_1} + \frac{1}{Z_2} + \frac{1}{Z_3} + \cdots (8)$$

In a series connection, the current flowing through is the same, and the overall voltage is the sum of voltages across individual elements. On the other hand in parallel connection, the voltage is the same for all elements, and the overall current is the sum of the current flowing through each element. Impedance contributions are additive in series and inverse additive in parallel. The models mentioned above are only applicable for ideal cases such as. smooth and uniform surfaces. In the real case, the electrode surfaces are

porous, have grain boundaries which result in non-uniform current distribution and mass transfer[85].

2.4.2.1.1 Electrolyte Resistance

The resistance of an ionic solution depends on the parameters such as. ionic concentration, type of ions, temperature, and the geometry of the area in which current is carried[85]. In a bounded area with area, A, density, ρ, and length, l, the resistance is defined as,

$$R = \rho \frac{l}{A} \text{.....(9)}$$

2.4.2.1.2 Double Layer Capacitance

An electrical double layer exists between the interface of an electrode and its surrounding electrolyte. Ions from the solution adsorb onto the electrode surface and thus forms this layer. The charged electrode and the charged ions are separated by an insulating space which is in the order of angstroms. Charges separated by an insulator form a capacitor and a bare metal immersed in an electrolyte will behave like a capacitor. This layer depends on some important factors such as. electrode potential, temperature, ionic concentrations, types of ions, oxide layers, electrode roughness[85].

2.4.2.1.3 Diffusion

An impedance caused by diffusion is called Warburg impedance. At high frequencies, the diffusing reactants do not have to move very far, so Warburg impedance is low. At low frequencies, the reactants have to diffuse farther, thus results in high Warburg-impedance. On a Nyquist plot, the Warburg impedance appears as a diagonal line

with a slope of 45°. This form of the Warburg impedance is known as infinite Warburg, and this is only valid if the diffusion layer has an infinite thickness[85].

2.4.2.1.4 Constant Phase Element (CPE)

Capacitors in EIS experiments are only valid for ideal cases where the surface of the cathode is not smooth, and the current distribution on the electrode surface is not uniform. To define the non-ideal condition a constant phase element (CPE) is used in place of capacitor[85].

2.4.2.2 Common Equivalent Circuit Models

Based on the Nyquist plot different types of equivalent circuit models have been used to fit the plot.

2.4.2.2.1 Randle Cells

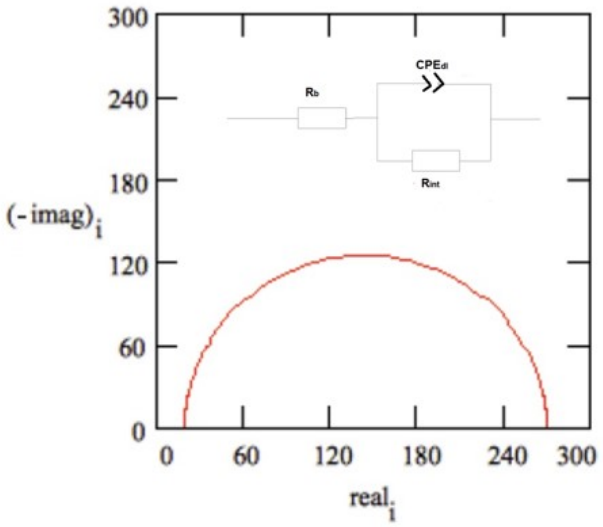

Figure 2-7 Nyquist plot with one semi-circle. Inset diagram shows a typical Randle cell[85].

This circuit model is one of the most common that includes an electrolyte resistance R_b, a double layer CPE with an interfacial resistance R_{int} connected in parallel. Figure 2-7

shows a typical Nyquist plot with the Randle cell in the inset diagram. In the diagram, the x-intercept is the R_b, and the diameter of the semi-circle is R_{int}.

2.4.2.2.2 Mixed Kinetic and Diffusion Control

When a semi-infinite diffusion is the rate determining step where polarization occurs due to a combination of kinetic and diffusion process, then Randle cell is not valid. In that case, a semi-infinite Warburg diffusion is added in series with R_{int} and parallel with CPE_{dl}. The electrolyte is connected with series. Nyquist plot with the circuit model in the inset diagram are shown in figure 2-8.

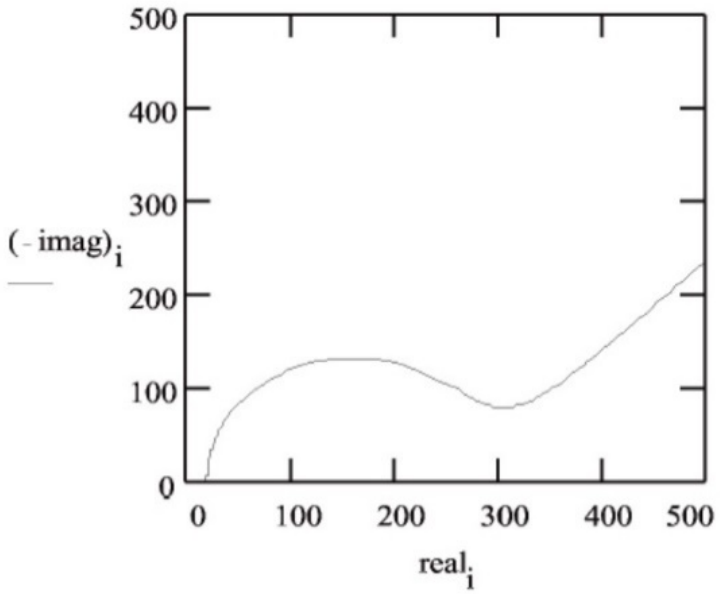

Figure 2-8 Nyquist plot where semi-infinite diffusion is the rate-determining step. Inset diagram shows the corresponding model[85].

2.4.2.2.3 Two semi-circles with Warburg

There is another case shown in fig. 2-9, where two semi-circles are observed which is common in lithium batteries. First one is at high-frequency while the second one is at the medium frequency. There is a semi-infinite Warburg at low frequency. The semi-circle

at high frequency is the interfacial resistance between the electrolyte and the electrodes and the corresponding CPE_{dl} is the distributed capacity of the interfaces. The second semi-circle at the medium frequency is due to the charge transfer resistance between the electrode and the conductive agent, and the corresponding CPE is the double layer capacitance. The semi-infinite Warburg line is related to the diffusion.

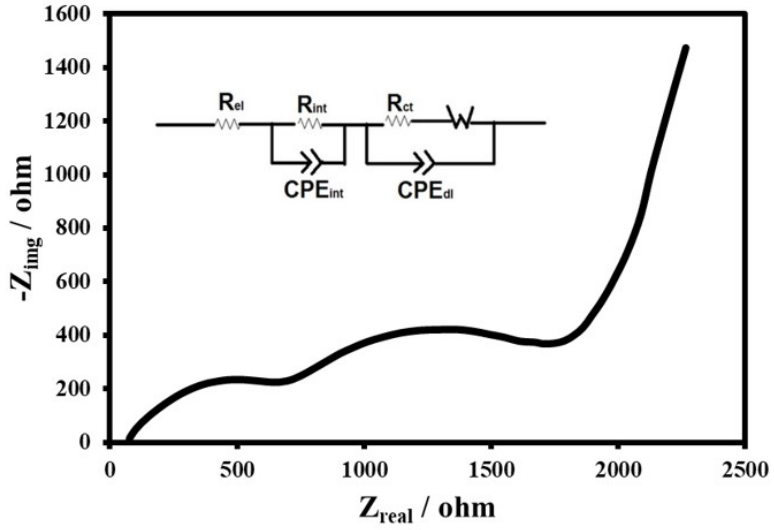

Figure 2-9 Typical Nyquist plot with two semi-circles and a Warburg. Inset diagram shows the corresponding EIS model.

2.4.3 Chronoamperometry

Chronoamperometry is an electrochemical technique where electrode potential is abruptly changed, and the resulting current variation has been recorded with time. In this dissertation, chronoamperometry was performed to determine Li^+ transference number in a lithium symmetry cell.

2.4.3.1 Li^+ Transference Number

Li^+ transference number was determined by the methods suggested by Bruce *et al.* [87]. According to the method, first a Li/Li symmetric cell was prepared by placing

electrolyte film in between the lithium and an EIS was measured before the polarization and from the EIS, initial resistance, R_o of the passivation layer was determined. Then chronoamperometry test was performed by applying a small DC voltage (10 mV) across the cell and ran until a steady state current was observed. From the test, the initial current I_o and the steady state current I_{ss} were determined. After the chronoamperometry test, an EIS was measured to determine the resistance R_{ss} after the chronoamperometry test. Finally, the transference number was calculated by the formula suggested by Bruce *et al.*

$$t_{Li} = \frac{I_{SS}(V - I_0 R_0)}{I_0(V - I_{SS} R_{SS})} \ldots\ldots\ldots (10)$$

Transference number t_{Li} is dimensionless and the value is in the range of 0 to 1[87].

2.4.4 Ionic Conductivity

The ionic conductivity of the electrolyte is the measure of electrolytes ability to transfer ions in between the electrodes. To determine the ionic conductivity, first electrolyte film was placed in between two stainless steel rod in a Swagelok type cell. A potentiostatic EIS was performed, and the x-intercept in the Nyquist plot determines the resistance R. The ionic conductivity σ was calculated by the following formula;

$$\sigma = \frac{L}{AR} \ldots\ldots\ldots (11)$$

Where L is the thickness of the electrolyte, A is the surface area of the electrolyte and R is the resistance determined from the Nyquist plot[36].

2.4.5 Galvanostatic Charge/Discharge

Galvanostatic charge-discharge tests are performed to determine the capacity of a battery and expressed in $mAh.g^{-1}$. A negative current is applied in a discharge process while

a positive current is applied for charge process. A predefined cut-off voltage is set-up, and the value depends on the chemistry of the electrode materials. A rate capability of a battery can be evaluated by cycling the battery at higher current rates. Cyclic stability of a battery is determined at a constant current for a pre-defined number of cycles. In this dissertation, the galvanostatic charge-discharge tests of LFP/(GPE) or (ILE)/Li cell performance was run at various C-rates for 40 cycles with a voltage cut-off ranging 2.5-4.2 V. On the later stage, S-CNT/(GPE) or (ILE)/Li cells were tested at various C-rates as high as 1C rate for 100 cycles to observe the rate capability. The cyclic stability at C/2 rate for 500 cycles was also performed for both the GPE and ILE containing battery. The cut-off voltage for Li-S battery was 1-3 V.

3 POLY (IONIC LIQUID) BASED GEL ELECTROLYTE FOR LITHIUM BATTERY APPLICATION

3.1 Background

As it is mentioned in an earlier section that much improvement in LIBs technologies is required in order to have a high specific energy density and specific capacity battery which can improve the performance of EVs. Safety remains one of the biggest concerns of LIB system due to the use of flammable and volatile organic liquid electrolyte[37,38,43]. Over the past few decades, the emergence of PEs opened up an avenue for safer battery technology[1,88,89]. The most notable advantages of PE containing batteries are their ability to overcome drawbacks such as electrolytes leakage and gas evolution during solvent decomposition. Since the introduction of PEs, numerous polymers and polymer/solvent mixtures have been reported with improved electrochemical and mechanical properties for applications in LIBs.

PEs are mainly classified as solid polymer electrolyte (SPE) and GPE. SPEs consists of a highly concentrated lithium salt dissolved in a polymer and the GPE consists of a polymer gelled by electrolyte solutions containing lithium salt. Armand *et al.* [90–92]for the first time investigated the performance of SPEs based on polyethylene oxide (PEO) for potential lithium-ion battery applications. However, low ionic conductivities of 10^{-5} S.cm^{-1} at 40-60°C was not good enough for LIBs to be operable at room temperature or below room temperature. Since then, numerous researches have been reported using SPEs in LIBs, based on PEO[91,92], polyacrylonitrile (PAN)[93,94], poly(vinyl alcohol)(PVA)[95,96], polyethylene carbonate (PEC)[97] polymethylmethacrylate

(PMMA)[95], polyvinylidene fluoride-co-hexafluoro propylene (PVDF-HFP)[98], polyvinyldene fluoride (PVDF) [99]and its copolymers with focusing to improve the room temperature ionic conductivity while maintaining the mechanical stability. One major problem of SPEs is their high crystallinity at room temperature which causes ions diffusion difficult and causes low room temperature ionic conductivity[100]. These problems have led to their predominant utilization in high temperature applications exceeding their glass transition temperatures.

To overcome the diffusional problem, GPEs take advantage over SPE which contains liquid electrolyte solution with lithium salt. The introduction of a liquid increases the ionic conductivity of GPEs as many as 100 times, especially at room temperatures. Other noticeable advantages of GPEs over SPEs are better interfacial contact with the electrodes. The first time application of GPE in LIBs were introduced by Tarascon *et al*. where his group prepared GPE with PVDF-HFP polymer as matrix and gelled by 1M $LiPF_6$ in ethylene carbonate (EC): dimethyl carbonate (DMC) (1:1 v/v) in $LiMn_2O_4$/C battery with a rate capability of 115 $mAh.g^{-1}$[62]. Mostly used solvents in GPEs include EC, DMC, 1,2-dioxolane, dimethoxymethane[101]. Although these solvents provide better performance for GPEs compared to SPEs in terms of ionic conductivity and battery performance, they still face the common problems that are observed in liquid electrolytes such as evaporation, leakage, and flammability. The search for a solvent which is non-flammable, non-volatile as well as have high electrochemical properties is therefore essential to GPE research.

As discussed in chapter 1, RTILs have been regarded as one of the best solvents for GPEs due to their low-volatility, non-flammability, and wide electrochemical stability window. Watanabe and Noda reported on the first use of the IL-based GPE which consisted of [EMIM][BF_4] and [BP][BF_4] IL with a polyvinyl [63] polymer. The reported ionic conductivities were 2×10^{-2} and 3×10^{-3} $mS.cm^{-1}$ at 30°C, respectively. The most used imidazolium cation based ionic liquid is 1-ethyl-3-methyl imidazolium bis(trifluoromethanesulfonylimide) [EMIM][TFSI] in lithium battery application. The major advantage of this IL is its high fluidity and ionic conductivity at room temperature. As it is mentioned in earlier chapter that an electrolyte consists of a solvent and a lithium salt. In most of the cases, LiTFSI is a commonly used salt for PEs because of the plasticizing ability of $TFSI^-$ anion and accelerating amorphous phase fraction[102]. Armand *et al.* [46]reported on a $Li_4Ti_5O_{12}$/EMIMTFSI-1M LiTFSI/$LiCoO_2$ with more than 90% capacity retention after 200 cycles at 1-C rate with 106 $mAh.g^{-1}$ capacity. Yang *et al.* reported on a GPE of [EMIM][TFSI] IL with PVDF-HFP polymer with 141.9 $mAh.g^{-1}$ discharge capacity at the initial cycling and after 20 cycles it retained 93.1% of the initial capacity at C/10 rate at 20°C[103]. Ohno *et al.* [104]proposed the utilization of PIL which are essentially polymers of the IL monomers used as matrices for GPEs as described in chapter 1. The main advantage of using PILs are their high chemical affinity with ILs which leads to the improved performance of the resulting GPEs. Furthermore, the high chemical affinity lowers phase separation and leakage problem. PILs also shows good electrochemical and thermal properties[58,70]. Marcilla *et al.* and Pont *et al.* [65,66] synthesized imidazolium and pyrrolidinium based PILs by a simple anion-exchange reaction with the halide form of the polymer using a lithium salt. These types of PILs were

generally hydrophobic, thermally stable at high temperatures, and have a wide ESW. Appetecchi *et al.* evaluated PILs performance in lithium-ion battery and reported impressive capacities of 140 $mAh.g^{-1}$ at 40°C for 70 cycles at C/10 rate[105].

In this work, we report on the preparation of a free-standing GPE composed of pyrrolidinium-based PIL poly[diallyldimethylammonium bis(trifluoromethane) sulfonimide] (PDADMATFSI), the imidazolium-based IL [EMIM][TFSI], and the lithium salt LiTFSI. Thermal and electrochemical properties of the GPE were evaluated to determine the utility of the synthesized GPE in lithium-ion battery applications. Compatibility of the GPE against lithium metal was also evaluated. Cyclability study of Li/GPE/LFP batteries were also performed at room temperature (22^{o}C) for rates up to 5C charge and discharge rates.

3.2 Experimental Details

The detail synthesis procedure of IL, PIL and GPE are described in chapter 2. Figure 3-1 depicts the chemical structures of the lithium salt, IL and PIL. For the preparation of GPE, first 1 M LiTFSI in [EMIM][TFSI] was prepared followed by mixing with 20 wt.% of PIL (final composition 80:20 electrolyte:PIL by weight). The mixture was magnetic stirred for 24 hrs and then drop-casted in a 0.5” circular PDMS template layered on a glass slide by using a syringe pump. Figure 3-2 illustrates the step-by-step procedure of GPE preparation.

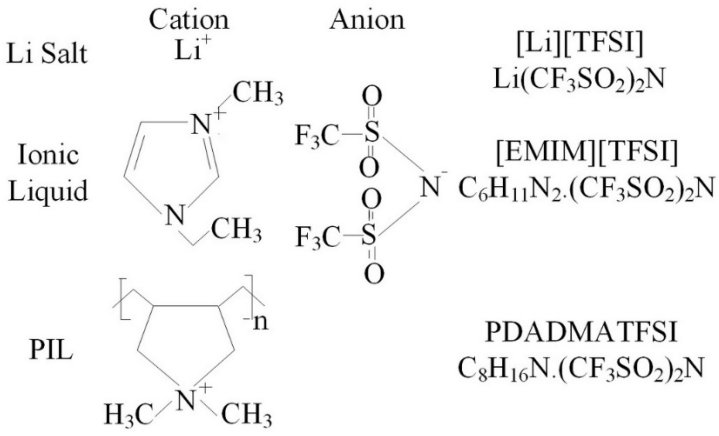

Figure 3-1 Chemical structures of the GPE and ILE components: [Li][TFSI], [EMIM][TFSI], and PDADMATFSI.

The detail procedure of preparing the LFP cathode is also described in chapter 2. For this work, 78 wt.% carbon pre-coated LFP, 10 wt.% PVDF, and 12 wt.% carbon black ratios were used.. LFP and carbon black were added to pre-dissolved PVDF solution in NMP and were bath sonicated for 2 hours. The resulting slurry was then casted on aluminum foil and dried at 90°C for 24 hours. The active material loading varied from 2 - 2.3 mg.cm^{-2}.

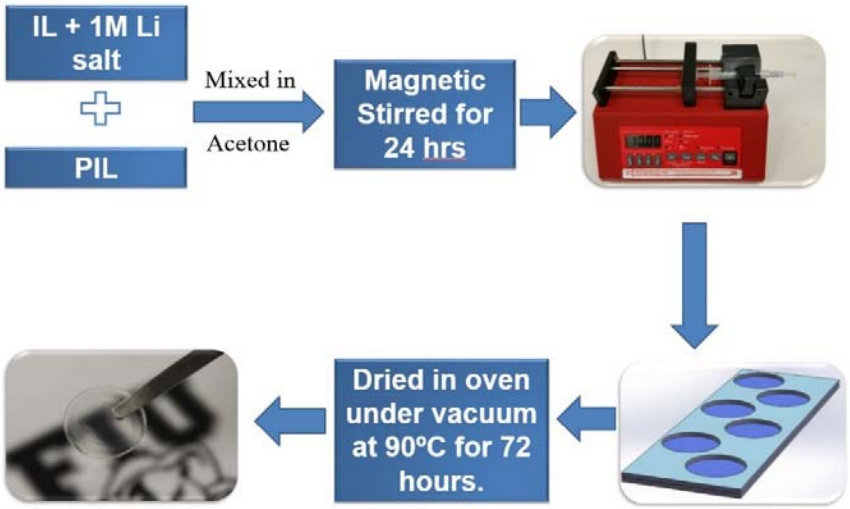

Figure 3-2 Step-by-step procedure of the preparation of GPE.

TGA studies were performed to determine the decomposition temperatures of the GPE using SDT Q600 from TA Instruments. To determine the thermal decomposition temperature, the sample was heated from room temperature to 600°C under nitrogen gas (flow rate: 50 mil.min^{-1}) with a scan rate of 10°C min^{-1}. Isothermal TGA analyses was also performed using the same equipment. Samples were tested at selected temperatures to confirm their thermal stability. Ionic conductivities of electrolyte films were obtained from the EIS data. To perform the test, electrolyte films were placed between the two stainless steel electrodes and analyzed at room temperature. The ionic conductivity, σ, was calculated following the equation 11. LSV was performed at room temperature (22°C) to investigate the anodic and cathodic stability limit of the electrolyte films. Two fresh cells were used to complete the experiment. One sample was used to determine the cathodic limit and the other one to determine the anodic limit. The scanning was performed from open circuit voltage (OCV) to 6 V (anodic limit) and to – 0.5 V (cathodic limit). For this experiment, two electrode setup where lithium was used as both reference and counter electrode and stainless steel as working electrode with a scan rate of 1 mVs^{-1}. Lithium transference number (t_{Li^+}) was determined following the procedure and equation suggested by Bruce *et al.* [39]. More details are discussed in chapter 2. To perform this test first, symmetrical cells using GPE (Li/GPE/Li) and ionic liquid electrolyte, ILE, (Li/ILE/Li) were monitored under chronoamperometry at ΔV=10 mV until a steady-state current was reached. The initial I_0 and steady-state I_{SS} currents in addition to the initial Z_0 and steady-state Z_{ss} resistances were obtained. t_{Li+} was calculated by following equation 10. The stability of GPE and ILE against lithium was evaluated by monitoring the electrochemical impedance spectra of Li/(GPE) or (ILE)/Li symmetrical cell after different storage time

under open circuit condition at 22ºC. All the above mentioned electrochemical measurements were carried out using a Gamry Reference 600 instrument. To investigate the compatibility of the GPE with the Li metal electrode, symmetric Li/GPE/Li, and Li/ILE/Li cells were prepared and galvanostatically cycled. Repeated 30 minutes charges and discharges were performed at a current density of 0.2 $mA.cm^{-2}$ for 100 cycles.

Cells using lithium anode, GPE or ILE, and LFP cathode were prepared in a Swagelok type assembly in an oxygen-free and humidity-free (< 1 ppm) argon filled glovebox. The electrodes in both cells were pre-soaked with IL-1M LiTFSI containing SEI forming additive, 5 wt.% VC solution[48,106]. Galvanostatic charge-discharge cycling was performed using variable rates at 22°C between 2.5–4.2 V using an MTI Corp battery analyzer.

3.3 Results and discussion

TGA curves in Figure 3-3 shows that the GPE composed of 80:20 electrolyte: PIL by weight decomposed in two stages. A slow decomposition can be observed around 160°C and a rapid decomposition between 390-450°C. The values are greatly improved from the various carbonate-containing GPEs, which affords our GPEs higher stability and protection from thermal runaway in LIBs[42].

The ionic conductivities of the synthesized GPE and ILE were measured at 25°C using EIS. Ionic resistance, *Z*, was determined from the intercept of the high-frequency AC impedance spectra with the real axis on a Nyquist plot. For the GPEs (80:20) the ionic conductivity was 3.4 ± 0.3 $mS.cm^{-1}$ (n=5) at 25°C which is comparatively high to other GPEs reported elsewhere[105]. GPEs using [EMIM][TFSI] (33.3 wt.%) with P(VDF-HFP) also reported a lower ionic conductivity of 2.11 $mS.cm^{-1}$ at 30°C[107]. The physical

stability and electrochemical affinity of the PIL: IL pair allowed improved ionic conductivity of GPE which is ~40% of the ionic conductivities of the pure IL (8.4 mS cm^{-1} at 25°C)[108].

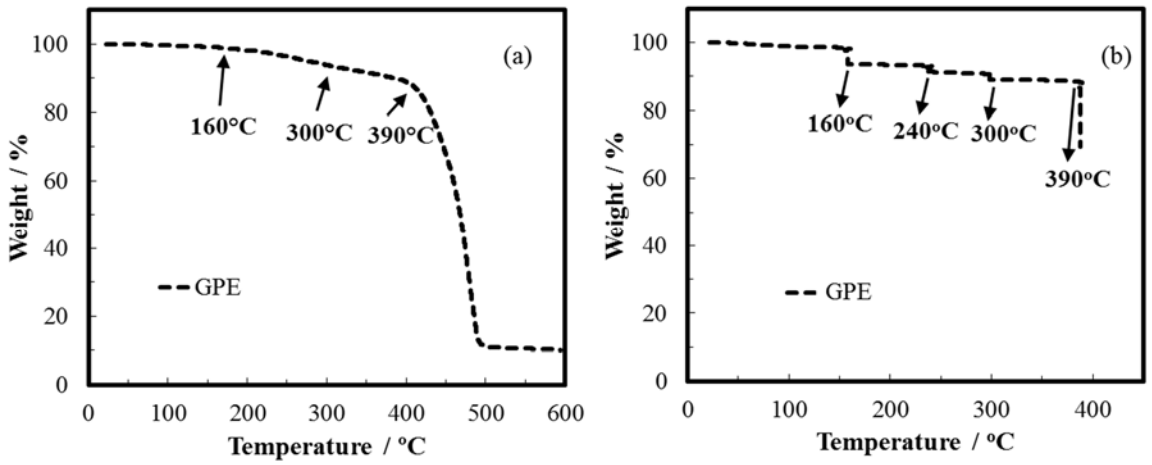

Figure 3-3 Thermogravimetric analysis (TGA) analysis of (a) GPE from 22 to 600°C (b) Isothermal TGA of GPE at different temperatures (Holding Time: 1 hour each) under nitrogen atmosphere (flow rate: 50 mL min^{-1}). Scan rate: 10°C min^{-1}.

The electrochemical stability window shows both the anodic and cathodic limit compatibility of the electrolyte with the electrode materials by performing LSV. Fig. 3-4 compares the LSV of ILE and GPE. From the figure, it can be seen that the anodic stabilities of both the ILE and the GPE reaching 4.9 V vs Li/Li^+. The smoothness of the anodic curve indicates the absence of oxidizing impurities in both ILE and GPE which indicates of its safe use at high voltage cells with high voltage cathode material without any oxidative decomposition. On the other hand, the cathodic limit of ILE is 1 V vs Li/Li^+ which is due to the decomposition of $EMIM^+$ cation as reported elsewhere[79]. In GPE however, the cathodic limit is in the range of 0.3 – (-0.1) V, significantly lower than the ILE. As seen from the figure, there is a small current increase at 0.3 V and a rapid increase

at -0.1 V. The former fluctuation were likely due to the presence of impurities in the hygroscopic GPE and have been reported elsewhere[67].

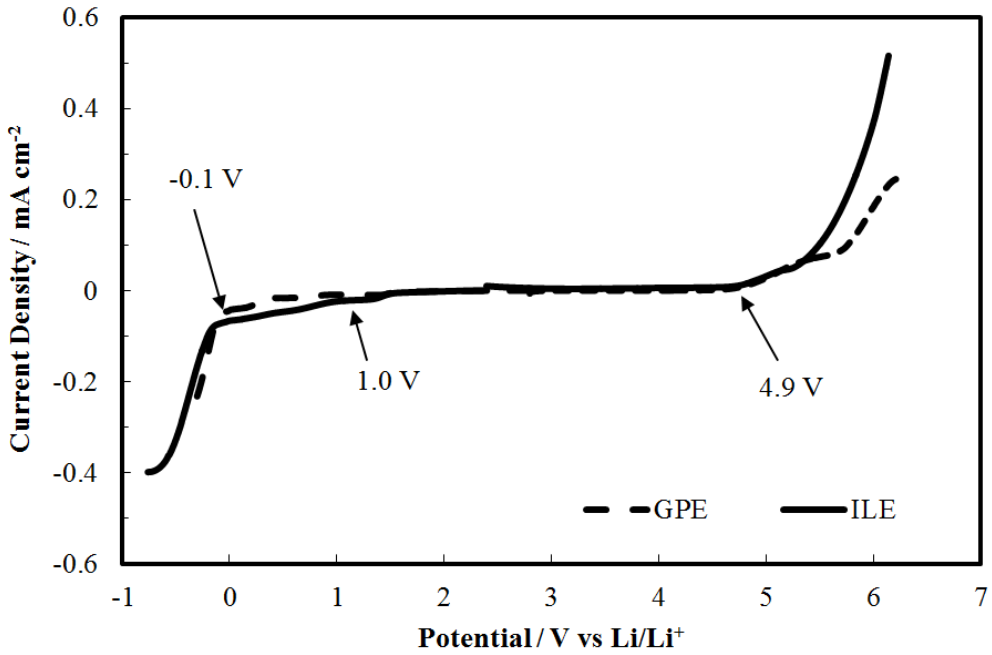

Figure 3-4 Linear sweep voltammograms of ILE and GPE at room temperature with stainless steel as working electrode and lithium as both reference and counter electrode. Scan rate: 1 mV s^{-1}.

It is safe to assume that the actual cathodic limit of the GPE is the lower limit of -0.1 V. The wider ESW for GPE (5 V) compared to the liquid electrolyte (3.9 V) can be attributed to the stabilizing properties of the PIL. This enhancement is due to the presence of pyrrolidinium cation of the PIL whose cathodic limit is below 0 V and has the ability to form SEI on the lithium anode[109]. Barghamadi *et al.* confirmed using XPS that pyrrolidinium cations and TFSI anions both participate in the formation of SEI[110]. The formation of such layer by the PIL can be credited to the improvement of the cathodic stability of EMIM. This stability improvement was also previously observed in the

stabilization of the cation of $PYR_{1A}TFSI$[111]. This wide ESW of GPE makes the IL a suitable electrolyte for Li/GPE/LFP cells[89].

The lithium ion transference number (t_{Li^+}) was determined by performing chronoamperometric tests in addition to initial and steady-state EIS to determine the interfacial resistances Z_0 and Z_{ss}, respectively. Fig. 3-5a and 3-5b show the polarization curve obtained by chronoamperometric test for the ILE and GPE with the inset figure showing the Nyquist curves for symmetric Li/electrolyte/Li cells. Interfacial resistances (Z_0 and Z_{ss}) values were obtained by analyzing the real resistance of the semicircle of EIS Nyquist plots. After 4000 seconds, a steady-state current was achieved. The transference number, t_{Li^+}, was calculated using the equation described in chapter 2. Table 3-1 summarizes the initial and steady-state currents and resistances and t_{Li^+} of both GPE and ILE. The transference number of GPE is 0.41 while the ILE's is 0.3. The increase in transference number for the GPE is indicative of a chemical affinity between PIL and LiTFSI, suggesting an interaction with the $TFSI^-$ anion that in turn afforded high Li^+ mobility.

Table 3-1 Values of initial and steady state currents and interfacial resistances of Li/Li symmetrical cells and Li^+ transference numbers of GPE and ILE.

Sample	I_0/μA	I_{SS}/μA	Z_0/Ω	Z_{SS}/Ω	t_{Li^+}
GPE	26.5	16.2	232.2	259.6	0.41
ILE	7.5	4.7	992.6	995.2	0.30

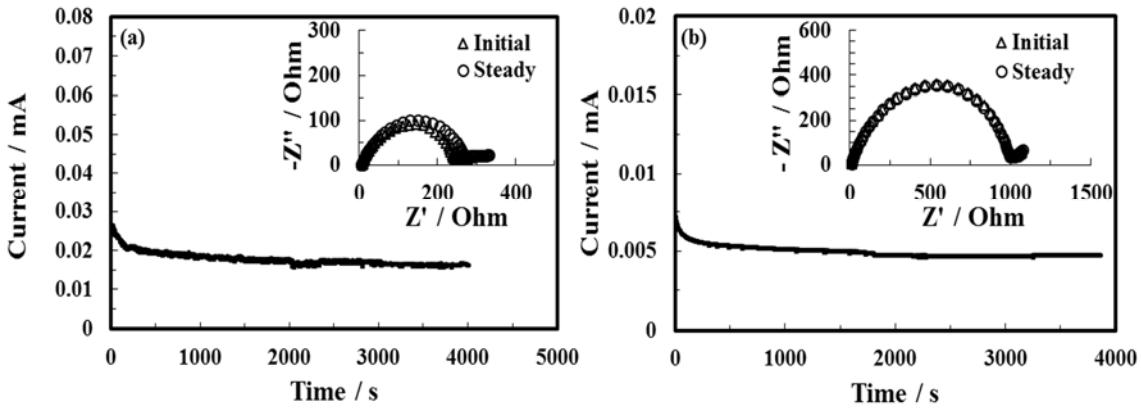

Figure 3-5 Chronoamperometry curves for a) GPE b) ILE. The insets show Nyquist plots before and after chronoamperometry.

The chemical compatibility of the GPE and ILE with the Li anode was tested by monitoring the interfacial resistances stability (Fig. 3-6). By assembling Li/GPE/Li and Li/ILE/Li symmetric cells, time-lapsed EIS tests were conducted on the cells kept under open-circuit conditions[97]. The interfacial resistances of both the GPE (Fig. 3-6a) and the ILE (Fig. 3-6b) increases with storage time due to the formation of a resistance layer on lithium metal. The resistance value for ILE increases from 328 $\Omega.cm^2$ (1 hr after preparation) to 1846 $\Omega.cm^2$ (after 10 days) while in the case of GPEs, the resistance increases from 158 $\Omega.cm^2$ (1 hr after preparation) to 613 $\Omega.cm^2$ (after 10 days). Although the resistance value for both the ILE and GPE increases with storage time, the growth rate is significantly lower for GPE compared to ILE. Fig. 3-6b also suggests higher resistance growth rate for ILE compared to GPE, indicating that the presence of PIL helps to reduce the growth of the resistive layer on lithium metal. This can be explained by the trapping of ions by the PIL matrix thus preventing liquid leakage and stabilizing the solid electrolyte interface (SEI) on lithium[112].

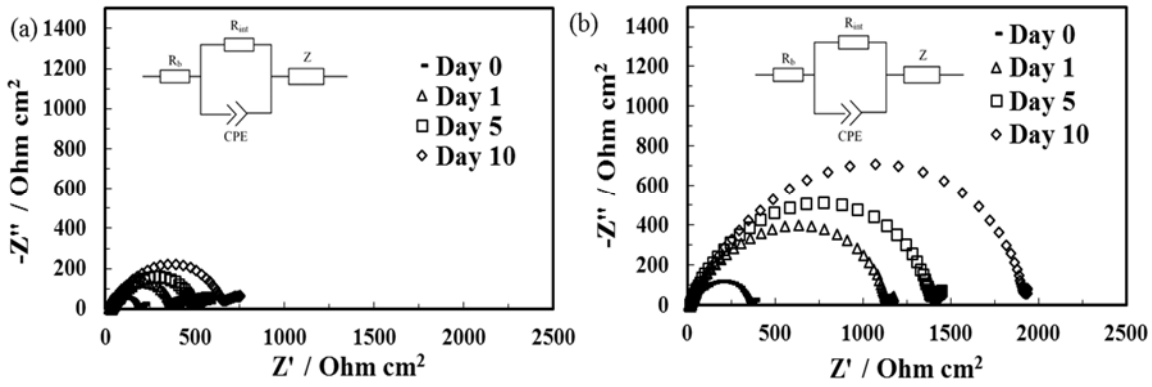

Figure 3-6 Nyquist plots after different storage time under open-circuit conditions for a) Li/GPE/Li and b) Li/ILE/Li symmetric cells at room temperature.

Galvanostatic cycling measurements were performed on Li/GPE/Li and Li/ILE/Li cells at a current density of 0.2 mA cm^{-2} in order to investigate the electrochemical compatibility of GPE and ILE against Li electrodes. Figure 3-7 shows the cycling profile for ILE (Fig. 3-7a) and GPE (Fig. 3-7b). The positive voltage value refers to Li stripping, and the negative value refers to Li plating[113]. From the figure, it is observed that the GPE cell had lower overpotentials compared to the ILE cell. The continuous voltage increase of ILE cells was indicative of growing non-uniform lithium depositions while the cell failure after 45 cycle was caused by an internal short circuit due to dendrite growth.

For the GPE however, a stable voltage profile is observed, indicating a uniform and stable lithium deposits and with no detectable failure in 100 cycles. This improvement can be attributed to the improved SEI forming properties of the GPE, afforded by the PIL as previously mentioned[114].

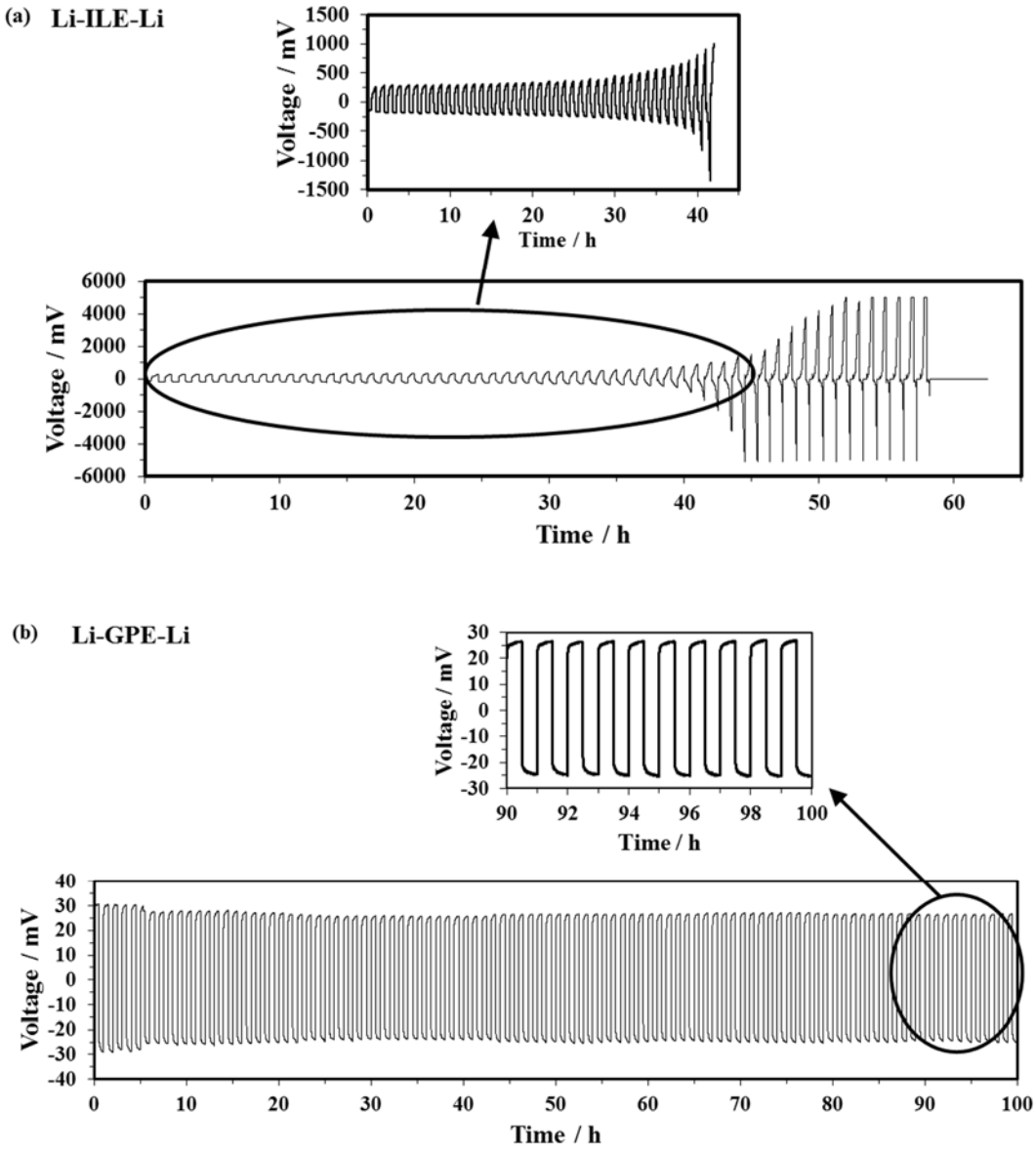

Figure 3-7 Galvanostatic cycling curves of (a) Li/ILE/Li and (b) Li/GPE/Li symmetrical cells at a current density of 0.2 mA.cm^{-2} at room temperature.

Cyclic charges-discharges at increasingly higher C-rates have been performed for 40 cycles at 22°C. The capacities of the charge and discharge cycles are shown in Fig. 3-8a and 3-8c for the GPE and ILE, respectively. The GPE demonstrated improved performance over their ILE counterparts at 22°C, with consistently higher discharge

capacities and improved capacity retention up to 5C rate. The GPE batteries discharge capacity at C/10 was 169.3 $mAh.g^{-1}$ which is 99.9% of the theoretical capacity of LFP (170 $mAh.g^{-1}$), indicating no ionic or interfacial limitations for the GPE at that rate. The ILE cells had a discharge capacity of 166.7 $mAh.g^{-1}$ (98.1%), slightly lower than the GPE cells. At higher rates the GPE cells had discharge capacities of 166.3 $mAh.g^{-1}$ (97.8%) versus 160.8 $mAh.g^{-1}$ (94.6%) for the ILE at C/5 and 153.8 $mAh.g^{-1}$ (90.5%) versus 126.1 $mAh.g^{-1}$ (74.2%) for the ILE at C/2. Similarly, higher discharge capacities for the GPE were observed at 1C and 2C rates, with 126.8 $mAh.g^{-1}$ (74.6%) versus 19.2 $mAh.g^{-1}$ (11.3%) for the ILE at 1C, then quickly dropping to 71.4 $mAh.g^{-1}$ (42.0%) versus 9.5 $mAh.g^{-1}$ (5.6%) for the ILE at 2C. At rates exceeding 2C, only the GPE cells remained functional with 36.7 $mAh.g^{-1}$ (22.0%) at 3C and 14.1 $mAh.g^{-1}$ (8.3%) at 5C. The capacity drop for both cells at C-rates exceeding 1C indicates limiting lithium ion diffusion within the electrolyte and the electrode/electrolyte interfaces previously observed elsewhere[115]. The improved performance of the GPE compared to the ILE counterparts was due to the electrochemical stability, interfacial stability, and increased transference number. The improved transference number can be credited for reducing the polarization and minimizing the effect of undesirable side reactions previously observed[116]. The same batteries that were cycled up to 5C rates were cycled for another set of 5 cycles at C/10 to confirm their stability, 98.4% capacity retention from the first discharge was obtained for GPEs versus 94.8% for the ILE. The coulombic efficiency was near 100% for all C-rates for GPE indicating excellent electrochemical stability of the GPE even at higher voltages and high compatibility with the electrodes and improved reversibility of lithium ion intercalation process[105]. These results suggest a method for enabling the utilization of the high

cathodic limit [EMIM][TFSI] in electrolytes in Li-ion batteries, previously deemed unsuitable for use with Li anode cells[46].

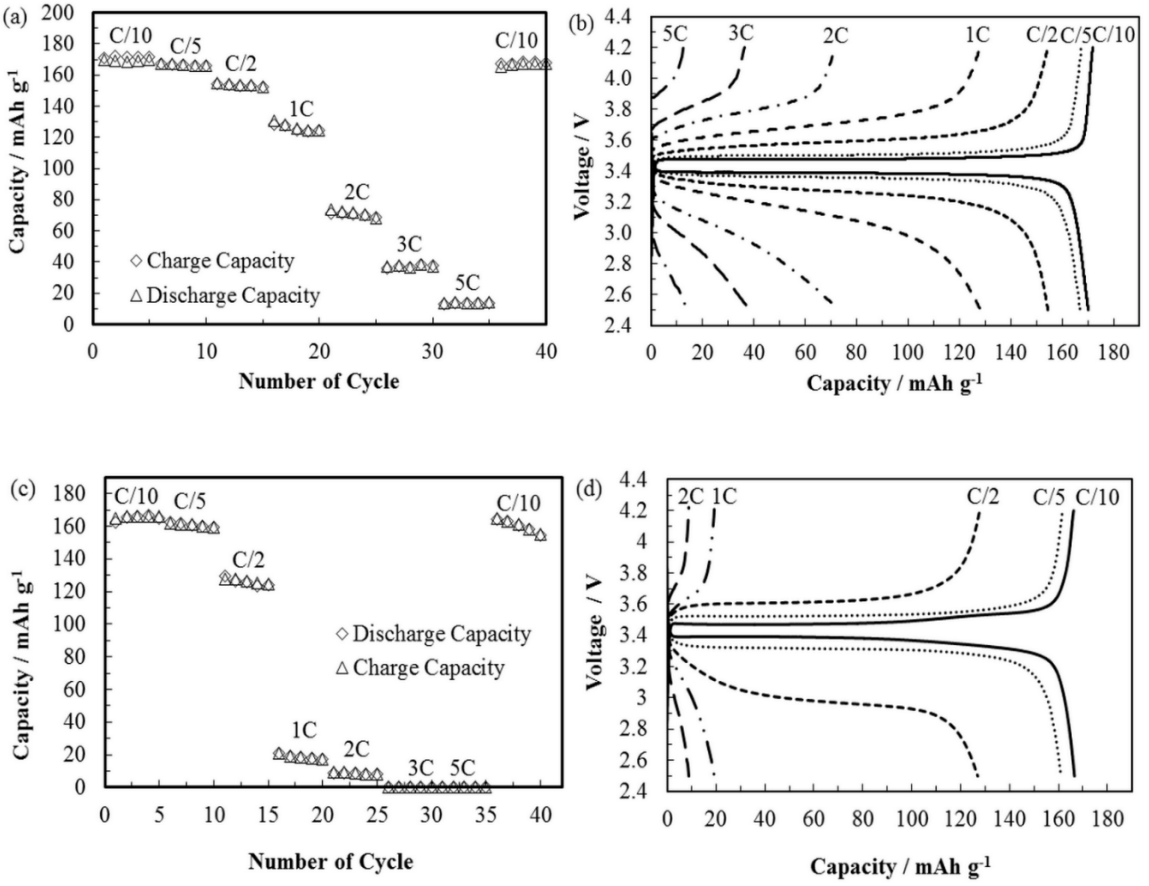

Figure 3-8 Cyclic charge-discharge plots (a) Rate performance (b) Voltage profiles of Li/$LiFePO_4$ cells using GPE as electrolyte. (c) Rate performance (d) Voltage profiles of Li/$LiFePO_4$ cells using ILE as electrolyte at varied rates of C/10 to 5C at 22°C. Capacities are reported per gram of $LiFePO_4$.

3.4 Conclusion

Free-standing GPEs based on a PIL and IL electrolyte have been developed with IL electrolyte content as high as 80 wt.%. These GPEs have been shown to have high ionic conductivities at 25ºC (3.35 $mS.cm^{-1}$), wide electrochemical window (5.0 V vs Li/Li^+), and improved transference number (0.41) compared to ILE (0.3). These GPEs have shown excellent discharge capacities at various rates, with impressive capacity retention

percentages in Li/$LiFePO_4$ cells. These GPE are expected to similarly perform with other Li-ion electrodes and under a wide range of conditions.

4 POLY (IONIC LIQUID) BASED GEL ELECTROLYTE FOR LI-S BATTERY APPLICATION

4.1 Background

Rechargeable LIBs with high safety and energy densities are in high demand for portable electronics and EVs[117–119]. Safety remains a major concern for LIBs because of the presence of flammable and volatile organic electrolytes[120]. The emergence of SPE improves the safety of LIBs due to the absence of flammable solvents. However, poor room temperature ionic conductivity limits its applications[121]. A solvent gelled with a polymer and lithium salt known as a GPE shows improved ionic conductivity while maintaining good mechanical stability[36,122]. On the other hand, the addition of highly flammable, volatile organic electrolytes as solvents to GPE, again promotes safety problems in LIBs[42]. RTIL as solvents in GPE have the edge over organic electrolytes due to their low volatility, low flammability, wide stability window, and high thermal stability[123].

To achieve higher energy densities, researchers are increasingly more focused on working beyond LIBs[124–127], as low theoretical capacities of the cathode materials limit the energy density to 300 $Wh \cdot kg^{-1}$. Li–S battery with a sulfur cathode and lithium anode has the theoretical capacity of ~1675 $Ah \cdot kg^{-1}$ and energy density of 2600 $Wh \cdot kg^{-1}$ which makes them some of the most promising candidates for high energy density batteries[128]. However, due to the highly insulating properties of sulfur, and the formation of intermediate sulfur products because of the dissolution of lithium polysulfides during the discharge process, it is difficult to achieve these high theoretical capacity and energy density[129]. A series of intermediate lithium polysulfides forms during the discharge

process of a Li-S cell with a general formula Li_2S_x ($2 \leq x \leq 8$) and at the end of discharge the final product is Li_2S. Initially, during discharge, elemental sulfur (S_8) dissolves in the electrolyte as solvated S_8 then is gradually reduced to intermediate lithium polysulfides. The formation of higher order (Li_2S_x, $4 \leq x \leq 8$) lithium polysulfides of longer chain lengths occurs, which are soluble in most solvents of electrolytes. After reduction, the chain length of the polysulfides shortens, and at the end of discharge, the final product is the lower order sulfides (Li_2S_2 and Li_2S) which are insoluble in the electrolyte. The formation of these insoluble sulfides yields a loss of active materials and results in a noticeable drop in discharge capacity in subsequent cycles[130].

A number of researches attempted to inhibit the polysulfides dissolution focusing on electrolyte modification. Previous studies reported that changing the solvents[131], salt[132], use of additives[133], and replacing with a solid-state electrolyte can prevent polysulfide shuttling. It has been reported that certain types of RTILs have the ability to suppress the lithium polysulfides formation during discharging[129]. Yuan *et al.*[134] reported on piperidinium-based IL with 1 M LiTFSI salt in Li-S battery and observed ~29% capacity drop over the first 10 cycles at 50 mA/g sulfur-acetylene black (1:3) cathode. Other studies have reported different cations that include imidazolium[135], pyrrolidinium[136], and ammonium[137], with anions such as $TFSI^-$, PF^-_6, BF^-_4, FSI^-, and others[138]. Park *et al*. reported that RTILs with $TFSI^-$ anions with various cations yields the least solubility of polysulfides due to its low donor number (DN). This low donor ability results in a weak Lewis basicity of the anion and suppresses polysulfides dissolution in the electrolyte. Wang *et al*.[139] reported on an imidazolium-based RTIL using mesoporous sulfur-carbon cathode. After 40 cycles, a rapid capacity drop of 61% was observed. The

same RTIL using a binder-free activated carbon cloth and sulfur cathode at C/17 showed approximately a 50% drop in capacity after 50 cycles [140]. These results suggest poor capacity retention in Li-S batteries using imidazolium-based RTIL.

Another attractive approach to suppress the loss of active sulfur material due to the dissolution of Li/S redox products in the electrolyte is by using GPEs. Ahn *et al.* reported on a GPE based on PVDF-co-HFP with tetra(ethylene glycol) dimethyl ether (TEGDME). Their batteries exhibited 68% capacity drop after 10 cycles at 0.14 $mA \cdot cm^{-2}$ using sulfur-carbon black cathode[141]. More recently, GPEs using polymers such as PEO[142], PMMA[143], PAN[144], and PVDF[145] have been investigated. In most studies, TEGDME and DOL/DME were used as solvents. However, only a handful of studies have been performed using RTILs as solvents for GPEs. Shin *et al.*[146] reported on the use of PEGDME-based GPE using pyrrolidinium-based RTIL in Li-S battery. A 55% capacity drop was observed after 5 cycles at 0.054 $mA \cdot cm^{-2}$. Rao *et al.*[144] reported a mixture of piperidinium ($PPR_{14}TFSI$) IL and PEGDME based gel electrolyte using electrospun PAN/PMMA membrane with 37% capacity drop after 50 cycles using carbon nanofiber-sulfur cathode. Jin *et al.* observed a 33% capacity drop after 20 cycles at a current density of 50 $mA.g^{-1}$ using GPE combined with pyrrolidinium IL and PVDF polymer[147]. PILs are the polymers of IL monomers which was reported by Ohno *et al.* for the first time[104] used as matrices for PE. Application of PILs in lithium batteries[36], indicates its high chemical affinity with ILs, low phase separation, good electrochemical and thermal properties[58]. Lithium-sulfur batteries using IL-PIL based GPE shows a massive 80% capacity drop at C/40 rate after just 30 cycles using carbon black-sulfur cathode at 55ºC [148].

In this work, we are reporting on the application of a free-standing GPE based on pyrrolidinium cation based PIL PDADMATFSI, lithium salt LiTFSI and imidazolium-based IL [EMIM][TFSI] in the lithium-sulfur battery using a sulfur-CNT composite cathode. Cyclic discharge/charge tests at various C-rates as well as cyclic stability up to 500 cycles at C/2-rate for GPE shows improved performances compared to ILE cell system. EIS studies at a various depth of discharge and during cycling show better interfacial contact properties for GPE and higher capacity than ILE.

4.2 Experimental Methods

For the preparation of GPE, first 1 M of LiTFSI salt was dissolved in [EMIM][TFSI] which yielded an ILE. The mixing ratio of ILE: PIL was optimized for performance and mechanical stability to be 60:40 by weight. Before mixing the ILE and PIL, PIL was dissolved in acetone. ILE was added to the PIL- acetone solution and was stirred for 2 h. The solution was then solvent cast in pre-cut 0.5" diameter and 150 μm deep cylindrical template. After air drying for 20 mins at room temperature, the films were heat treated at 90 ^{o}C under vacuum for 72 hours before recovery and storage in the glove box. The detailed procedure is described in chapter 2 and the schematic diagram of preparation are shown in figure 3-2. A transparent and free-standing GPE was obtained as shown in Fig. 4-1.

The sulfur-CNT composite was obtained by electrochemical reaction deposition method as demonstrated in previous work [149]. The detailed procedure of the composite cathode preparation is described in chapter 2 under cathode preparation section.

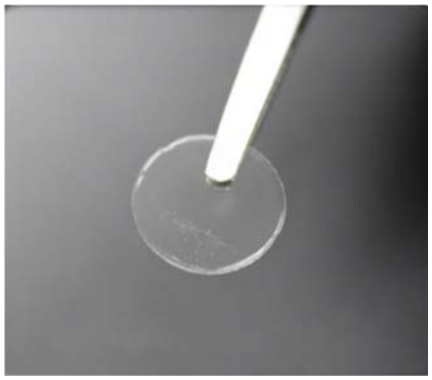

Figure 4-1 Photograph of a transparent and free-standing GPE (0.5” diameter).

The weight percentage of the sulfur in the cathode was determined by performing TGA using SDT Q600 from TA Instruments. The sample was heated from room temperature to 400ºC at a heating rate of 5ºC/min under a nitrogen atmosphere (flow rate. 50 mL/min). Characterization of the cathode material was performed by Raman spectroscopy using BaySpec’s Nomadic^{TM} with an excitation wavelength of 532 nm. To identify the crystallinity of the S-CNT composite, X-ray diffusion (XRD) patterns were recorded with Siemens 5000D diffractometer using Cu Kα radiation (λ = 1.5405Å). The surface morphology of the S-CNT composite and cycled cathode films were studied using a scanning electron microscope (JOEL SEM 6330F). TGA studies were also performed to determine the thermal decomposition temperature of the GPE using SDT Q600 from TA Instruments. The sample was heated from room temperature to 600ºC under a nitrogen atmosphere (flow rate. 50 mL·min^{-1}) with a scan rate of 10ºC min^{-1}.

LSV was performed to determine the ESW of the electrolyte. The CV experiments were performed, to illustrate the electrochemical properties of the GPE, for Li/GPE or ILE/S-CNT cell at the scan rate of 0.1 mV/sec from 1 to 3 V. For both the LSV and CV experiments, two electrode techniques were performed. The detailed procedure of the tests

was discussed in chapter 2. For LSV, stainless steel was used as working electrode and lithium as both reference and counter electrode. Potentiostatic EIS was performed between 100 kHz and 50 mHz with a perturbation voltage of 5 mV to study the electrochemical processes occurring in cells at different depths of discharge and during galvanostatic charge-discharge cycles. The experimental data were analyzed using circuit models derived by Gamry Echem Analyst software. All experiments were performed using a Gamry Reference 600 instrument.

Cells using lithium anodes, sulfur-CNT cathode, and GPE or ILE (soaked in separator) as an electrolyte was prepared. Rate capability of the cells using the GPE and ILE was evaluated by performing galvanostatic charge-discharge tests at variable rates at room temperature, and cyclic stability of the cells was performed up to 500 cycles at a rate of C/2.

4.3 Results and discussion

TGA curve of the GPE composed of 60:40 (ILE: PIL) by weight shows a thermal stability as high as 405ºC (Fig. 4-3a). This stability combined with the non-volatility suggest the ability of the GPE to protect the cell from thermal runaway in lithium batteries[150]. TGA curve for the sulfur-CNT cathode (Fig. 4-2a) shows the percentage of weight loss of the cathode material with the temperature increasing from 100 to 250ºC, indicates 42 wt. % sulfur content in the cathode. Fig. 4-2b shows the Raman spectra of the sulfur-CNT cathode where the peak at 1350 cm^{-1} representing the D band which is caused by defects and disorder structure in sp^2-hybridized carbon system and the peak at 1590 cm^{-1} is assigned to G band which arises from the stretching of the sp^2 C-C bonded carbon

atoms[151]. Two peaks at 805 cm^{-1} and 900 cm^{-1} are attributed to the binder, PVDF [152]. Meanwhile, the peak 500 cm^{-1} represents the peak for A_1 symmetry mode of S-S bond[151]. Fig. 4-2c shows XRD patterns of S-CNT composite cathode while the inset figure shows the standard Bragg positions of the orthorhombic S_8 with the space group Fddd (ICDD PDF database: entry no. 01-077-0145). The peak of CNT is observed at 26°[153], and the other peaks for sulfur indicate the composites crystalline nature and absence of any impurities in the sample. SEM image in Fig. 4-2d shows the morphology of the S-CNT composite where CNT is stacked with sulfur.

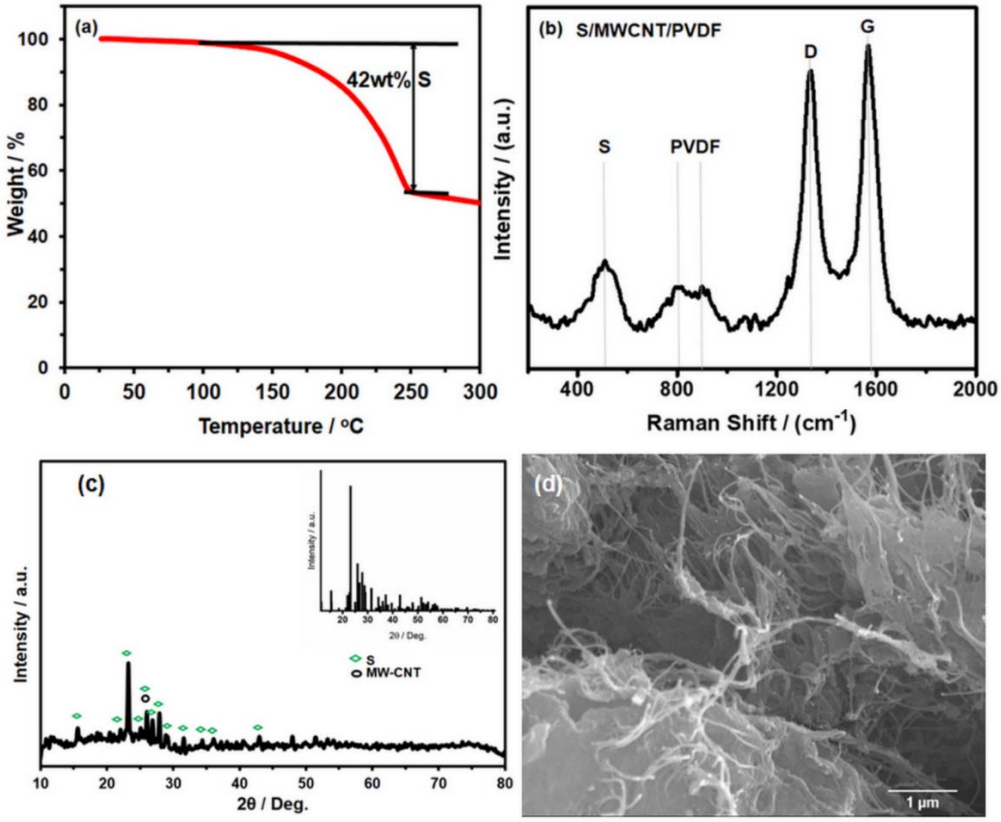

Figure 4-2 (a) Thermogravimetric analysis (TGA) of S-CNT composite from 22 to 300°C Scan Rate: 5°C·min^{-1} under nitrogen atmosphere (flow rate: 50 mL·min-1) (b) Raman spectrum of the PVDF/S-CNT-composite cathode (c) XRD patterns of S-CNT-composite (inset: Standard data for orthorhombic S, ICDD PDF database: entry number 01-077-0145) (d) SEM micrograph of S-CNT composite cathode.

LSV determines both the anodic and cathodic limits of the electrolyte to understand its compatibility with the electrode. Figure. 4-3b compares the LSV results of both the GPE and ILE systems and indicates the anodic limit of GPE and ILE as 5.1 V and 4.9 V vs. Li/Li^+, respectively. The cathodic limit is determined as -0.1 V and 1 V vs. Li/Li^+ for GPE and ILE respectively. The cathodic limit at 1 V for ILE is due to the decomposition of $EMIM^+$, rendering it incompatible with lithium anodes[46]. However, for GPE the cathodic limit of -0.1 V makes the GPE suitable for use with lithium anodes. In addition, the anodic limit for the GPE is also improved from 4.9 V for ILE to 5.1 V for GPE. This improvement is consistent with our previous results discussed in chapter 3[36]. The widening of the ESW from 3.9 V for ILE to 5.2 V for GPE is attributed to the PIL which can help passivate the reactive lithium in addition to contributing to the stabilization of the imidazolium ions[66,109].

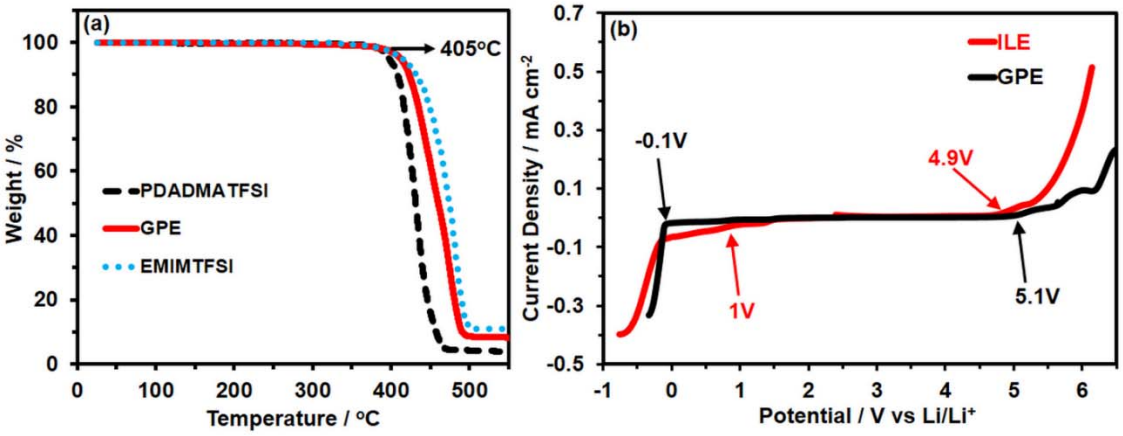

Figure 4-3 (a) Thermogravimetric analysis (TGA) of PDADMATFSI, EMIMTFSI and GPE from 22 to 600°C Scan Rate: 10°C·min^{-1} under nitrogen atmosphere (flow rate: 50 ml·min^{-1}) (b) Linear Sweep Voltammograms (LSV) of ILE and GPE at room temperature (22°C) against lithium. Scan rate: 1 mV·s^{-1}.

Figure 4-4 compares cyclic voltammetry of Li/GPE/S-CNT and Li/ILE/S-CNT for the 1st cycle. Fig. 4-5(a) and fig. 4-5(b) shows 1st, 2nd and 3rd cycle voltammograms for

GPE and ILE containing cells respectively, scanning from 1 to 3 V at a scan rate of 0.1 $mV \cdot s^{-1}$. Previous reports on Li-S[154] observed mostly two reduction peaks; however, in this work, two major reduction peaks at 2.17 V and 2 V were observed, with additional minor peaks around 2.09 V and 1.5 V for the first cycle of both GPE and ILE cells. In the 2^{nd} and consecutive cycles, the major reduction peaks remained, while the minor peaks are no longer apparent for GPE while for ILE a small peak at 1.5 V is still observed for the 2^{nd} and 3^{rd} cycle. The first reduction peak at 2.17 V indicates the transformation of elemental sulfur (S_8) to higher order soluble lithium polysulfides (Li_2S_n, $n \geq 4$)[128]. The second minor reduction peak at 2.09 V is the result of medium ordered polysulfides (S_4^{2-}) as evidenced by UV-vis, HPLC and ERS technique[155]. Similar types of peaks were also observed for solid electrolyte systems[156]. This second peak indicates a gradual decrease of the polysulfide chain lengths as reported elsewhere [157]. The reduction peak at 2 V indicates the formation of lower order polysulfides (Li_2S_2 and Li_2S) and as discussed by Barghamadi *et al*. [158], below 2 V the Li_2S_2 further reduces to Li_2S and the reduction peak at 1.5 V can be attributed to the formation of Li_2S due to the reduction of the polysulfide species [159]. The broad appearance of the reduction and oxidation peaks rather than the sharp appearance indicates slow reaction kinetics, commonly observed in IL electrolytes [139] and GPE systems [144][160]. Higher redox peak intensity for GPE compared to ILE also suggests better redox kinetic activity of the GPE system[161].

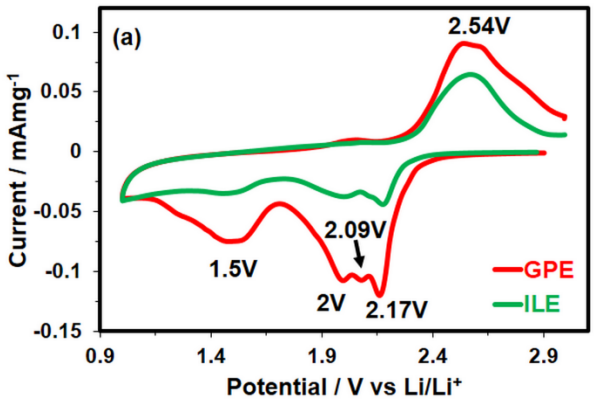

Figure 4-4 Cyclic Voltammograms (CV) of S-CNT/GPE (red) or ILE (green)/Li at the first cycle Scan Rate: 0.1 $mV \cdot s^{-1}$.

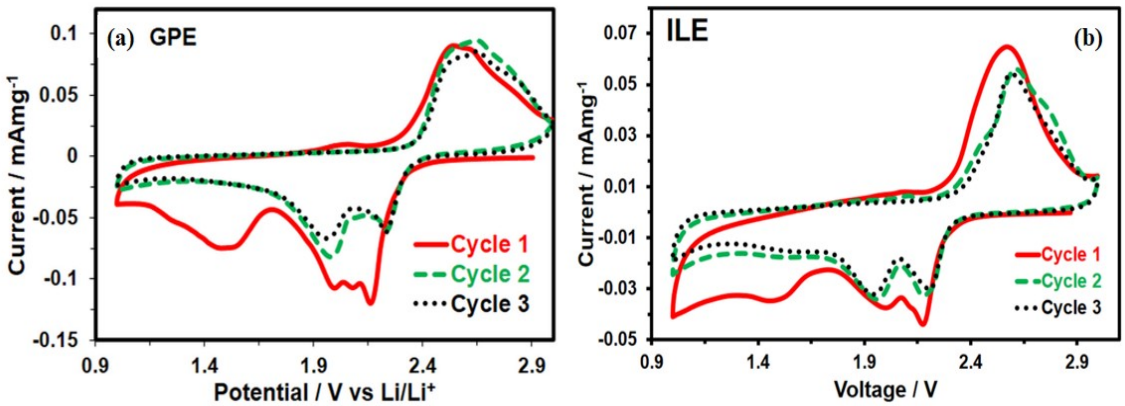

Figure 4-5 (a) S-CNT/GPE/Li (b) S-CNT/ILE/Li for the first 3 cycles. Voltage range: 1 to 3V vs Li/Li^+ at room temperature (22ºC).

Galvanostatic cyclic charge-discharges at various C-rates up to 1C were performed for 100 cycles at room temperature to investigate the rate capability of the cells. Fig. 4-6(a) shows the discharge capacity of both GPEs and ILE at C/10, C/5, C/2, 1C and again at C/10 for 20 cycles each. The initial capacity for GPE is 966 $mAh \cdot g^{-1}$ while for ILE the initial capacity is 768 $mAh \cdot g^{-1}$. A rapid capacity drop is observed for both systems, with a first cycle capacity drop of 20% and 31% for GPE and ILE, respectively. This drop has been previously observed in Li-S batteries using S-CNT cathode with TEGDME/DOL [153] and DOL/DME electrolytes [149]. Lower capacity drop for GPE indicates improved

reversibility and sulfur utilization than for ILE. A rapid capacity drop for ILE has been observed at C/2 and 1C rates compared to GPE. A capacity of 253 and 85 $mAh \cdot g^{-1}$ at the 50^{th} cycle are observed for GPE and ILE, respectively. Similarly, a capacity of 170 and 21 $mAh \cdot g^{-1}$ at the 70^{th} cycle are observed for GPE and ILE, respectively. This stark difference between the two batteries performances indicates better rate capability of GPE than ILE at higher C-rates. When the current was brought back to C/10 for the last 20 cycles, the discharge capacities recovered to 298 and 178 $mAh \cdot g^{-1}$ at the 90^{th} cycle for GPE and ILE, respectively. This difference indicates a larger permanent capacity loss in ILE than GPE cells.

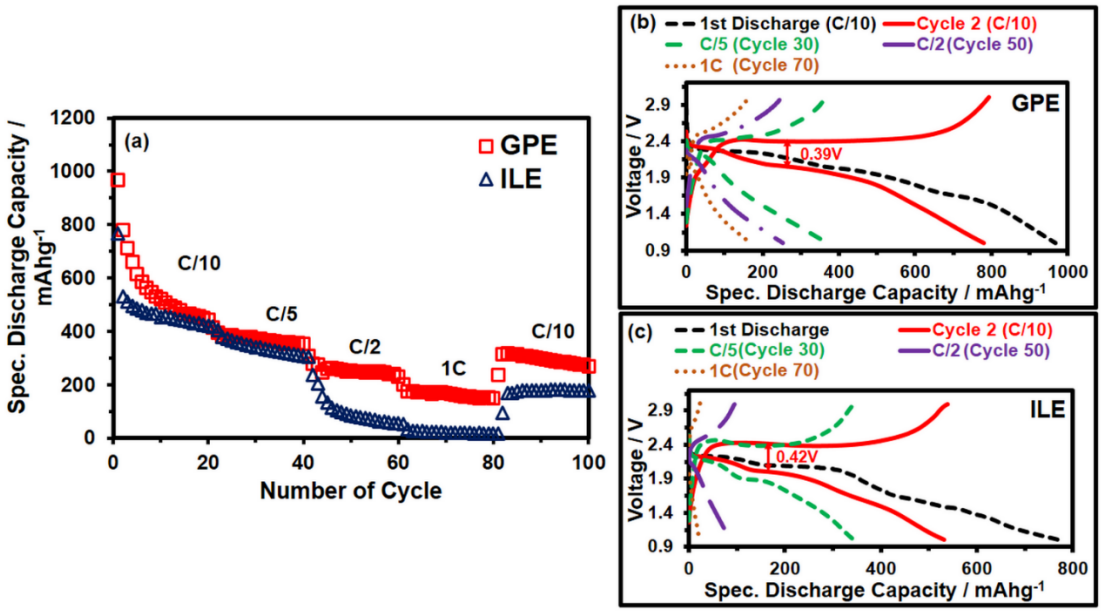

Figure 4-6 (a) Galvanostatic cyclic charge-discharge at various rates for GPE (red) and ILE (blue) based Li-S cells at room temperature (22°C) for 100 cycles. Corresponding charge-discharge voltage profiles for (b) GPE and (c) ILE at various C-rates.

Fig. 4-6 (b) and (c) show the voltage profiles at various C-rates for GPE and ILE cells, respectively. For the first discharge, three plateaus at 2.2 V, 2 V, and 1.5 V are

observed for both the GPE and ILE cells which are also evidenced in CV curves shown in fig. 4-4. The second cycle's discharge profile does not show the 1.5 V plateau for GPE while it remains for ILE, which can be indicative of the further formation of irreversible Li_2S on the electrodes for ILE[159]. Moreover, the charge-discharge overpotential for cycle 2 is 0.39 V and 0.42 V (using the second discharge plateau) for the GPE and ILE, respectively, which suggests less polarization for GPE than ILE due to the lower internal resistance of the electrode material [162].

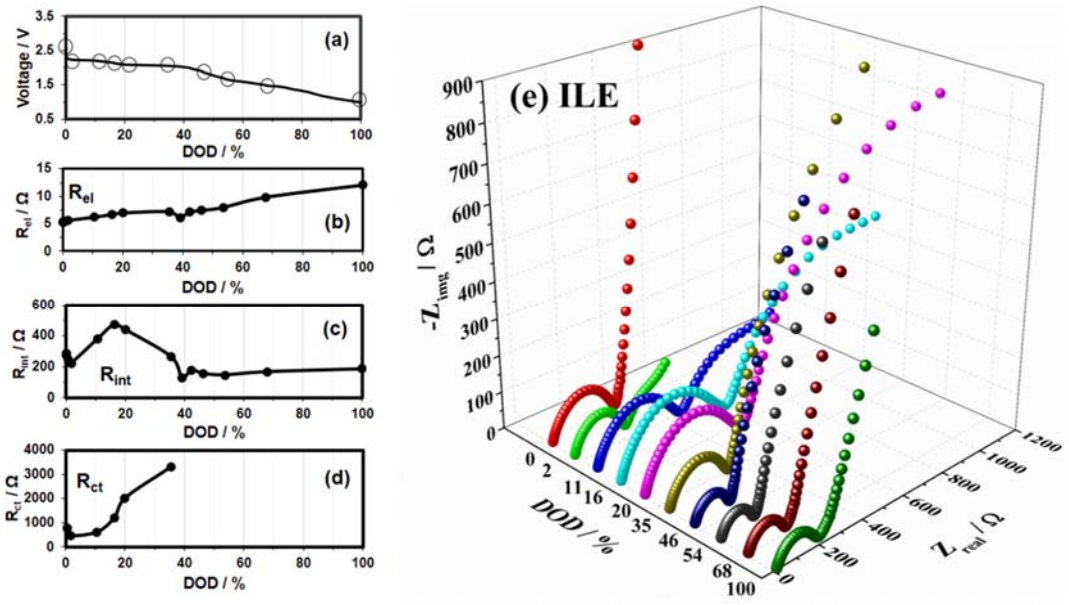

Figure 4-7 Discharge curve of S-CNT/ILE/Li cell at the first cycle at different DOD. Each circle on the curve represents Nyquist plots shown in (e). Change of resistance values with the function of %DOD where (b) electrolyte resistance, R_{el} (c) electrode/ILE interfacial resistance, R_{int} (d) charge transfer resistance, R_{ct} (e) Nyquist plots as a function of % of DOD for ILE. Frequency range: 100 kHz to 50 mHz.

To shed light on the reaction mechanism, EIS tests as a function of depth of discharge (DOD) were performed. Figs. 4-7 (a) and 4-8 (a) show the first discharge profile

of ILE and GPE cells respectively, and the circles indicate the depth of discharge (DOD) of our point of interest which are shown in Figs. 4-7 (e) and 4-8 (e) for both the systems.

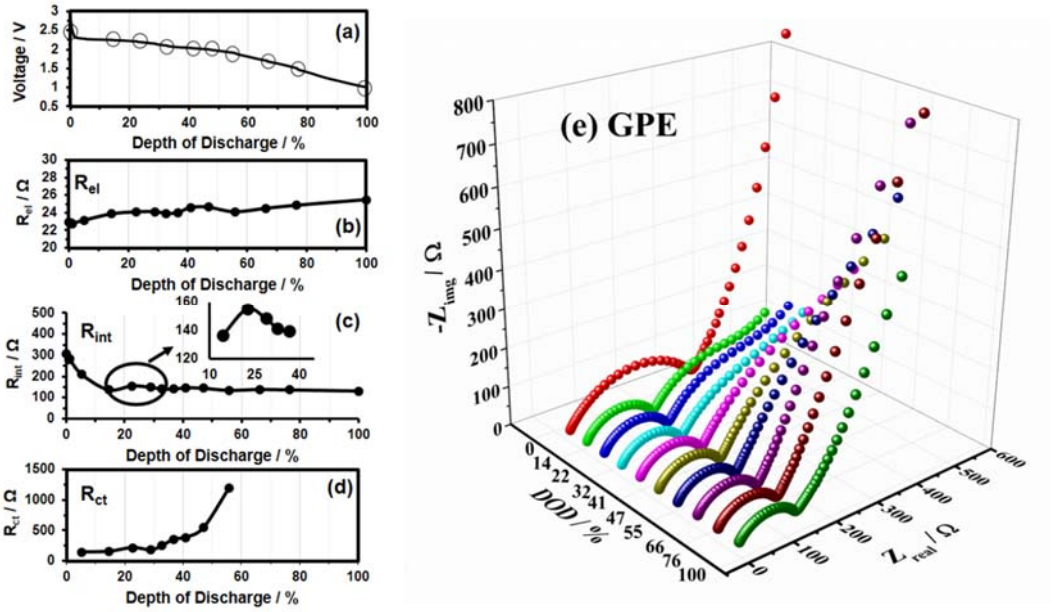

Figure 4-8 Discharge curve of S-CNT/GPE/Li cell at the first cycle at different DOD. Each circle on the curve represents Nyquist plots shown in (e). Change of resistance values with the function of %DOD where (b) electrolyte resistance, R_{el} (c) electrode/ILE interfacial resistance, R_{int} (d) charge transfer resistance, R_{ct} (e) Nyquist plots as a function of % of DOD for GPE. Frequency range : 100 kHz to 50 mHz.

For ILE, as shown in Fig. 4-7 (a) the first plateau at 2.2 V corresponds to the 10% DOD while for GPE (Fig. 4-8 (a)) it is 23% of DOD whereas, the second plateau at 2 V for ILE completes at 42% DOD comparing to GPE as 55% DOD. The third plateau at 1.5 V is at 68% for ILE and 76% for GPE. For the analysis of the plots, equivalent circuit models are suggested as shown in Fig. 4-9, indicated as model 1 and model 2. Model 1 is used for the fully charged and discharged state, while model 2 is used for the other DOD states. In both models, R_{el} represents the resistance of the electrolyte while semi-circle observed at high frequencies (HF) is described as R_{int}//CPE_{int}. R_{int} is the combined interfacial resistance of the interfaces between the electrolyte with the electrodes, and constant phase element

CPE_{int} is the distributed capacity of the surface layers of both the interfaces of the electrodes[163,164]. CPE is used instead of a capacitor because of the non-ideal behavior of the cathode due to surface inhomogeneity, roughness and the porous nature of the electrode[165,166].

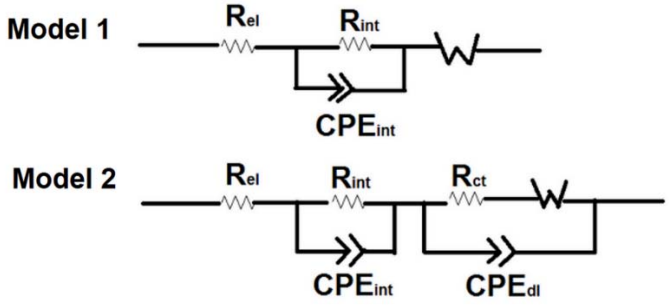

Figure 4-9 Equivalent circuit models to fit Nyquist plots. Model 1 for fully charged and discharged state. Model 2 for intermediate discharged state.

At the beginning of discharge, a semi-circle at medium frequencies (MF) shown in model 2 represented as $R_{ct}//CPE_{dl}$ where R_{ct} denotes the charge transfer resistance while CPE_{dl} is the double layer capacitance on the electrode surface. At lower frequencies (LF), a straight line is observed which is due to the blocking character of the cathodes known as the semi-infinite Warburg diffusion (W_0). In model 1, W_o is connected in series with $R_{int}//CPE_{int}$ while in model 2, W_o is connected in series with R_{ct} and parallel to CPE_{dl}. Fig. 4-7 (b) and 4-8 (b) shows the change of R_{el} values as a function of DOD. At the end of discharge, an increase in electrolyte resistance for both ILE and GPE is observed which may be the results of increased viscosity of the electrolyte due to changes in chemical composition during the discharge process[167]. Moreover, Fig. 4-7 & 4-8 (c) represents the resistance value of the semicircle at HF region. This resistance R_{int} is the combined interfacial resistance between the electrode/electrolyte interfaces as mentioned earlier. It is

seen that the resistance values drop at the initial part of the discharge process indicating improved interfacial contact between sulfur particles due to changes in composition and morphology of the cathode[167]. After the initial decrease, the resistance increased to its maximum in both the systems at the end of first voltage plateau (16% DOD for ILE and 22% for GPE) then it dropped and remains almost unchanged from the beginning part of the second plateau in both the systems. The increase of interfacial resistance can be the result of the formation of longer chain polysulfide films in the electrode pores, as a similar type of behavior was observed in TEGDME/DOL[54] and Sulfolane[58] based electrolyte. Moreover, we observed the increment of the resistance for ILE was much more significant than the GPE system. The maximum resistance at the end of first voltage plateau for GPE is 175.9 Ω while for ILE the value is 475 Ω. The lower interfacial resistance for GPE indicates an improved and more stable electrode and electrolyte contact[156,169].

The second semi-circle emerged at the MF region as shown in Fig. 4-7 (d) and 4-8 (d) is because of the charge transfer reaction on the sulfur electrodes. From the figures, we can see that in both the cases the resistance remain stable at the first and just before second voltage plateau region. At this region, electrochemical reduction of sulfur is more dominating as long chain soluble lithium polysulphides forms which make the resistance value low. However, at the beginning of the second plateau, an intense increase in the charge transfer resistance starts which is the cause of slower reduction reaction of sulfur, as less soluble Li_2S_2 and Li_2S forms[163,168]. Moreover, from the figure, it is also seen that the resistance increment for ILE is higher than the GPE cells. At the end of the second plateau for ILE, the R_{ct} value is 3316 Ω while for GPE the resistance is 1190 Ω which indicates better electrical conduction for charge transfer for GPE[170].

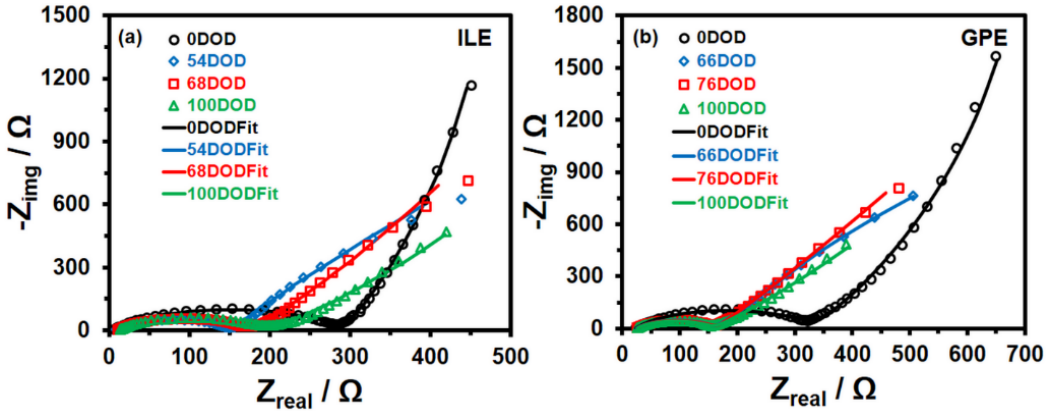

Figure 4-10 Nyquist plots at the initial and at the end of discharge with fitting using model 1 (a) ILE (b) GPE.

At the end of the second plateau, the semicircle at the MF got replaced by a straight line which is the Warburg diffusion results from the blocking character of the electrode. At this stage, poorly soluble and insulating short chain polysulfides continues to form and deposits on the electrode thus forms a blocking layer on the cathode[171]. From Fig. 4-10 (a) and (b) it is also seen that at 1.7 V (66% DOD for GPE and 54% DOD for ILE) and at 1.5 V (68% for ILE and 76% for GPE) the angle of the Warburg is 45° which indicates the flatness of the electrode surface. However, at 100% DOD, the angle of the Warburg reduced to 26° for ILE. This behavior can be described as the slow diffusion process due to the increase of Li_2S concentration on the cathode surfaces[172] for ILE while for GPE, a small decrease of the Warburg angle 45° at 100% DOD indicates less Li_2S formation and better reversibility.

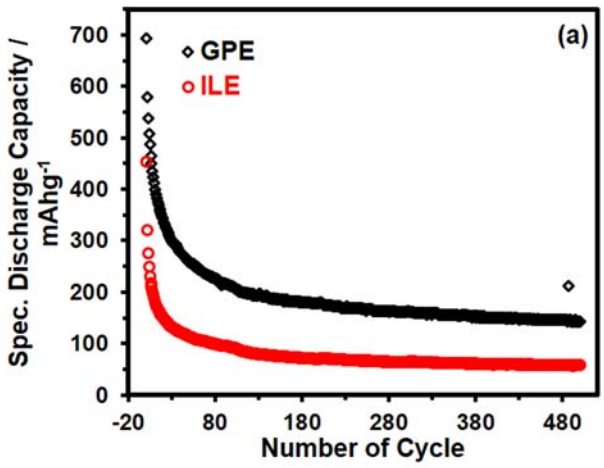

Figure 4-11 Cycling performance of GPE (black) and ILE (red) at C/2 rate for 500 cycles at room temperature (22ºC).

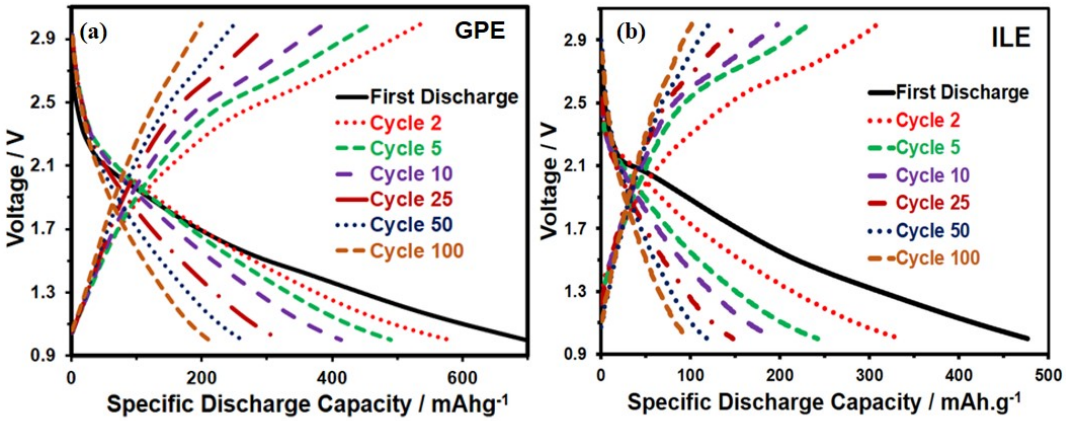

Figure 4-12 Charge-discharge voltage profile for (a) GPE and (b) ILE for the first 100 cycles at C/2.

Fig. 4-11 further compares the cyclic stability of GPE and ILE at C/2 rate for 500 cycles. It has been seen that the initial capacity for GPE is 693 $mAh \cdot g^{-1}$ which is higher than the ILE (453 $mAh \cdot g^{-1}$) system which indicates better electrochemical and interfacial stability of the GPE with electrodes than ILE. However, a rapid capacity drop is observed for both the cells with just 31% (211 $mAh \cdot g^{-1}$) capacity retention for GPE and only 21% (92 $mAh \cdot g^{-1}$) for ILE after 100 cycles comparing with the initial cycle. From 100 to 500

cycles the capacity drop is much lower than the first 100 cycles with 32% (142 $mAh \cdot g^{-1}$) for GPE and 38% (57 $mAhg^{-1}$) for ILE. Fig. 4-12 (a) and (b) shows the voltage profile for GPE and ILE system respectively for the first 100 cycles. From the figures, it can be seen that for the first discharge cycle the first reduction plateau is around 2.1 V while a second plateau is seen at around 1.6 V.

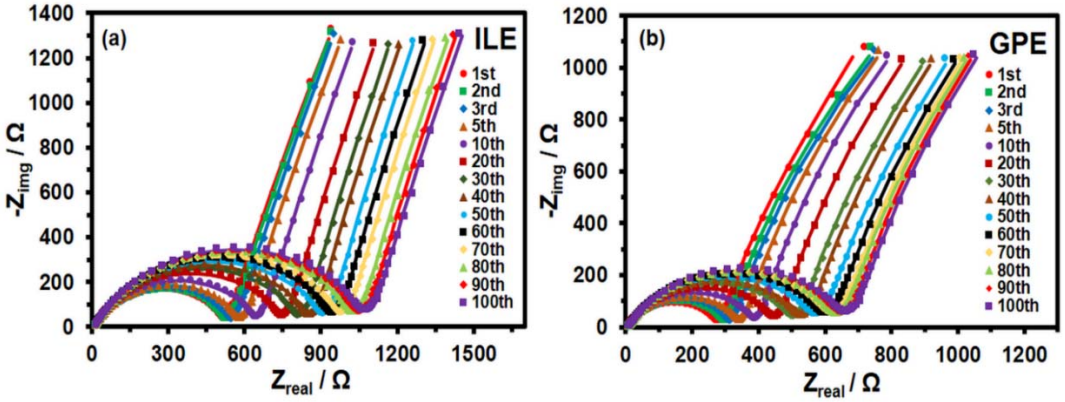

Figure 4-13 Nyquist plots with fitting at fully charged state for (a) ILE (b) GPE (Frequency range: 100 kHz to 50 mHz).

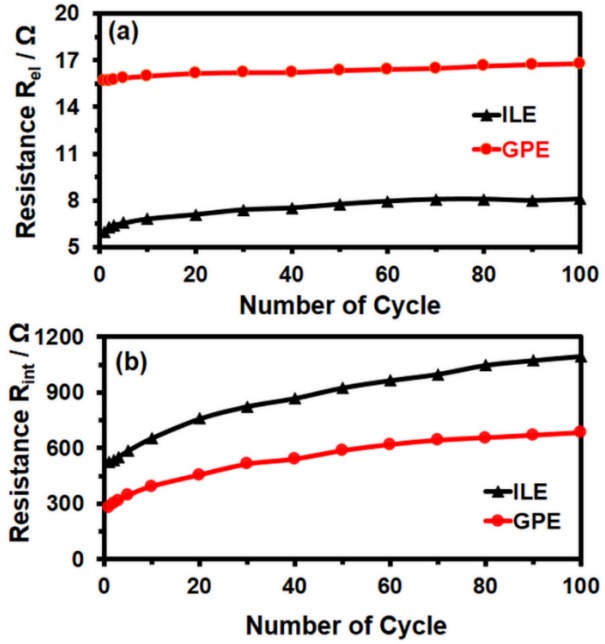

Figure 4-14 Plots of resistance values for ILE (black) and GPE (red) against cycle number (a) electrolyte resistance, R_{el} (b) electrode/electrolyte interfacial resistance, R_{int}.

To investigate the capacity fading of the cells, potentiostatic EIS was performed during the cycling of both the cells for the first 100 cycles at C/2 rate. Fig. 4-13 (a) and (b) shows the Nyquist plots at various cycles for ILE and GPE at fully charged state respectively. For both the cases, one semicircle is observed throughout the HF and MF region which represents the interfacial resistance between the electrolyte and electrodes. At the LF region, a large Warburg impedance represents the mass diffusion characteristics of the electrolyte/electrode interfaces[156,167]. To analyze the Nyquist plots, model 1 shown in Fig. 4-9 has been applied. In an earlier section it is evidenced that at the end of first discharge, the second semicircle at MF region which is due to charge transfer resistance got replaced by a Warburg diffusion line. It can be the cause of accumulation of insoluble Li_2S_2 and Li_2S on the cathode surface and thus blocks the pores of the cathode. Fig. 4-14 (a) and (b) shows the growth of the electrolyte resistance (R_{el}) and interfacial resistance (R_{int}) of the electrolyte/electrode interfaces respectively with the increasing number of cycles for both GPE and ILE. The resistance value for R_{el} is higher for GPE than ILE which is due to the higher thickness of the GPE (150 μm) comparing to ILE (25 μm). However, the electrolyte resistance almost remains same for GPE while for ILE 8% increase of resistance has been observed after the 5^{th} cycle and 25% increase after 100 cycles from the initial cycle suggesting less dissolution of lithium polysulfides[170]. Meanwhile, in Fig. 4-14 (b) the R_{int} resistance increases rapidly for the first 10 cycles then moderate increase up to 30 cycles. After that, a slow increase is observed from 30 cycles to 100 cycles for both GPE and ILE which indicates a connection between capacity fading and interfacial impedance growth. From Fig. 4-14 (b) it is also seen that the R_{int} value is higher for ILE than the value for GPE. For ILE the resistance after the first charge was 527

Ω and raised up to 654 Ω at the 10th cycle which is 127 Ω higher than the initial value. On the other hand, for GPE after the first charge, the resistance is 282 Ω while 392 Ω after the 10th cycle which is 110 Ω higher than the initial. Moreover, for ILE the resistance from cycle 70 to 100 increases from 998 Ω to 1095 Ω which is 10% increase while for GPE, it is from 641 to 682 Ω that is only 5% increase. The reasons behind the increase in interfacial resistance and capacity fading with cycling can be the cause of insoluble Li_2S_2 and Li_2S precipitation on cathode/electrolyte interfaces[162,167] and also on lithium anode/electrolyte interfaces[173]. Additionally, GPE has better interfacial compatibility with lithium anode than ILE as it can form stable solid electrolyte interphase (SEI) on lithium anode [36]. During the first discharge process, elemental sulfur reacts with lithium ions and forms lower order polysulfides as the end product of discharge as discussed earlier. However, during charging, not all the Li_2S_2/Li_2S can reoxidize to soluble polysulfides as they deposits on the cathode surface and results in a decrease of active material thus capacity fading occurs with cycling. Moreover, the formation of Li_2S results in volumetric expansion[128] which leads to cracks on the cathode surface exposing more sulfur to the electrolyte and generating more insulating Li_2S, as the cracks on the cathode using ILE is evidenced by SEM images obtained after 100 cycles of charge/discharge at C/2 rate (Fig. 4-15 a) This insulating product agglomerates and thickens on the electrode surface and impedes ion transport. Therefore, the interfacial resistance increases and causes a drop in the capacity of subsequent cycles[162,167,174–176]. An improvement using cells with GPE indicates a stable passivation layer formation on the surface of the electrode (Fig. 4-15 (b) which suppresses the cracking and instability of the cathode by impeding volumetric expansion of sulfur thus resulting in less capacity fading.

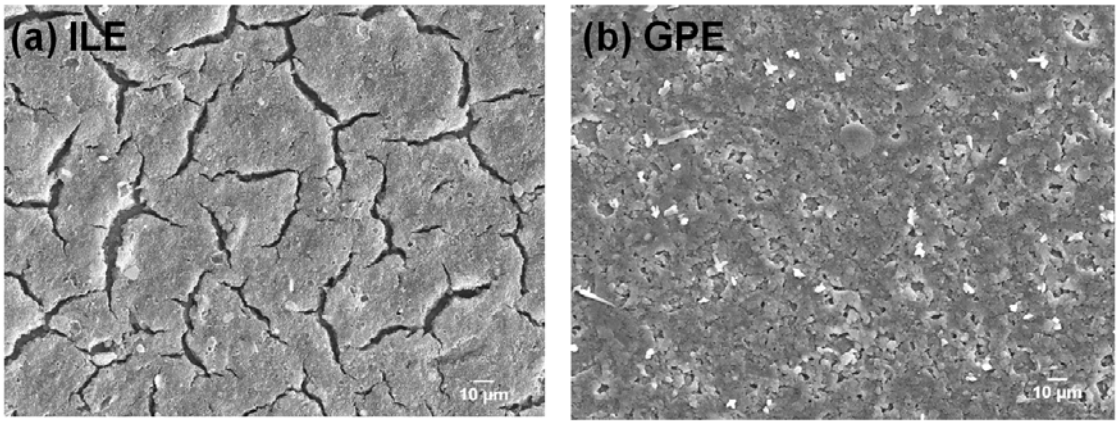

Figure 4-15 SEM micrographs to understand the morphology of the cathode surface of (a) ILE and (b) GPE after 100 cycles at C/2 rate.

4.4 Conclusions

A polymeric ionic liquid-based GPE in Li-S batteries using S-CNT cathode is presented. The GPE shows high thermal stability (405^{o}C) and wider stability window (5.2 V vs. Li/Li^{+}). An EIS study as a function of the state of discharge revealed that the interfacial resistance is the critical step at the first voltage plateau, while charge transfer resistance is dominant at the second voltage plateau. After discharge, a Warburg diffusion indicates an accumulation of insoluble Li_2S_2/Li_2S on the cathode surface which results in blockage of the pores of the cathode. GPE shows better rate capability compared to ILE at higher C-rates and performs better cyclic stability at C/2 rate for 500 cycles. Continuous growth of interfacial resistance at the electrode/electrolyte interfaces caused by the continuous deposition of Li_2S_2/Li_2S on the electrodes causes capacity fading due to loss of active sulfur material during cycling. However, better interfacial properties of GPE lowers the continuous deposition of Li_2S_2/Li_2S and shows higher discharge capacity.

5 POLY (IONIC LIQUID) BASED COMPOSITE GEL ELECTROLYTE FOR LITHIUM BATTERY APPLICATION

5.1 Background

Rechargeable lithium-ion batteries (LIBs) have been studied widely for the past decades due to its high demand for modern technological devices, to power consumer electronics, stationary energy grids and electric vehicles[88,177,178]. The major advantages of using LIBs is its high energy-to-weight ratio (180 Wh/kg), power-to-weight ratios (1500 W/kg) and low self-discharge rate[179,180]. However, safety remains one of the major concerns for LIBs due to its wide use of liquid organic electrolyte which has poor chemical stability, is highly flammable and has leakage concern[181,182]. A number of research has been going on to replace the electrolyte with a non-flammable, both chemically and thermally stable electrolyte. Polymer electrolyte (PE) as electrolyte shows a safer route to LIB technology as there is no issue of leakage, flammability, chemical instability problems as associated with liquid electrolyte[183,184]. PEs for LIBs are mainly consisted of a polymer dissolved in a high concentration of lithium salts. Although PEs have advantages over liquid electrolytes, poor room temperature ionic conductivity (~10^{-8} – 10^{-5} $S.cm^{-1}$) due to ion diffusion restrictions causing a major problem for them to be applied in LIBs[88]. To overcome the issue, RTIL have emerged as a solvent for electrolyte which is nonflammable and shows excellent chemical and thermal stabilities as well as good ionic conductivity at room temperature[36,185]. PE gelled with a solvent is known as GPE. Watanabe and Noda *et al.* for the first time reported RTIL based GPE using vinyl monomers as polymer with imidazolium and pyridinium based IL[63]. Since then, numerous researches have been reported using IL as a solvent for GPE and polymers based

on PEO[186], PAN/PMMA[187], PVDF-HFP[188], PVA[189] for the use in LIB application. Another approach of making GPE is the application of polymeric ionic liquid (PIL) which is the polymers of IL monomers used as polymer matrices for GPE. Major advantages of using PILs are their excellent chemical affinity with IL which results in improved compatibility, minimal phase separation, and leakage. PILs also possess better electrochemical stability and room temperature ionic conductivity resulting in high cyclic stability when used as polymer matrices for GPE in energy storage devices[36,107]. Since the introduction of the concept of PIL by Ohno *et al*.[104], a number of researches have been reported using PIL as polymer matrices for electrolyte in energy storage devices[190]. Appetecchi *et al.* reported pyrrolidinium cationic-based GPE using PDADMATFSI PIL with $PYR_{14}TFSI$ IL with a reported capacity of 140 $mAh.g^{-1}$ at 40ºC for 70 cycles at C/10 rate[105]. In our earlier study, we investigated the PDADMATFSI PIL combined with imidazolium-based IL using Li/LFP cell and reported 166 $mAh.g^{-1}$ discharge capacity after 40 cycles at C/10 rate at room temperature[36]. Li *et al.* investigated GPE using guanidinium-based PILs and IL in LIBs with a reporting discharge capacities of 140 $mAh.g^{-1}$ at C/10 rate after 100 cycles at 80ºC[191]. Kun *et al.* reported imidazolium-based PIL using Li/LFP cells with a discharge capacity of 157.5 $mAh.g^{-1}$ after 80 cycles at C/10 rate at 60ºC[192].

However, the ionic conductivity problem remains if the content of RTIL is lower in GPE while the mechanical strength and dimensional stability is another issue if the RTIL content is higher than the polymer[70]. From the past few decades, it is well established that addition of ceramic filler materials (e.g., SiO_2, Al_2O_3, TiO_2, ZrO_2, etc.) at a certain percentage to GPE not only help the mechanical and dimensional stability but also

improves ionic conductivity and lithium ion transport through the electrolyte[193]. GPEs containing fillers has been named as composite gel polymer electrolyte (cGPE) later on. Scrosati *et al.* for the first time incorporated 10 wt.% Al_2O_3 and TiO_2 separately in PEO-LiX electrolyte and reported improved in low-temperature ionic conductivity[193]. Wei *et al.* observed 127.9 $mAh.g^{-1}$ discharge capacity at the first discharge capacity at C/2 rate using nano-TiO_2 filler in piperidinium IL and PVDF-HFP matrix[194]. Diego *et al.* added 5 wt% fumed SiO_2 in GPE containing pyrrolidinium IL/LiTFSI and PEO and reported 155 $mAh.g^{-1}$ at C/10 rate after 20 cycles at 90ºC[195]. Kimura *et al.* observed improved in ionic conductivity and mechanical properties by adding 5 wt% silica fiber in IL-based cGPE where polyethylene carbonate (PEC) acted as a polymer matrices[73]. There are only a few works that have been done adding ceramic filler materials in PIL based ionic liquid containing GPE. Shun *et al.* added 8 wt% mesoporous silica nanoplates in PIL based GPE and reported an initial discharge capacity of 117 $mAh{\cdot}g^{-1}$ (C/10 rate) at 40ºC[196].

ESD is a thin film deposition technique where a liquid precursor solution is atomized into an aerosol spray by the application of a high electric field between the feeding source and a preheated substrate[75]. After reaching the substrate, the solvent of the solution evaporates, and a solid or porous film can be obtained. By varying the flow rate, the distance between the source and the substrate, dc potential, substrate temperature and the composition of the solution one can control the morphology and thickness of the deposited film[76]. This technique operates without vacuum which makes the method less costly compared to other thin film deposition techniques such as. Chemical vapor deposition (CVD), electrophoretic deposition (EPD) and layer-by-layer (LBL) deposition technique[77]. Electrodes prepared with this technique does not need any polymeric

binders thus lowers resistance and dead weight to the electrode[78]. Porous, high surface area and homogenous film forming ability make ESD technique suitable for the application as electrodes in energy storage devices. A number of researches have been reported using the ESD technique in LIBs and super-capacitors[197,198]. A detailed description and a schematic illustration of the ESD technique are shown in figure 2-1.

In this present work, we are reporting the influence of incorporation of the various content of glass micro-fillers in GPE composed of pyrrolidinium-based PIL PDADMATFSI and LiTFSI salt gelled by imidazolium-based IL EMIMTFSI solvent and a binder-free LFP/C cathode deposited by ESD technique. Galvanostatic charge/discharge tests along with various electrochemical characterization have been used to evaluate the performances of composite gel polymer electrolyte (cGPE).

5.2 Experimental Methods

EMIMTFSI solvent and PDADMATFSI PIL were prepared following the procedures detailed in our previous work[36]. The chemical structure of the chemicals are depicted in figure 3-1, and the detailed procedure are described in chapter 2. For the preparation of GPE, 1M LiTFSI salt was first dissolved in EMIMTFSI then the solution and PIL (60:40 by weight) were dissolved in acetone. While for cGPE, the glass micro-filler was shredded into pieces and fragmented using probe sonication for 3 hours in acetone. The fragmented micro-fillers were dried in air at room temperature to let the acetone evaporate and then finally at 300°C under vacuum for 48 hours. For the preparation of cGPE, various ratios of glass micro-fillers (0.5%, 1%, 2%, 3% and 5% by weight) were separately added in the PIL/acetone solution then IL with 1M salt solution was added in

the solution. Finally, the mixed solution was magnetically stirred for 24 hrs. The dispersed solution was drop cast in 0.5" circular PDMS template layered on a glass slide. A syringe pump was used to cast the solution to distribute the micro fillers uniformly in each sample. The cast samples were then air dried for 20 minutes to let the acetone evaporate then finally dried at 90ºC under vacuum for 72 hrs and stored in the argon filled glovebox until further used. Later on, cGPEs with 1 wt% micro-filler is named as cGPE-1 while cGPEs with 0.5, 2, 3, and 5 wt% micro-fillers are mentioned as cGPE-0.5, cGPE-2, cGPE-3, and cGPE-5 respectively. A schematic figure of the GPE and cGPE preparation process along with the photographs of GPE and cGPE-1wt% are shown in Fig. 3-2 and Fig. 5-1 respectively.

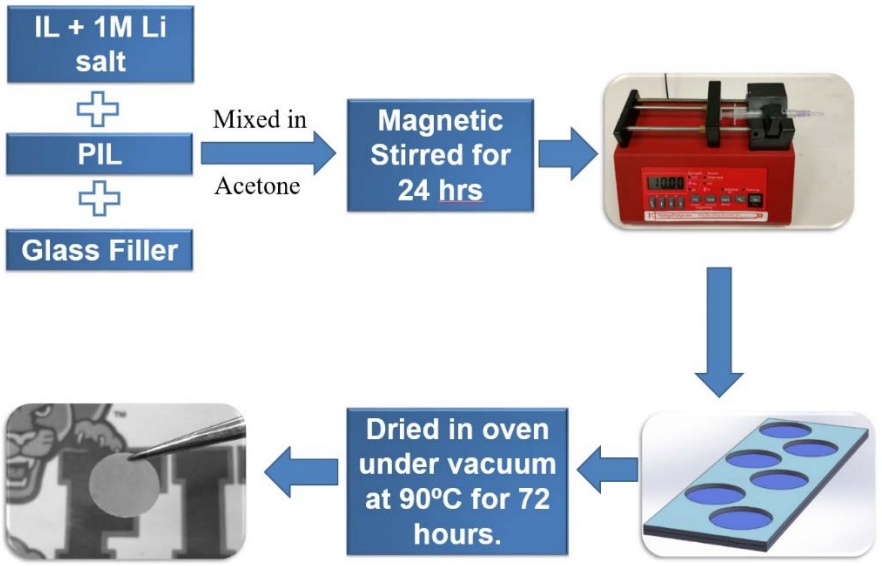

Figure 5-1 Step-by-step procedure of the preparation of cGPE.

A binder-free cathode was prepared by applying ESD technique. At first 90wt% carbon pre-coated LFP and 10wt.% super P carbon black was dissolved in 1,2-propanediol in the ratio of 2.4mg.mL^{-1} under stirring for 30 minutes. The solution was then fed on a heated substrate through a syringe pump under the application of a high DC voltage. A

schematic experimental setup of the ESD technique has been shown in Fig. 2-1. The feeding rate of the solution to the substrate was 0.5 $mL.hr^{-1}$, and the applied DC voltage between the needle tip and the preheated substrate was 8 kV. The distance between the needle tip and stainless steel substrate was 4 cm, and the temperature of the substrate was 180ºC. The typical loading of the active material LFP was 0.7 ± 0.05 $mg.cm^{-2}$.

TGA was performed to identify the decomposition temperature of the GPE and cGPE (1%, 3% and 5%) using SDT Q600 from TA instrument. The samples were heated from room temperature to 600ºC under a nitrogen atmosphere with a flow rate of 50 $mL.min^{-1}$ (Scan rate: 10 $^{o}C\ min^{-1}$).

ESW were determined for both the GPE and cGPE systems by performing LSV at a scan rate of 1 $mV.sec^{-1}$. The CV tests were performed for GPE and cGPE-1 at the scan rate of 0.1 $mV.sec^{-1}$ from 2.5 – 4.2 V for the first 3 cycles to illustrate the electrochemical properties. Two electrode techniques were used for both the LSV and CV experiments. For LSV, stainless steel was used as working electrode and lithium metal as both counter and reference electrode while for CV experiment Li/GPE or cGPE/$LiFePO_4$ cell system was used. The ionic conductivity (σ) of the samples were determined by using equation 11 as described in chapter 2. Lithium transference number (t_{Li^+}) were evaluated by following the method and equation suggested by Bruce *et al.* [87]. The detailed technique of the electrochemical technique is described in chapter 2. Chronoamperometry tests were performed at 10 mV dc polarization to determine the initial and steady-state currents as well as the impedances before and after polarization by performing EIS of Li/GPE or cGPE/Li symmetric cells. Potentiostatic EIS were performed between 100 kHz to 50 mHz

with a perturbation voltage of 5 mV to investigate the electrochemical processes occurring during the galvanostatic cyclic discharge-charge cycles. All the electrochemical experiments were performed using Gamry Reference 600 instrument. Raman spectroscopy was performed on various electrolyte systems using IL, GPE, and cGPE-1 using Bayspec's Nomadic Raman spectrometer using a wavelength of 532 nm.

5.3 Results and Discussion

TGA curve in Fig. 5-2 shows the high thermal stability up to 400ºC of the GPE and cGPE-1%. The PIL starts to decompose at 390ºC while the IL starts to decompose at 405ºC. Fig. 5-3 compares the ESW of the GPE and cGPE-1/3/5 by performing LSV experiments. From the figure it can be concluded that the addition of glass micro-fillers in GPE does not contribute any significant changes in ESW as for all the cases, the cathodic limit is 5.1 V, and the anodic limit is -0.1 V (ESW: 5.2 V vs. Li/Li^+). The smoothness of both the anodic and cathodic curve indicates the absence of impurities in the electrolyte. The high anodic and cathodic (less than 0 V) limit for the GPE and cGPEs makes them suitable for high voltage cathode materials and lithium metal respectively[36,89]. Fig. 5-4 shows the CV curves of GPE and cGPE-1 where a slightly higher redox peak value for cGPE-1 than GPE indicates a better redox kinetic activity of the former system. The Li/cGPE-1/LFP cell also shows smaller potential separation between the oxidation and reduction peaks than the Li/GPE/LFP cell which is considered as better reversibility for cGPE-1 than the latter one[161].

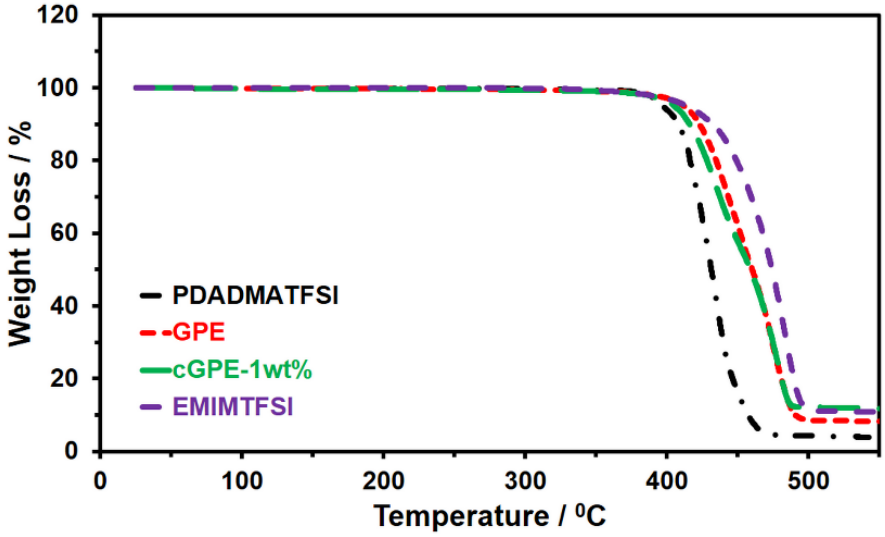

Figure 5-2 Thermogravimetric analysis (TGA) analysis of PIL, IL, GPE, and cGPE-1 from 22 to 600°C under nitrogen atmosphere (flow rate: 50 mL min^{-1}). Scan rate: 10°C min^{-1}.

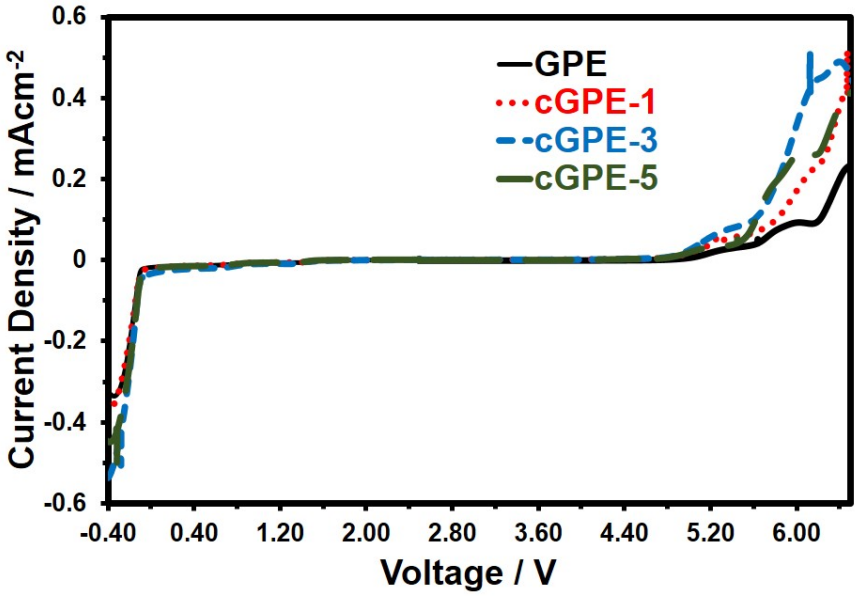

Figure 5-3 Linear sweep voltammograms of GPE, cGPE-1, 3, and 5 at room temperature with stainless steel as working electrode and lithium as both reference and counter electrode. Scan rate: 1 mV s^{-1}.

Fig. 5-5 (a) and (b) shows the change in ionic conductivity (σ) and lithium transference number (t_{Li^+}) of the GPE at different percentages of filler contents at room temperature respectively. From the figures, it can be seen that cGPE-1 shows the highest ionic conductivity and transference number compared to GPE and other cGPEs. Upon

addition of 1wt% micro-filler improves the ionic conductivity of 33.33% and transference number of 10.77% than GPEs at room temperature. However, further addition of micro-fillers to the GPE decreased both the conductivity and transference number of the cGPE-3 and cGPE-5. The increase at 1wt% can be ascribed as an improved interaction between the adsorbed $TFSI^-$ anions and the Lewis acid group of the micro-fillers surface, forming ion-ceramic complexes thus increases ion pair dissociation[69,199]. The increase in ion dissociation helps Li-ions to transfer more freely through the percolating pathways of complex ion-micro fillers. However, the decrease in conductivity and transference number in cGPEs consisting more than 1wt% micro-filler is caused by the agglomeration of particles, hence decreases the surface area of particles to interact. The agglomeration causes less salt dissociation and thus reduced or blocks Li-ion movement through the electrolyte[122,176,200].

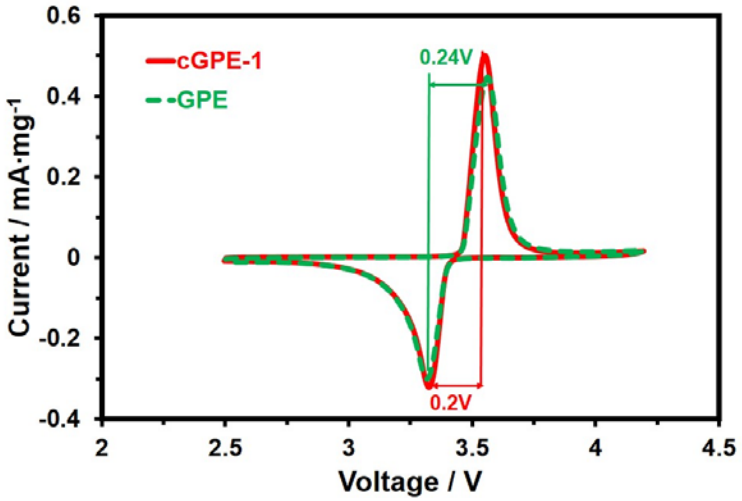

Figure 5- 4 Cyclic Voltammograms (CV) of LFP/GPE (green) or cGPE-1 (red)/Li at the first cycle. Voltage range: 2.5 to 4.2 V vs Li/Li+ at room temperature (22°C). Scan Rate: 0.1 $mV \cdot s^{-1}$.

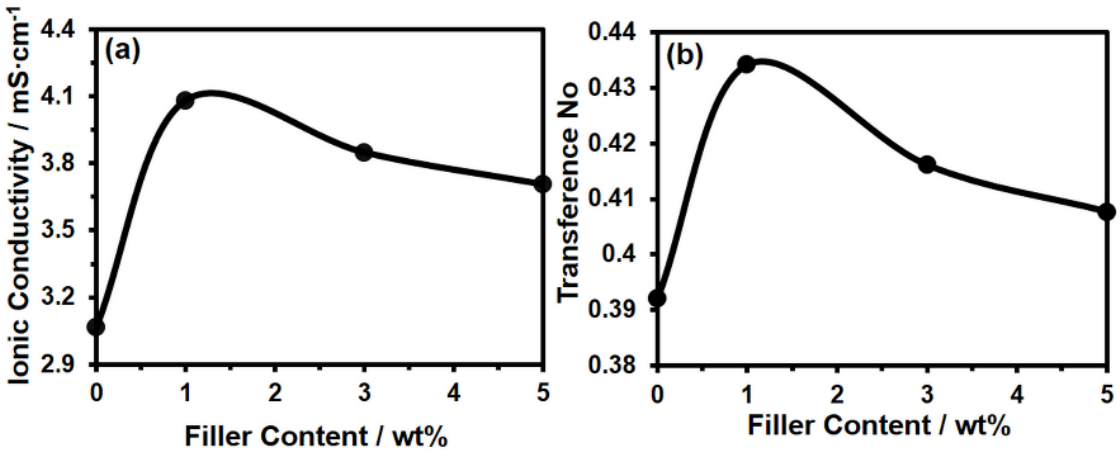

Figure 5-5 Change in (a) Ionic Conductivity (b) Transference number of GPEs and cGPEs with various contents of glass fillers.

To further understand the interaction of micro-fillers with ionic liquid-lithium salt (ILE), and PIL, Raman spectroscopy was performed at room temperature. Figure 5-6 (a – c) shows the deconvoluted Raman spectra in the frequency range of 725-765 cm^{-1} to probe the conformational changes and Li^+ coordination with the $TFSI^-$ anion[201,202] in the electrolyte. Fig 5-6 (a) and (b) shows the spectra for ILE and GPE respectively while Fig. 5-6 (d) depicts the spectra where 1 wt% micro-fillers added to the GPE (cGPE-1). The spectra are fit using the Voigt profile (Gaussian: Lorentzian = 1:1). From the figures, it is seen that the small shoulder at 735 cm^{-1} and the peak at ~741 cm^{-1} are the conformers of the free $TFSI^-$ anion C_1(cisoid) and C_2(transoid) respectively. The peaks ranging from 735 – 742 cm^{-1} correspond to the unbounded free $TFSI^-$, also known as solvent-separated ion pairs (SSIPs)[203,204]. The third Raman peak at 749 cm^{-1} corresponds to the bounded $TFSI^-$ which is the contact ion pairs (CIPs) and ion aggregates (AGGs) between the Li^+ and $TFSI^-$[205].

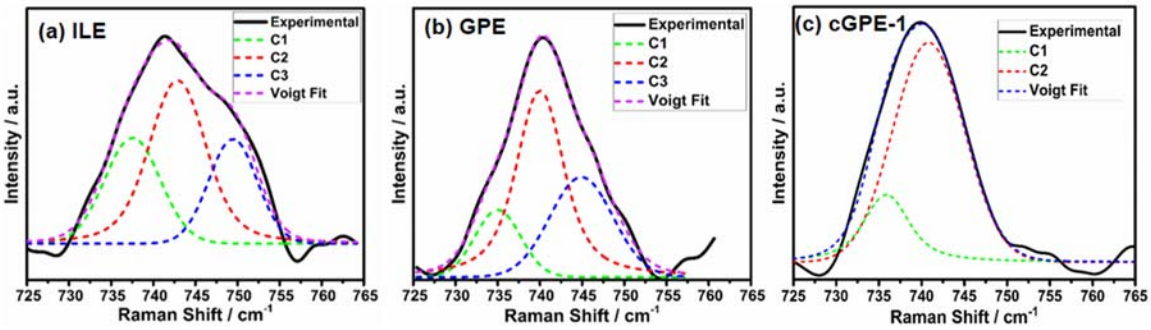

Figure 5-6 Raman Spectra of (a) ILE (b) GPE and (c) cGPE-1 in the range of 725 – 765 cm^{-1}.

From Fig 5-6 (a) and (b) it is seen that both the ILE and GPE shows a peak ~ 748 cm^{-1} which indicates the formation of anionic complexes by the coordination of Li^+ with $TFSI^-$ anion[203,204]. However, the peak intensity ratio of bounded to unbounded $TFSI^-$ for GPE is lower than the ILE indicates the addition of PIL in the system improves the charge carrier mobility in the electrolyte. On the other hand, the addition of 1 wt% micro filler in GPE (cGPE-1), the peak ~748 cm^{-1} is unnoticeable. Qing *et al.* also observed a similar behavior using pyrrolidinium cation based PIL-functionalized cGPE with cellulose as a nanofiller[206]. The above results suggest weak Li^+ and $TFSI^-$ interactions which free up Li^+ by inducing ion pair dissociation in the cGPE-1 which results in high ion conductivity and mobility[207].

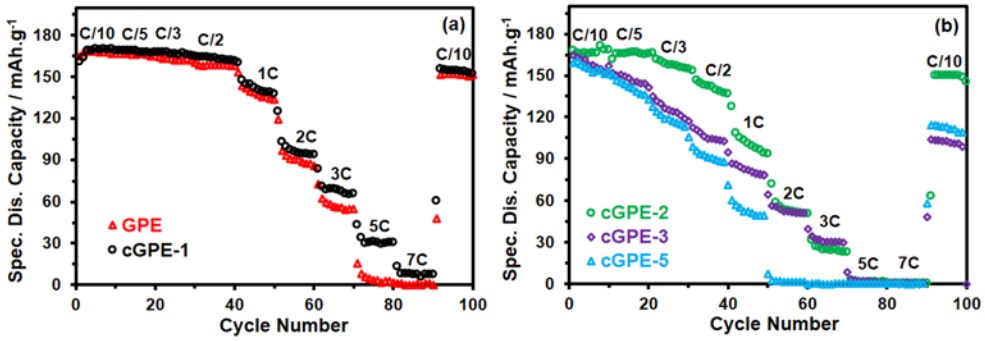

Figure 5-7 Galvanostatic cyclic charge-discharge at various rates for (a) GPE and cGPE-1 (b) cGPEs with various contents of fillers for 100 cycles at 22ºC.

Figure 5-7 (a) shows the discharge capacities at various C-rates for GPE and cGPE-1 while figure 5-7 (b) shows the discharge rate capacities for cGPE-2, cGPE-3, and cGPE-5 while fig. 5-8 (a) and (b) shows the charge-discharge voltage profiles for GPE and cGPE-1 at various C-rates up to 7C for 100 cycles at room temperature (22ºC). The figures compares the discharge capacities of GPE and cGPEs (-1, -2, -3, -5) at C/10, C/5, C/3, C/2, 1C, 2C, 3C, 5C, 7C, and again at C/10 for 10 cycles each. The cGPE-1 demonstrates the best performance over GPE and other cGPEs regarding both discharge capacities and rate capability up to 7C rate. After the 5th cycle at C/10 rate cGPE-1 recorded a discharge capacity of 169.43 mAh.g^{-1} while GPE shows 168.86 mAhg^{-1}. On the other hand, cGPE-3 and cGPE-5 show lower capacity of 157.59 mAh.g^{-1} and 154.95 mAh.g^{-1} respectively after the same number of cycles. Similarly, slightly higher discharge capacities are observed for cGPE-1 compared to GPE, and other cGPEs at 1C rate, with 142.85 mAh.g^{-1} for cGPE-1 compared to 138.86 mAh.g^{-1} for GPE. For high filler content such as cGPE-3 and cGPE-5, lower capacities of 81.64 mAh.g^{-1} and 52.06 mAh.g^{-1} are observed respectively.

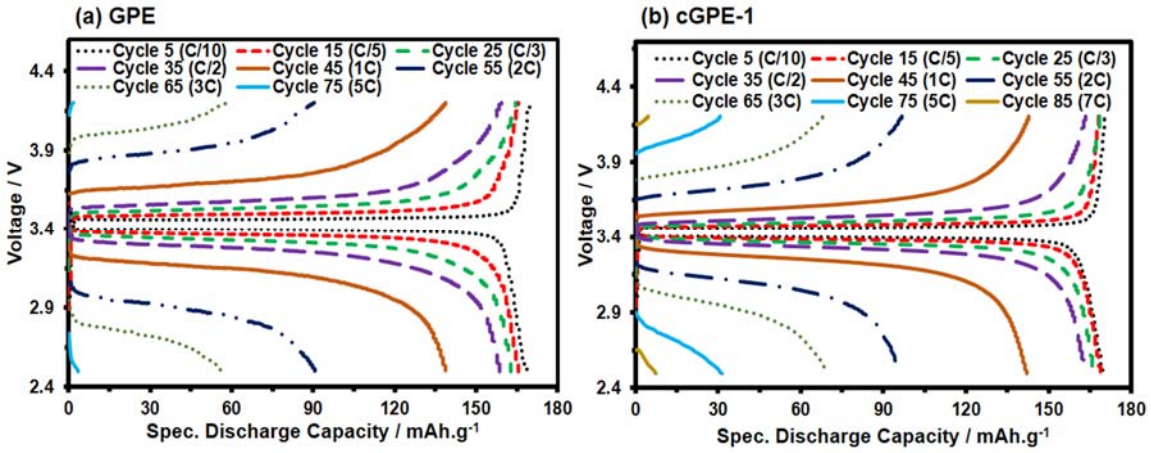

Figure 5- 8 Voltage profiles for (a) GPE and (b) cGPE-1 at various C-rates.

However, a rapid capacity drop is observed for cGPE-2 (98.99 mAh.g^{-1}) and cGPE-3 (52.53 mAh.g^{-1}) while cGPE-5 cell is not functional above 1C. The discharge capacity of cGPE-1 at 5C and 7C are 31.4 and 7.19 mAh.g^{-1} respectively. On the other hand, very low discharge capacities are recorded for GPE and cGPE-3 cells at this high C-rates. The cells were then charge-discharged again at C/10 rate for the last 10 cycles, and the discharge capacities recovered to 154.2 and 152.31 mAh.g^{-1} for cGPE-1 and GPE respectively. The improved performance for cGPE-1 over other electrolytes at higher C-rates is due to the limiting lithium ion diffusion in between the electrolytes and electrolyte/electrode interfaces[36] as evidenced earlier by having the maximum transference number, ionic conductivity, and lithium-ion dissociation.

To further understand the improved electrochemical performance of the cGPE-1 over GPE, compatibility of the electrolytes against lithium metal was performed by running a galvanostatic cyclic test on a Li/GPE or cGPE-1/Li symmetric cell at a current density of 0.1 mA.cm^{-2}.

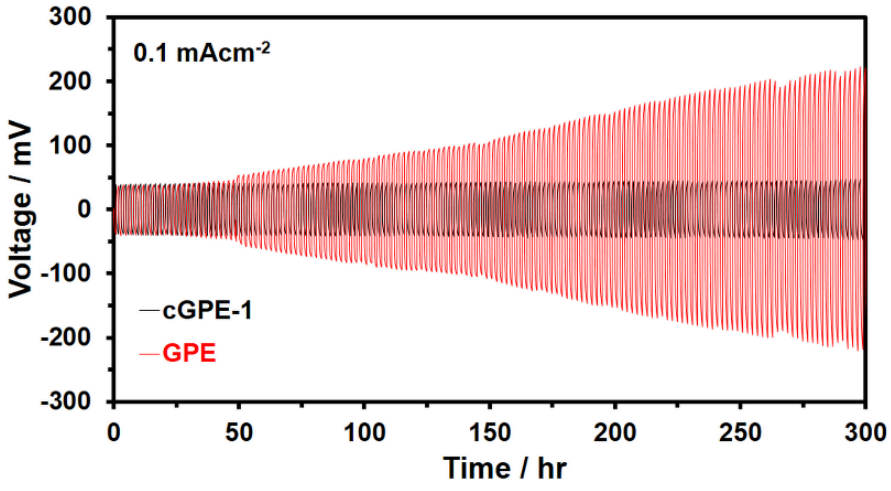

Figure 5- 9 Galvanostatic cycling curves of Li/GPE and cGPE-1/Li symmetrical cells at a current density of 0.1 mA.cm^{-2} for 300 hrs at 22ºC.

Fig. 5-9 compares the overpotential of both the systems up to 300 hrs where one charge-discharge cycle is 2 hrs. In the figure the positive voltage plateau indicates Li stripping while the negative plateau refers to Li plating[36,116]. The figure also illustrates that both the cells show very similar overpotential (40 mV) for the first 45 hrs. However, the overpotential for GPE gradually started to increase after 45 hrs of charge-discharge, and it continued to increase to 210 mV after 300 hrs of Li plating and stripping. On the other hand, no increase in overpotential is observed for cGPE-1 cell indicating the addition of micro-fillers promotes uniform Li^+ deposition and hence inhibits dendrite growth thus prevents short-circuit[200].

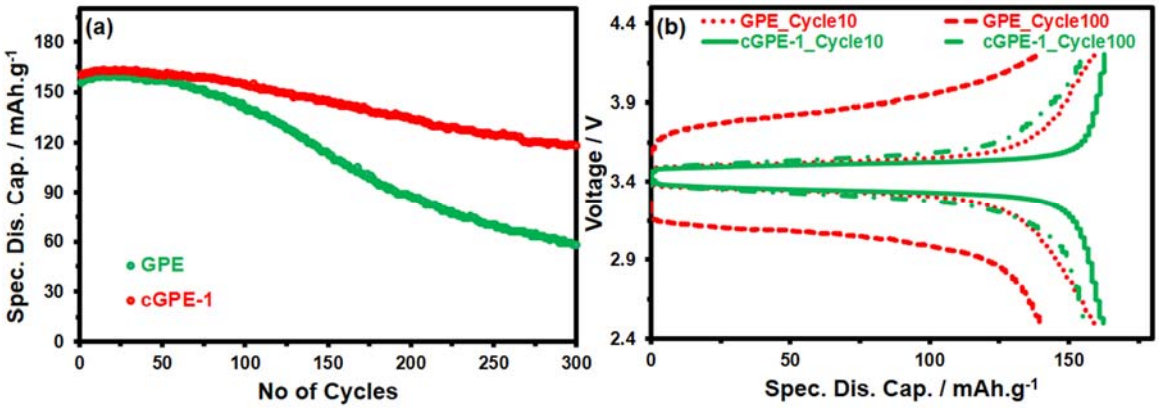

Figure 5- 10 (a) Cyclcing performance of GPE (green) and cGPE-1 (red) at C/2 rate for 100 cycles at 22ºC (b) Voltage profiles comparison of GPE (red) and cGPE-1 (green) after 10 and 100 cycles.

Figure 5-10 (a) compares the cyclic stability of the GPE and cGPE-1 at C/2 rate for 300 cycles at room temperature (22ºC) while Fig. 5-10 (b) shows the charge-discharge voltage profiles for GPE and cGPE-1 after 10 and 100 cycles. From figure 5-10 (a) it is seen that the initial discharge capacity of the GPE and cGPE-1 are 155.4 and 160.42 $mAh.g^{-1}$ respectively and after an initial increase of capacity which is due to the SEI formation[208], the maximum discharge capacity of 160.81 and 163.33 $mAh.g^{-1}$ are

achieved at the 14th cycle. The batteries with the cGPE-1 containing electrolyte maintained a stable discharge capacity up to the 70th cycle while for GPE the capacity started to drop slightly after the 40th cycles. The capacity for GPE cell experiences a faster drop in capacity than cGPE-1with the increase of cycles. After 100 cycles, a 12.6% (140.54 mAh.g^{-1}) drop in capacity from the highest discharge capacity at the 14th cycle is observed for GPE while for cGPE-1 the drop is only 5.1% (155 mAh.g^{-1}). After 300 cycles of cycling the drop percentage for GPE is 63.87% (58.1 mAh.g^{-1}) for GPE, by contrast, 27.55% (118.33 mAh.g^{-1}) discharge capacity is observed for cGPE-1. Figure 5-10 (b) compares the galvanostatic voltage profiles of GPE and cGPE-1 after 10 and 100 cycles. The polarization voltage for GPE increased significantly from 0.2 V to 0.77 V. In contrast, for cGPE-1 the value increased from 0.17 V to 0.23 V which indicates improved interfacial contact between the cGPE-1and the electrodes[209,210].

Potentiostatic EIS was performed during the galvanostatic cycling shown in Fig. 5-10 for the first 100 cycles to understand the capacity fading of the cells at C/2 rate. Figure 5-11 (a) and (b) shows the Nyquist plots at various cycles for GPE and cGPE-1 at fully discharge state while the inset figures show the fitting using the model shown in Fig. 5-11 (a) respectively. In both cases, two semi-circles are observed, one at high frequency (HF) while the other one is at medium frequency (MF), and a straight line has been observed at low frequencies (LF). In the model, R_{el} is the resistance of the bulk electrolyte while the first semi-circle at HF region represents as R_{int} || CPE_{int} which is the interfacial resistance between the electrolyte and the electrodes and the corresponding constant phase element (CPE) is the distributed capacity of the electrode/electrolyte interfaces[122,164]. The use of CPE instead of a capacitor is due to the non-ideal behavior of the electrode mostly the

inhomogeneity, roughness and porous nature of the electrode[166,209]. The second semi-circle at the MF is represented as R_{ct} || CPE_{dl} in the model which is the charge transfer resistance between the electrolyte and the conductive agent while the CPE_{dl} is related to the double layer capacitance[209]. In the model, a semi-infinite Warburg diffusion W_o is connected in series with the R_{ct} || CPE_{dl}, represents the straight line observed at LF which is due to the blocking characteristics of the cathode[209,211].

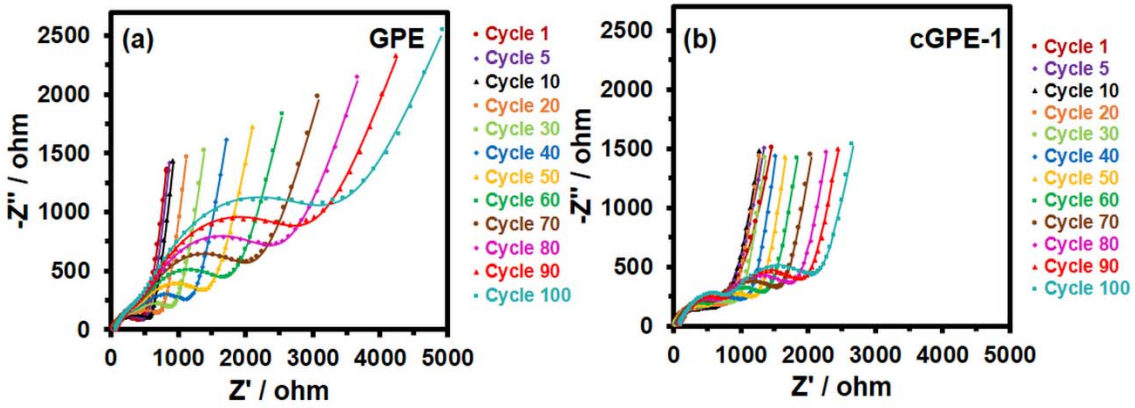

Figure 5- 11 Nyquist plots with fitting at fully charged state for (a) GPE (b) cGPE-1 for the first 100 cycles. Frequency range: 100 kHz to 50 mHz.

Figure 5-12 (b) compares the change in resistance values of R_{el}, $R_{int,}$ and R_{ct} as a function of cycle number up to 100 cycles for GPE (black) and cGPE-1(red) cells. There is no significant change of bulk electrolyte resistance R_{el} observed for both the cells. On the other hand, at the initial cycles, the R_{int} resistance is slightly higher than the R_{ct} resistances for both the cases. After 20 cycles of the charge-discharge process, a rapid increase of R_{ct} is observed compared to a much lower rate of increment in R_{int} for both the cells. However, the rate of increase in R_{ct} is much higher for GPE than cGPE-1 cell. After 100 cycles, 22.45 times increase in R_{ct} for GPE while for cGPE-1 the increment is only 5.95 times from the initial cycle. Based on this observation it can be concluded that R_{ct}

plays a crucial role in the capacity drop for both the cells. It has been studied that the charge transfer reaction occurs at the interface of the electrolyte and the conductive agent[212]. As cycling proceeds, insulating reaction products agglomerates and accumulates on the cathode surface thus decreases the conductive surface area on the cathode and hinder the ion transportation inside the cathode. This blocking of ion transfer causes slow transfer kinetic reaction and results drop in capacity[167]. Moreover, the lower R_{ct} for cGPE-1 than GPE may be due to the better adherence between the micro-fillers and the GPE with the electrodes which provides improved charge transport[213]. From the above discussions, it can be concluded that the improved rate capability and cyclic stability for the cGPE-1 than GPE reflects the better dendrite suppressing ability and interfacial contact between the electrodes/electrolyte interfaces which is due to the uniform deposition of reaction products on the electrodes using cGPE-1. The improvement is also attributable to the improvement in ionic conductivity, lithium ion mobility and ion-pair dissociation inducing pathways for free lithium ion movement for cGPE-1 cell.

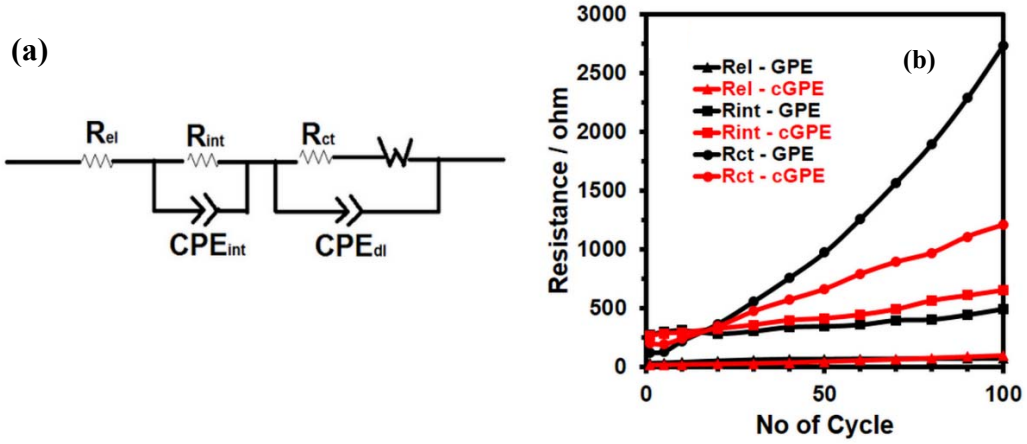

Figure 5- 12 (a) Equivalent circuit models to fit Nyquist plots. (b) Plot of resistance values for GPE (black) and cGPE-1(red) with cycle number.

5.4 Conclusion

In this study, polymeric ionic liquid-based GPE containing various content of glass micro-fillers were prepared, and the performance as an electrolyte was evaluated in lithium battery application. With the addition of 1 wt% micro-filler in GPE (cGPE-1) helps to form complex ceramic ions with the anion and creates a free pathway for lithium ion to transport between the electrodes as it is evidenced by improved ionic conductivity, lithium transference number and also dissociation of lithium salt. Additionally, cGPE-1 shows better rate capability for 100 cycles as high as 7C rate and also shows better cyclic stability for 300 cycles at C/2 rate. The cGPE-1 shows improved stability against lithium metal, and improved interfacial contact after cycling indicates uniform deposition of reaction products on the electrode surfaces which improves charge transfer kinetic reaction and hence improved battery performance. The application of glass micro-fillers in poly(ionic liquid) based GPE offers a new way of the application of composite gel electrolyte in energy storage devices.

6 CONCLUDING REMARKS AND FUTURE WORKS

6.1 Concluding Remarks

Due to their high theoretical energy densities, lithium batteries have been considered as the future of energy storage. A breakthrough in this battery technology could lead to improvement in performance in various applications including in EVs. The present state-of-the-art batteries do not meet the specific energies required for the automotive industry. Lithium as anode could deliver this high specific energy. However, safety remains one of the biggest concerns using lithium due to its poor interfacial properties with most organic liquid electrolytes which are often very volatile and flammable. Replacing these organic electrolytes with a non-flammable, non-volatile electrolytes in addition to improving the interfacial contacts with the electrodes can help remedy this problem. Over the past few years, numerous attempts have been made to produce an electrolyte with the aforementioned properties. SPEs and derivatives of PEs such as composite polymer electrolytes have been shown to improved interfacial contact with lithium. They were also shown to overcome the safety issues caused by volatile and flammable organic solvents. However, their poor room temperature ionic conductivity impedes their progress and their applicability in battery systems. Instead, polymer electrolytes gelled by a non-flammable solvent such as ionic liquids have been considered as viable compromise since they can drastically improve the ionic conductivity over solid electrolytes while remaining safe from solvent leakage and flammability risks.

This dissertation aims to develop and characterize GPEs based on pyrrolidinium cation PIL, imidazolium based IL as a solvent, and a lithium salt. Investigation of the effect of glass micro-fiber fillers at various contents was also carried out in lithium batteries.

In the first stage of this dissertation, GPEs with high IL content (up to 80% of ILE) were prepared. The free-standing GPEs were thermally stable up to 390ºC and highly ionically conductive with ionic conductivities as high as 3.4 $mS.cm^{-1}$. The affinity between the PIL, IL, and lithium salt in GPE allowed for a wide electrochemical stability window (5 V) and helped increase Li^+ transference number from 0.3 to as high as 0.41. Also, a repeating symmetric lithium plating/stripping test showed better GPE compatibility with lithium anodes than ILE. Furthermore, galvanostatic charge-discharge cycling of Li/GPE/LFP cells showed high discharge capacity of 169.3 $mAh.g^{-1}$ at C/10 rate and moderate capacity of 126.8 $mAh.g^{-1}$ at 1C rate. Cells using GPE also showed excellent rate capability up to 5 C rate as well as 98.4% capacity retention after 40 cycles at 22ºC.

In the second phase of this dissertation, the performance of the GPEs was evaluated with S-CNT composite cathodes in lithium-sulfur batteries. The major advantage of using Li-S is its high energy densities of 400-600 $Wh.kg^{-1}$ which is two to three times higher than LIBs. The galvanostatic charge-discharge performance of the GPE was compared to ILE-containing cells. The GPE-containing cells showed superior rate capability up to 1-C rate for 100 cycles and cyclic stability for 500 cycles at C/2 rate than ILE. However, rapid capacity fading for the first few cycles for both GPE and ILE cells was observed. EIS study revealed a higher depth-of-discharge dependent impedance growth during the first discharge cycle for ILE, followed by a subsequent interfacial resistance growth between

the electrode/electrolyte interfaces. At the end of discharge, a Warburg diffusion line indicated an accumulation of insoluble Li_2S_2/Li_2S on the cathode surface thus blocked the pores of the cathode. With subsequent cycling, the continuous deposition of the insoluble products increased the interfacial resistances and loss of capacity fading occurred. However, lower impedance growth for GPE compared to ILE indicated less deposition of these insoluble products and resulted in higher discharge capacity for the cells using GPE. SEM imaging of the cycled cathodes showed cracks in the ILE-containing cells supporting the hypothesis of the formation of insoluble charge and discharge products, which volumetrically expanded and yielded cracks.

In the last phase of the dissertation, various contents of glass micro-filler were added to GPE (cGPE), and their performances were evaluated for Li/(GPE) or (cGPE)/LFP cells setup. The optimum filler content in cGPE was determined based on the electrochemical performance of the batteries. It turned out that the cGPE containing 1wt% optimized glass micro-filler content (cGPE-1) had the highest ionic conductivity (4.1 $mS.cm^{-1}$ vs 3.06 $mS.cm^{-1}$) and Li^+ transference number (0.43 vs 0.39) compared to GPE. Furthermore, Raman spectroscopy showed that the addition of fillers increased ion-pair dissociation of lithium salt. Based on this observations, it was suggested that for cGPE-1 containing cells, 1wt% filler helped form complex ion ceramics with the anion and created a free transport pathway for Li^+ to between the electrodes. The cGPE-1 containing cells also showed improved stability against lithium during repeated stripping/platting tests. Galvanostatic cyclic charge-discharge tests showed the rate capability as high as 7C rate for 100 cycles and 300 cycles at C/2 rate. An in-situ EIS investigation during cycling indicated improved interfacial contact between the electrode/electrolyte interfaces for cGPE-1 compared to

ILE, thus improved charge transfer reaction kinetics and improved the overall battery performance. The application of glass micro-filler in PIL based GPE was shown to offer a stabilizing and performance increasing effect when included in lithium batteries.

6.2 Future Works

Due to their measurable improvement in various lithium batteries systems, GPE electrolyte based ionic liquids have been shown to improve the stability and performance of Li/LFP and Li-S batteries. It is anticipated that the type of system that would most benefit from this improvement would be lithium oxygen batteries. The high thermal stability, wide electrochemical window, non-volatility, and chemical compatibility of the poly (ionic liquid) electrolyte with lithium would likely provide much needed improvement in the performance of Li-O_2 batteries. Along with efforts to reduce the thickness, increase the liquid phase content, and introduction of ceramic fillers, it is anticipated that a suitable PIL based GPE or cGPE can be developed with tailored properties to eliminate problems common in Li-O_2 batteries such as Li_2CO_3 formation, solvent evaporation, anode interfacial resistance growth, and oxygen/water crossover.

REFERENCES

[1] J.-M. Tarascon, M. Armand, Issues and challenges facing rechargeable lithium batteries, in: Mater. Sustain. Energy A Collect. Peer-Reviewed Res. Rev. Artic. from Nat. Publ. Gr., World Scientific, 2011: pp. 171–179.

[2] W. Li, B. Song, A. Manthiram, High-voltage positive electrode materials for lithium-ion batteries, Chem. Soc. Rev. (2017).

[3] P. Albertus, S. Babinec, S. Litzelman, A. Newman, Status and challenges in enabling the lithium metal electrode for high-energy and low-cost rechargeable batteries, Nat. Energy. (2017) 1.

[4] B.D. McCloskey, Attainable Gravimetric and Volumetric Energy Density of Li–S and Li Ion Battery Cells with Solid Separator-Protected Li Metal Anodes, J. Phys. Chem. Lett. 6 (2015) 4581–4588. doi:10.1021/acs.jpclett.5b01814.

[5] M.N. Obrovac, V.L. Chevrier, Alloy Negative Electrodes for Li-Ion Batteries M.N. Obrovac, Chem. Rev. 114 (2014) 11444–11502. doi:10.1021/cr500207g.

[6] X.-B. Cheng, R. Zhang, C.-Z. Zhao, Q. Zhang, Toward Safe Lithium Metal Anode in Rechargeable Batteries: A Review, Chem. Rev. 117 (2017) 10403–10473. doi:10.1021/acs.chemrev.7b00115.

[7] L. Grande, J. von Zamory, S.L. Koch, J. Kalhoff, E. Paillard, S. Passerini, Homogeneous lithium electrodeposition with Pyrrolidinium-based ionic liquid electrolytes, ACS Appl. Mater. Interfaces. 7 (2015) 5950–5958.

[8] J. Voelcker, Bollore Bluecar: Sharing Paris's Most Popular Electric Car, (2012). https://www.greencarreports.com/news/1079516_bollore-bluecar-sharing-pariss-most-popular-electric-car (accessed March 27, 2018).

[9] J. Spector, Why Toyota's Next Move Is Solid-State Batteries | Greentech Media, (2017). https://www.greentechmedia.com/articles/read/toyotas-next-move-solid-state-batteries#gs.VCIJygQ (accessed March 27, 2018).

[10] M.S. Reisch, Solid-state batteries inch their way toward commercialization (vol 95, pg 19, 2017), Chem. Eng. News. 95 (2017) 3.

[11] Z. Estrada, Fisker's "autonomous" EMotion electric car promises 400 miles of range - The Verge, (2018). https://www.theverge.com/2018/1/9/16867184/fisker-emotion-electric-luxury-car-lidar-autonomous-ces-2018 (accessed March 27, 2018).

[12] Z. Estrada, There could be an entire line of Dyson electric cars - The Verge, (2018). https://www.theverge.com/2018/2/14/17013694/dyson-electric-car-lineup (accessed March 27, 2018).

[13] S. O'Kane, Riding in Byton's far-out concept SUV is like being in first class - The Verge, (2018).

https://www.theverge.com/transportation/2018/1/9/16867332/byton-electric-ev-car-ride-first-look-test-touchscreen-ces-2018 (accessed March 27, 2018).

[14] J.W. Choi, D. Aurbach, Promise and reality of post-lithium-ion batteries with high energy densities, Nat. Rev. Mater. 1 (2016) 16013.

[15] J.L. Schaefer, Y. Lu, S.S. Moganty, P. Agarwal, N. Jayaprakash, L.A. Archer, Electrolytes for high-energy lithium batteries, Appl. Nanosci. 2 (2012) 91–109. doi:10.1007/s13204-011-0044-x.

[16] Z. Li, D. Zhang, F. Yang, Developments of lithium-ion batteries and challenges of LiFePO4 as one promising cathode material, J. Mater. Sci. 44 (2009) 2435–2443. doi:10.1007/s10853-009-3316-z.

[17] P. Poizot, S. Laruelle, S. Grugeon, L. Dupont, J.M. Tarascon, P. Poizot, S. Laruelle, S. Grugeon, L. Dupont, Nano-sized transition-metal oxides as negative-electrode materials for lithium-ion batteries, Nature. 407 (2000) 496. doi:10.1038/35035045.

[18] Y. Zhang, Q. Huo, P. Du, L. Wang, A. Zhang, Y. Song, Y. Lv, G. Li, Advances in new cathode material LiFePO4 for lithium-ion batteries, Synth. Met. 162 (2012) 1315–1326. doi:10.1016/j.synthmet.2012.04.025.

[19] A. Ritchie, W. Howard, Recent developments and likely advances in lithium-ion batteries, J. Power Sources. 162 (2006) 809–812.

[20] A.K. Padhi, K.S. Nanjundaswamy, J.B. Goodenough, Phospho-olivines as positive-electrode materials for rechargeable lithium batteries, J. Electrochem. Soc. 144 (1997) 1188–1194.

[21] G. Cheruvally, Lithium iron phosphate: a promising cathode-active material for lithium secondary batteries, Trans Tech Publications Limited, 2008.

[22] S. Franger, C. Benoit, C. Bourbon, F. Le Cras, Chemistry and electrochemistry of composite LiFePO4 materials for secondary lithium batteries, J. Phys. Chem. Solids. 67 (2006) 1338–1342.

[23] M.-R. Yang, T.-H. Teng, S.-H. Wu, LiFePO4/carbon cathode materials prepared by ultrasonic spray pyrolysis, J. Power Sources. 159 (2006) 307–311.

[24] C. Yada, Y. Iriyama, S.-K. Jeong, T. Abe, M. Inaba, Z. Ogumi, Electrochemical properties of LiFePO4 thin films prepared by pulsed laser deposition, J. Power Sources. 146 (2005) 559–564.

[25] M. Sathiya, Synthetic routes for the preparation of rechargeable Li-ion battery electrode materials, (2012).

[26] N. Ravet, Y. Chouinard, J.F. Magnan, S. Besner, M. Gauthier, M. Armand, Electroactivity of natural and synthetic triphylite, J. Power Sources. 97 (2001) 503–507.

[27] N.J. Yun, H.-W. Ha, K.H. Jeong, H.-Y. Park, K. Kim, Synthesis and electrochemical properties of olivine-type LiFePO4/C composite cathode material prepared from a poly (vinyl alcohol)-containing precursor, J. Power Sources. 160 (2006) 1361–1368.

[28] Y. Xia, M. Yoshio, H. Noguchi, Improved electrochemical performance of LiFePO4 by increasing its specific surface area, Electrochim. Acta. 52 (2006) 240–245.

[29] Y. Meesala, A. Jena, H. Chang, R.-S. Liu, Recent Advancements in Li-Ion Conductors for All-Solid-State Li-Ion Batteries, ACS Energy Lett. 2 (2017) 2734–2751.

[30] D. Zhou, R. Liu, J. Zhang, X. Qi, Y.-B. He, B. Li, Q.-H. Yang, Y.-S. Hu, F. Kang, In Situ Synthesis of Hierarchical Poly(ionic liquid)-Based Solid Electrolytes for High-Safety Lithium-ion and Sodium-ion Batteries, Nano Energy. 33 (2017) 45–54. doi:10.1016/j.nanoen.2017.01.027.

[31] H. Kim, G. Jeong, Y.-U. Kim, J.-H. Kim, C.-M. Park, H.-J. Sohn, Metallic anodes for next generation secondary batteries, Chem. Soc. Rev. 42 (2013) 9011–9034. doi:10.1039/C3CS60177C.

[32] F. Ding, W. Xu, G.L. Graff, J. Zhang, M.L. Sushko, X. Chen, Y. Shao, M.H. Engelhard, Z. Nie, J. Xiao, Dendrite-free lithium deposition via self-healing electrostatic shield mechanism, J. Am. Chem. Soc. 135 (2013) 4450–4456.

[33] J. Jeong, J.-N. Lee, J.-K. Park, M.-H. Ryou, Y.M. Lee, Stabilizing effect of 2-(triphenylphosphoranylidene) succinic anhydride as electrolyte additive on the lithium metal of lithium metal secondary batteries, Electrochim. Acta. 170 (2015) 353–359.

[34] M. Ishikawa, M. Morita, Y. Matsuda, In situ scanning vibrating electrode technique for lithium metal anodes, J. Power Sources. 68 (1997) 501–505.

[35] Q. Pan, D.M. Smith, H. Qi, S. Wang, C.Y. Li, Hybrid electrolytes with controlled network structures for lithium metal batteries, Adv. Mater. 27 (2015) 5995–6001.

[36] M. Safa, A. Chamaani, N. Chawla, B. El-Zahab, Polymeric Ionic Liquid Gel Electrolyte for Room Temperature Lithium Battery Applications, Electrochim. Acta. 213 (2016) 587–593. doi:10.1016/j.electacta.2016.07.118.

[37] K. Xu, Electrolytes and interphases in Li-ion batteries and beyond, Chem. Rev. 114 (2014) 11503–11618. doi:10.1021/cr500003w.

[38] K. Xu, Nonaqueous Liquid Electrolytes for Lithium-Based Rechargeable Batteries Nonaqueous Liquid Electrolytes for Lithium-Based Rechargeable Batteries, Chem. Rev. 104 (2004) 4303. doi:10.1021/cr030203g.

[39] P. Arora, Z. Zhang, Battery separators, Chem. Rev. 104 (2004) 4419–4462.

[40] G. Pistoia, M. De Rossi, B. Scrosati, M. De Rossi, B. Scrosati, Study of the behavior of ethylene carbonate as a nonaqueous battery solvent, J. Electrochem. Soc. 117 (1970) 500–502. doi:10.1149/1.2407550.

[41] J.M. Tarascon, D. Guyomard, New electrolyte compositions stable over the 0 to 5 V voltage range and compatible with the Li1+xMn2O4/carbon Li-ion cells, Solid State Ionics. 69 (1994) 293–305. doi:10.1016/0167-2738(94)90418-9.

[42] G.G. Eshetu, J.P. Bertrand, A. Lecocq, S. Grugeon, S. Laruelle, M. Armand, G. Marlair, Fire behavior of carbonates-based electrolytes used in Li-ion rechargeable batteries with a focus on the role of the LiPF6 and LiFSI salts, J. Power Sources. 269 (2014) 804–811. doi:10.1016/j.jpowsour.2014.07.065.

[43] J. Kalhoff, G.G. Eshetu, D. Bresser, S. Passerini, Safer electrolytes for lithium-ion batteries: State of the art and perspectives, ChemSusChem. 8 (2015) 2154–2175. doi:10.1002/cssc.201500284.

[44] R. Hayes, G.G. Warr, R. Atkin, Structure and Nanostructure in Ionic Liquids, Chem. Rev. 115 (2015) 6357–6426. doi:10.1021/cr500411q.

[45] A. Matic, B. Scrosati, Ionic liquids for energy applications, MRS Bull. 38 (2013) 533–537. doi:10.1557/mrs.2013.154.

[46] B. Garcia, S. Lavallée, G. Perron, C. Michot, M. Armand, Room temperature molten salts as lithium battery electrolyte, Electrochim. Acta. 49 (2004) 4583–4588. doi:10.1016/j.electacta.2004.04.041.

[47] M. Gali??ski, A. Lewandowski, I. Stepniak, M. Galiński, A. Lewandowski, I. Stepniak, Ionic liquids as electrolytes, Electrochim. Acta. 51 (2006) 5567–5580. doi:10.1016/j.electacta.2006.03.016.

[48] T. Sato, T. Maruo, S. Marukane, K. Takagi, Ionic liquids containing carbonate solvent as electrolytes for lithium ion cells, J. Power Sources. 138 (2004) 253–261. doi:10.1016/j.jpowsour.2004.06.027.

[49] M. Holzapfel, C. Jost, P. Novák, Stable cycling of graphite in an ionic liquid based electrolyte., Chem. Commun. (Camb). (2004) 2098–2099. doi:10.1039/b407526a.

[50] V. Borgel, E. Markevich, D. Aurbach, G. Semrau, M. Schmidt, On the application of ionic liquids for rechargeable Li batteries: High voltage systems, J. Power Sources. 189 (2009) 331–336. doi:10.1016/j.jpowsour.2008.08.099.

[51] M. Ue, K. Ida, S. Mori, Electrochemical properties of organic liquid electrolytes based on quaternary onium salts for electrical double-layer capacitors, J. Electrochem. Soc. 141 (1994) 2989–2996.

[52] R.D. Rauh, T.F. Reise, S.B. Brummer, Efficiencies of cycling lithium on a lithium substrate in propylene carbonate, J. Electrochem. Soc. 125 (1978) 186–190.

[53] L.J. Krause, W. Lamanna, J. Summerfield, M. Engle, G. Korba, R. Loch, R. Atanasoski, Corrosion of aluminum at high voltages in non-aqueous electrolytes

containing perfluoroalkylsulfonyl imides; new lithium salts for lithium-ion cells, J. Power Sources. 68 (1997) 320–325.

[54] J. Foropoulos Jr, D.D. DesMarteau, Synthesis, properties, and reactions of bis ((trifluoromethyl) sulfonyl) imide,(CF3SO2) 2NH, Inorg. Chem. 23 (1984) 3720–3723. doi:10.1021/ic00191a011.

[55] L.A.A. Dominey, V.R.R. Koch, T.J. Blakley, Thermally stable lithium salts for polymer electrolytes, Electrochim. Acta. 37 (1992) 1551–1554. doi:10.1016/0013-4686(92)80109-Y.

[56] R. Corporation, I. Madison, W. Ebner, D. Fouchard, L. Xie, The LiNiO2/carbon lithium-ion battery, Solid State Ionics. 69 (1994) 238–256. doi:10.1016/0167-2738(94)90413-8.

[57] P. V. Wright, Electrical conductivity in ionic complexes of poly(ethylene oxide), Br. Polym. J. 7 (1975) 319–327. doi:10.1002/pi.4980070505.

[58] S. Passerini, M. Montanino, G.B. Appetecchi, Lithium polymer batteries based on ionic liquids, (2013) 53–101. doi:10.1002/9781118734162.ch3.

[59] E. Quartarone, P. Mustarelli, Electrolytes for solid-state lithium rechargeable batteries: recent advances and perspectives, Chem. Soc. Rev. 40 (2011) 2525–2540. doi:10.1039/c0cs00081g.

[60] J.W. Fergus, Ceramic and polymeric solid electrolytes for lithium-ion batteries, J. Power Sources. 195 (2010) 4554–4569. doi:10.1016/j.jpowsour.2010.01.076.

[61] G. Feuillade, P. Perche, Ion-conductive macromolecular gels and membranes for solid lithium cells, J. Appl. Electrochem. 5 (1975) 63–69. doi:10.1007/BF00625960.

[62] A. Du Pasquier, P.C. Warren, D. Culver, A.S. Gozdz, G.G. Amatucci, J.M. Tarascon, Plastic PVDF-HFP electrolyte laminates prepared by a phase-inversion process, Solid State Ionics. 135 (2000) 249–257. doi:10.1016/S0167-2738(00)00371-4.

[63] A. Noda, M. Watanabe, Highly conductive polymer electrolytes prepared by in situ polymerization of vinyl monomers in room temperature molten salts, Electrochim. Acta. 45 (2000) 1265–1270. doi:10.1016/S0013-4686(99)00330-8.

[64] M. Yoshizawa, H. Ohno, Synthesis of molten salt-type polymer brush and effect of brush structure on the ionic conductivity, Electrochim. Acta. 46 (2001) 1723–1728. doi:10.1016/S0013-4686(00)00777-5.

[65] R. Marcilla, J.A. Blazquez, J. Rodriguez, J.A. Pomposo, D. Mecerreyes, Tuning the Solubility of Polymerized Ionic Liquids by Simple Anion-Exchange Reactions, J. Polym. Sci. Part A Polym. Chem. 42 (2003) 208–212. doi:10.1002/pola.11015.

[66] A.L. Pont, R. Marcilla, I. De Meatza, H. Grande, D. Mecerreyes, Pyrrolidinium-based polymeric ionic liquids as mechanically and electrochemically stable

polymer electrolytes, J. Power Sources. 188 (2009) 558–563. doi:10.1016/j.jpowsour.2008.11.115.

[67] G.B. Appetecchi, G.T. Kim, M. Montanino, F. Alessandrini, S. Passerini, Room temperature lithium polymer batteries based on ionic liquids, J. Power Sources. 196 (2011) 6703–6709. doi:10.1016/j.jpowsour.2010.11.070.

[68] J.E. Weston, B.C.H. Steele, EFFECTS OF INERT FILLERS ON THE MECHANICAL AND ELECTROCHEMICAL PROPERTIES OF LITHIUM SALT-POLY (ETHYLENE OXIDE) POLYMER ELECTROLYTES _ i b, Solid State Lonics. 7 (1982) 75–79. doi:10.1016/0167-2738(82)90072-8.

[69] F. Croce, L.L. Persi, B. Scrosati, F. Serraino-Fiory, E. Plichta, M.A. Hendrickson, Role of the ceramic fillers in enhancing the transport properties of composite polymer electrolytes, Electrochim. Acta. 46 (2001) 2457–2461. doi:10.1016/S0013-4686(01)00458-3.

[70] Y.-S. Ye, J. Rick, B.-J. Hwang, Ionic liquid polymer electrolytes, J. Mater. Chem. A. 1 (2013) 2719–2743. doi:10.1039/C2TA00126H.

[71] N.S.T. Do, D.M. Schaetzl, B. Dey, A.C. Seabaugh, S.K. Fullerton-Shirey, Influence of Fe $_2$ O $_3$ Nanofiller Shape on the Conductivity and Thermal Properties of Solid Polymer Electrolytes: Nanorods versus Nanospheres, J. Phys. Chem. C. 116 (2012) 21216–21223. doi:10.1021/jp3059454.

[72] W. Liu, N. Liu, J. Sun, P.C. Hsu, Y. Li, H.W. Lee, Y. Cui, Ionic Conductivity Enhancement of Polymer Electrolytes with Ceramic Nanowire Fillers, Nano Lett. 15 (2015) 2740–2745. doi:10.1021/acs.nanolett.5b00600.

[73] K. Kimura, H. Matsumoto, J. Hassoun, S. Panero, B. Scrosati, Y. Tominaga, A QuaternaryPoly(ethylene carbonate)-Lithium Bis(trifluoromethanesulfonyl)imide-Ionic Liquid-Silica Fiber Composite Polymer Electrolyte for Lithium Batteries, Electrochim. Acta. 175 (2015) 134–140. doi:10.1016/j.electacta.2015.03.117.

[74] A.A. Van Zomeren, E.M. Kelder, J.C.M. Marijnissen, J. Schoonman, The production of thin films of LiMn2O4 by electrospraying, J. Aerosol Sci. 25 (1994) 1229–1235.

[75] M. Beidaghi, Z. Wang, L. Gu, C. Wang, Electrostatic spray deposition of graphene nanoplatelets for high-power thin-film supercapacitor electrodes, J. Solid State Electrochem. 16 (2012) 3341–3348.

[76] R. Agrawal, C. Chen, S. Dages, C. Wang, A High Energy 3V Lithium-Ion Capacitor Synthesized via Electrostatic Spray Deposition, Adv. Mater. Lett. 8 (2017) 783–790.

[77] R. Agrawal, E. Adelowo, A.R. Baboukani, M.F. Villegas, A. Henriques, C. Wang, Electrostatic Spray Deposition-Based Manganese Oxide Films—From Pseudocapacitive Charge Storage Materials to Three-Dimensional Microelectrode Integrands, Nanomaterials. 7 (2017) 198.

[78] V. Presser, L. Zhang, J.J. Niu, J. McDonough, C. Perez, H. Fong, Y. Gogotsi, Flexible Nano-felts of Carbide-Derived Carbon with Ultra-high Power Handling Capability, Adv. Energy Mater. 1 (2011) 423–430.

[79] P. Bonhôte, A.-P. Dias, M. Armand, N. Papageorgiou, K. Kalyanasundaram, M. Grätzel, Hydrophobic, Highly Conductive Ambient-Temperature Molten Salts., Inorg. Chem. 35 (1996) 1168–1178. doi:10.1021/ic951325x.

[80] P. Inc, Thermogravimetric Analysis (TGA) The Thermogravimetric Instrument Family, (n.d.). https://www.perkinelmer.com/lab-solutions/resources/docs/faq_beginners-guide-to-thermogravimetric-analysis_009380c_01.pdf (accessed April 1, 2018).

[81] M. Toledo, Decomposition of Calcium Oxalate Monohydrate - METTLER TOLEDO, (n.d.). https://www.mt.com/us/en/home/supportive_content/matchar_apps/MatChar_HB602.html (accessed April 1, 2018).

[82] H.H. Girault, Analytical and physical electrochemistry, CRC Press, 2004.

[83] M. Hayyan, F.S. Mjalli, M.A. Hashim, I.M. AlNashef, T.X. Mei, Investigating the electrochemical windows of ionic liquids, J. Ind. Eng. Chem. 19 (2013) 106–112. doi:https://doi.org/10.1016/j.jiec.2012.07.011.

[84] A.A.J. Torriero, ELECTROCHEMISTRY IN IONIC LIQUIDS., Springer, 2015. doi:10.1007/978-3-319-15132-8.

[85] Basics of EIS: Electrochemical Research-Impedance, (n.d.). https://www.gamry.com/application-notes/EIS/basics-of-electrochemical-impedance-spectroscopy/ (accessed April 5, 2018).

[86] NPTEL Phase-II: Fuel Cell Technology, (n.d.). http://nptel.ac.in/courses/103102015/fuel cell characterization/in situ characterization.html (accessed April 5, 2018).

[87] P.G.B. James Evans, Colin A. Vincent, Electrochemical measuremnet of transference numbers in polymer electrolytes, Polymer (Guildf). 28 (1987) 2324–2328.

[88] B. Scrosati, J. Hassoun, Y.-K. Sun, Lithium-ion batteries. A look into the future, Energy Environ. Sci. 4 (2011) 3287–3295. doi:10.1039/C1EE01388B.

[89] S. Seki, M. Watanabe, Polymer and Ionic Liquid Electrolytes for Advanced Lithium Batteries, in: Nanoscale Technol. Adv. Lithium Batter., Springer, 2014: pp. 51–61.

[90] M.B. Armand, J.M. Chabagno, M.J. Duclot, Fast ion transport in solids, Eds. Vashishta, P., Mundy, JN Shenoy, G. K, North Holland, Amsterdan. 52 (1979).

[91] Y. Kang, H.J. Kim, E. Kim, B. Oh, J.H. Cho, Photocured PEO-based solid polymer electrolyte and its application to lithium–polymer batteries, J. Power Sources. 92 (2001) 255–259.

[92] G.B. Appetecchi, J. Hassoun, B. Scrosati, F. Croce, F. Cassel, M. Salomon, Hot-pressed, solvent-free, nanocomposite, PEO-based electrolyte membranes: II. All solid-state Li/LiFePO4 polymer batteries, J. Power Sources. 124 (2003) 246–253.

[93] X. Huang, A facile approach to make high performance nano-fiber reinforced composite separator for lithium ion batteries, J. Power Sources. 323 (2016) 17–22. doi:10.1016/j.jpowsour.2016.05.022.

[94] Y.S. Lee, D.W. Kim, Cycling performance of lithium polymer cells assembled by in situ polymerization of a non-flammable ionic liquid monomer, Electrochim. Acta. 106 (2013) 460–464. doi:10.1016/j.electacta.2013.05.137.

[95] S. Rajendran, M. Sivakumar, R. Subadevi, Effect of salt concentration in poly (vinyl alcohol)-based solid polymer electrolytes, J. Power Sources. 124 (2003) 225–230.

[96] Y.S. Zhu, X.J. Wang, Y.Y. Hou, X.W. Gao, L.L. Liu, Y.P. Wu, M. Shimizu, A new single-ion polymer electrolyte based on polyvinyl alcohol for lithium ion batteries, Electrochim. Acta. 87 (2013) 113–118. doi:10.1016/j.electacta.2012.08.114.

[97] K. Kimura, J. Hassoun, S. Panero, B. Scrosati, Y. Tominaga, Electrochemical properties of a poly(ethylene carbonate)-LiTFSI electrolyte containing a pyrrolidinium-based ionic liquid, Ionics (Kiel). 21 (2015) 895–900. doi:10.1007/s11581-015-1370-x.

[98] P. Yang, W. Cui, L. Li, L. Liu, M. An, Characterization and properties of ternary P(VdF-HFP)-LiTFSI-EMITFSI ionic liquid polymer electrolytes, Solid State Sci. 14 (2012) 598–606. doi:10.1016/j.solidstatesciences.2012.02.005.

[99] C.M. Costa, M.M. Silva, S. Lanceros-Méndez, Battery separators based on vinylidene fluoride (VDF) polymers and copolymers for lithium ion battery applications, RSC Adv. 3 (2013) 11404. doi:10.1039/c3ra40732b.

[100] B. Scrosati, K.M. Abraham, W. van Schalkwijk, J. Hassoun, Lithium Batteries: Advanced Technologies and Applications, 2013. doi:10.1002/9781118615515.

[101] M. Liu, D. Zhou, Y.-B. He, Y. Fu, X. Qin, C. Miao, H. Du, B. Li, Q.-H. Yang, Z. Lin, Novel gel polymer electrolyte for high-performance lithium–sulfur batteries, Nano Energy. 22 (2016) 278–289.

[102] G.G. Eshetu, M. Armand, B. Scrosati, S. Passerini, Energy storage materials synthesized from ionic liquids, Angew. Chemie - Int. Ed. 53 (2014) 13342–13359. doi:10.1002/anie.201405910.

[103] Y. Yan, Y.X. Yin, S. Xin, J. Su, Y.G. Guo, L.J. Wan, High-safety lithium-sulfur battery with prelithiated Si/C anode and ionic liquid electrolyte, Electrochim. Acta. 91 (2013) 58–61. doi:10.1016/j.electacta.2012.12.077.

[104] H. Ohno, Molten salt type polymer electrolytes, Electrochim. Acta. 46 (2001) 1407–1411. doi:10.1016/S0013-4686(00)00733-7.

[105] G.B. Appetecchi, G.T. Kim, M. Montanino, M. Carewska, R. Marcilla, D. Mecerreyes, I. De Meatza, Ternary polymer electrolytes containing pyrrolidinium-based polymeric ionic liquids for lithium batteries, J. Power Sources. 195 (2010) 3668–3675. doi:10.1016/j.jpowsour.2009.11.146.

[106] M. Egashira, T. Kiyabu, I. Watanabe, S. Okada, J.-I. Yamaki, The effect of additives in room temperature molten salt-based lithium battery electrolytes, Electrochemistry. 71 (2003) 1114–1116.

[107] M. Rao, X. Geng, Y. Liao, S. Hu, W. Li, Preparation and performance of gel polymer electrolyte based on electrospun polymer membrane and ionic liquid for lithium ion battery, J. Memb. Sci. 399–400 (2012) 37–42. doi:10.1016/j.memsci.2012.01.021.

[108] A.B. McEwen, H.L. Ngo, K. LeCompte, J.L. Goldman, Electrochemical properties of imidazolium salt electrolytes for electrochemical capacitor applications, J. Electrochem. Soc. 146 (1999) 1687–1695. doi:10.1149/1.1391827.

[109] P.C. Howlett, D.R. MacFarlane, A.F. Hollenkamp, High Lithium Metal Cycling Efficiency in a Room-Temperature Ionic Liquid, Electrochem. Solid-State Lett. 7 (2004) A97. doi:10.1149/1.1664051.

[110] M. Barghamadi, A.S. Best, A.I. Bhatt, A.F. Hollenkamp, P.J. Mahon, M. Musameh, T. Rüther, Effect of LiNO3 additive and pyrrolidinium ionic liquid on the solid electrolyte interphase in the lithium–sulfur battery, J. Power Sources. 295 (2015) 212–220. doi:10.1016/j.jpowsour.2015.06.150.

[111] G.B. Appetecchi, M. Montanino, D. Zane, M. Carewska, F. Alessandrini, S. Passerini, Effect of the alkyl group on the synthesis and the electrochemical properties of N-alkyl-N-methyl-pyrrolidinium bis(trifluoromethanesulfonyl)imide ionic liquids, Electrochim. Acta. 54 (2009) 1325–1332. doi:10.1016/j.electacta.2008.09.011.

[112] H.Y. Liu, L.L. Liu, C.L. Yang, Z.H. Li, Q.Z. Xiao, G.T. Lei, Y.H. Ding, A hard-template process to prepare three-dimensionally macroporous polymer electrolyte for lithium-ion batteries, Electrochim. Acta. 121 (2014) 328–336. doi:10.1016/j.electacta.2014.01.013.

[113] X.B. Cheng, T.Z. Hou, R. Zhang, H.J. Peng, C.Z. Zhao, J.Q. Huang, Q. Zhang, Dendrite-Free Lithium Deposition Induced by Uniformly Distributed Lithium Ions for Efficient Lithium Metal Batteries, Adv. Mater. 28 (2016) 2888–2895. doi:10.1002/adma.201506124.

[114] W. Xu, J. Wang, F. Ding, X. Chen, E. Nasybulin, Y. Zhang, J.-G. Zhang, Lithium metal anodes for rechargeable batteries, Energy Environ. Sci. 7 (2014) 513–537. doi:10.1039/C3EE40795K.

[115] P.P. Prosini, M. Lisi, D. Zane, M. Pasquali, Determination of the chemical diffusion coefficient of lithium in LiFePO4, Solid State Ionics. 148 (2002) 45–51. doi:10.1016/S0167-2738(02)00134-0.

[116] D. Zhou, R. Liu, Y.B. He, F. Li, M. Liu, B. Li, Q.H. Yang, Q. Cai, F. Kang, SiO2 Hollow Nanosphere-Based Composite Solid Electrolyte for Lithium Metal Batteries to Suppress Lithium Dendrite Growth and Enhance Cycle Life, Adv. Energy Mater. 6 (2016) 1–10. doi:10.1002/aenm.201502214.

[117] D. Ma, Z. Cao, H. Wang, X. Huang, L. Wang, X. Zhang, Three-dimensionally ordered macroporous FeF3 and its in situ homogenous polymerization coating for high energy and power density lithium ion batteries, Energy Environ. Sci. 5 (2012) 8538–8542. doi:10.1039/C2EE22568A.

[118] Z.-L. Wang, D. Xu, H.-G. Wang, Z. Wu, X.-B. Zhang, In situ fabrication of porous graphene electrodes for high-performance energy storage, ACS Nano. 7 (2013) 2422–2430.

[119] X. Huang, R. Wang, D. Xu, Z. Wang, H. Wang, J. Xu, Z. Wu, Q. Liu, Y. Zhang, X. Zhang, Batteries: Homogeneous CoO on Graphene for Binder-Free and Ultralong-Life Lithium Ion Batteries (Adv. Funct. Mater. 35/2013), Adv. Funct. Mater. 23 (2013) 4274.

[120] J. Wang, F. Lin, H. Jia, J. Yang, C.W. Monroe, Y. NuLi, Towards a safe lithium–sulfur battery with a flame-inhibiting electrolyte and a sulfur-based composite cathode, Angew. Chemie Int. Ed. 53 (2014) 10099–10104.

[121] L. Chen, L.L. Shaw, Recent advances in lithium-sulfur batteries, J. Power Sources. 267 (2014) 770–783. doi:10.1016/j.jpowsour.2014.05.111.

[122] A. Chamaani, M. Safa, N. Chawla, B. El-Zahab, Composite Gel Polymer Electrolyte for Improved Cyclability in Lithium–Oxygen Batteries, ACS Appl. Mater. Interfaces. 9 (2017) 33819–33826. doi:10.1021/acsami.7b08448.

[123] M. Watanabe, M.L. Thomas, S. Zhang, K. Ueno, T. Yasuda, K. Dokko, Application of Ionic Liquids to Energy Storage and Conversion Materials and Devices, Chem. Rev. 117 (2017) 7190–7239. doi:10.1021/acs.chemrev.6b00504.

[124] N. Chawla, A. Chamaani, M. Safa, B. El-Zahab, Palladium-Filled Carbon Nanotubes Cathode for Improved Electrolyte Stability and Cyclability Performance of Li-O 2 Batteries, J. Electrochem. Soc. 164 (2017) A6303–A6307. doi:10.1149/2.0491701jes.

[125] J.-J. Xu, Z.-L. Wang, D. Xu, L.-L. Zhang, X.-B. Zhang, Tailoring deposition and morphology of discharge products towards high-rate and long-life lithium-oxygen batteries, Nat. Commun. 4 (2013) 2438.

[126] J. Xu, D. Xu, Z. Wang, H. Wang, L. Zhang, X. Zhang, Synthesis of perovskite-based porous La0. 75Sr0. 25MnO3 nanotubes as a highly efficient electrocatalyst for rechargeable lithium–oxygen batteries, Angew. Chemie Int. Ed. 52 (2013) 3887–3890.

[127] Z.-L. Wang, D. Xu, J.-J. Xu, X.-B. Zhang, Oxygen electrocatalysts in metal–air batteries: from aqueous to nonaqueous electrolytes, Chem. Soc. Rev. 43 (2014) 7746–7786.

[128] A. Manthiram, Y. Fu, S. Chung, C. Zu, Y. Su, Rechargeable Lithium − Sulfur Batteries, Chem. Rev. 114 (2014) 11751–87. doi:10.1021/cr500062v.

[129] S. Zhang, K. Ueno, K. Dokko, M. Watanabe, Recent Advances in Electrolytes for Lithium-Sulfur Batteries, Adv. Energy Mater. 5 (2015) 1–28. doi:10.1002/aenm.201500117.

[130] M. Barghamadi, A.S. Best, A.I. Bhatt, A.F. Hollenkamp, M. Musameh, R.J. Rees, T. Rüther, Lithium–sulfur batteries—the solution is in the electrolyte, but is the electrolyte a solution?, Energy Environ. Sci. 7 (2014) 3902–3920. doi:10.1039/C4EE02192D.

[131] G. Li, Z. Li, B. Zhang, Z. Lin, Developments of electrolyte systems for lithium–sulfur batteries: a review, Energy Storage. 3 (2015) 5. doi:10.3389/fenrg.2015.00005.

[132] K. Ueno, J. Park, A. Yamazaki, T. Mandai, N. Tachikawa, K. Dokko, M. Watanabe, 232 Anionic E ff ects on Solvate Ionic Liquid Electrolytes in Rechargeable Lithium − Sulfur Batteries, (2013) 7–8.

[133] S.S. Zhang, A new finding on the role of LiNO3 in lithium-sulfur battery, J. Power Sources. 322 (2016) 99–105. doi:10.1016/j.jpowsour.2016.05.009.

[134] L.X.X. Yuan, J.K.K. Feng, X.P.P. Ai, Y.L.L. Cao, S.L.L. Chen, H.X.X. Yang, Improved dischargeability and reversibility of sulfur cathode in a novel ionic liquid electrolyte, Electrochem. Commun. 8 (2006) 610–614. doi:10.1016/j.elecom.2006.02.007.

[135] Y. Yan, Y. Yin, Y. Guo, L.-J. Wan, Effect of cations in ionic liquids on the electrochemical performance of lithium-sulfur batteries, Sci. China Chem. 57 (2014) 1564–1569.

[136] X. Sun, X. Wang, R.T. Mayes, S. Dai, Lithium–Sulfur Batteries Based on Nitrogen-Doped Carbon and an Ionic-Liquid Electrolyte, ChemSusChem. 5 (2012) 2079–2085.

[137] J.-W. Park, K. Yamauchi, E. Takashima, N. Tachikawa, K. Ueno, K. Dokko, M. Watanabe, Solvent Effect of Room Temperature Ionic Liquids on Electrochemical Reactions in Lithium–Sulfur Batteries, J. Phys. Chem. C. 117 (2013) 4431–4440. doi:10.1021/jp400153m.

[138] J.W. Park, K. Ueno, N. Tachikawa, K. Dokko, M. Watanabe, Ionic liquid electrolytes for lithium-sulfur batteries, J. Phys. Chem. C. 117 (2013) 20531–20541. doi:10.1021/jp408037e.

[139] J. Wang, S.Y. Chew, Z.W. Zhao, S. Ashraf, D. Wexler, J. Chen, S.H. Ng, S.L. Chou, H.K. Liu, Sulfur-mesoporous carbon composites in conjunction with a novel ionic liquid electrolyte for lithium rechargeable batteries, Carbon N. Y. 46 (2008) 229–235. doi:10.1016/j.carbon.2007.11.007.

[140] A. Swiderska-Mocek, E. Rudnicka, Lithium–sulphur battery with activated carbon cloth-sulphur cathode and ionic liquid as electrolyte, J. Power Sources. 273 (2015) 162–167.

[141] J.H. Shin, S.S. Jung, K.W. Kim, H.J. Ahn, J.H. Ahn, Preparation and characterization of plasticized polymer electrolytes based on the PVdF-HFP copolymer for lithium/sulfur battery, J. Mater. Sci. Mater. Electron. 13 (2002) 727–733. doi:10.1023/A:1021521207247.

[142] B.H. Jeon, J.H. Yeon, K.M. Kim, I.J. Chung, Preparation and electrochemical properties of lithium–sulfur polymer batteries, J. Power Sources. 109 (2002) 89–97.

[143] K. Jeddi, M. Ghaznavi, P. Chen, A novel polymer electrolyte to improve the cycle life of high performance lithium–sulfur batteries, J. Mater. Chem. A. 1 (2013) 2769. doi:10.1039/c3ta01169k.

[144] M. Rao, X. Geng, X. Li, S. Hu, W. Li, Lithium-sulfur cell with combining carbon nanofibers-sulfur cathode and gel polymer electrolyte, J. Power Sources. 212 (2012) 179–185. doi:10.1016/j.jpowsour.2012.03.111.

[145] H.-S. Ryu, H.-J. Ahn, K.-W. Kim, J.-H. Ahn, J.-Y. Lee, Discharge process of Li/PVdF/S cells at room temperature, J. Power Sources. 153 (2006) 360–364.

[146] J.H. Shin, E.J. Cairns, N-Methyl-(n-butyl)pyrrolidinium bis(trifluoromethanesulfonyl)imide-LiTFSI-poly(ethylene glycol) dimethyl ether mixture as a Li/S cell electrolyte, J. Power Sources. 177 (2008) 537–545. doi:10.1016/j.jpowsour.2007.11.043.

[147] J. Jin, Z. Wen, X. Liang, Y. Cui, X. Wu, Gel polymer electrolyte with ionic liquid for high performance lithium sulfur battery, Solid State Ionics. 225 (2012) 604–607. doi:10.1016/j.ssi.2012.03.012.

[148] M. Baloch, A. Vizintin, R.K. Chellappan, J. Moskon, D. Shanmukaraj, R. Dedryvère, T. Rojo, R. Dominko, Application of Gel Polymer Electrolytes Based on Ionic Liquids in Lithium-Sulfur Batteries, J. Electrochem. Soc. 163 (2016) A2390–A2398.

[149] Y. Hao, X. Li, X. Sun, C. Wang, Nitrogen-doped graphene nanosheets/sulfur composite as lithium???sulfur batteries cathode, Mater. Sci. Eng. B Solid-State Mater. Adv. Technol. 213 (2016) 83–89. doi:10.1016/j.mseb.2016.04.009.

[150] G.G. Eshetu, S. Grugeon, S. Laruelle, S. Boyanov, A. Lecocq, J.-P. Bertrand, G. Marlair, In-depth safety-focused analysis of solvents used in electrolytes for large scale lithium ion batteries, Phys. Chem. Chem. Phys. 15 (2013) 9145. doi:10.1039/c3cp51315g.

[151] F. Wu, J. Qian, R. Chen, T. Zhao, R. Xu, Y. Ye, W. Li, L. Li, J. Lu, K. Amine, Sulfur cathode based on layered carbon matrix for high-performance Li–S batteries, Nano Energy. 12 (2015) 742–749.

[152] R. Kumaran, M. Alagar, S. Dinesh Kumar, V. Subramanian, K. Dinakaran, Ag induced electromagnetic interference shielding of Ag-graphite/PVDF flexible nanocomposites thinfilms, Appl. Phys. Lett. 107 (2015) 113107.

[153] W. Ahn, K.-B. Kim, K.-N. Jung, K.-H. Shin, C.-S. Jin, Synthesis and electrochemical properties of a sulfur-multi walled carbon nanotubes composite as a cathode material for lithium sulfur batteries, J. Power Sources. 202 (2012) 394–399.

[154] M. Wild, L. O'Neill, T. Zhang, R. Purkayastha, G. Minton, M. Marinescu, G.J. Offer, Lithium sulfur batteries, a mechanistic review, Energy Environ. Sci. 8 (2015) 3477–3494. doi:10.1039/C5EE01388G.

[155] C. Barchasz, F. Molton, C. Duboc, J.C. Leprêtre, S. Patoux, F. Alloin, Lithium/sulfur cell discharge mechanism: An original approach for intermediate species identification, Anal. Chem. 84 (2012) 3973–3980. doi:10.1021/ac2032244.

[156] Y. Zhu, J. Li, J. Liu, A bifunctional ion-electron conducting interlayer for high energy density all-solid-state lithium-sulfur battery, J. Power Sources. 351 (2017) 17–25.

[157] J.-H. Yu, J.-W. Park, Q. Wang, H.-S. Ryu, K.-W. Kim, J.-H. Ahn, Y. Kang, G. Wang, H.-J. Ahn, Electrochemical properties of all solid state Li/S battery, Mater. Res. Bull. 47 (2012) 2827–2829. doi:10.1016/j.materresbull.2012.04.086.

[158] M. Barghamadi, A. Kapoor, C. Wen, A Review on Li-S Batteries as a High Efficiency Rechargeable Lithium Battery, J. Electrochem. Soc. 160 (2013) A1256–A1263. doi:10.1149/2.096308jes.

[159] M. Agrawal, S. Choudhury, K. Gruber, F. Simon, D. Fischer, V. Albrecht, M. Göbel, S. Koller, M. Stamm, L. Ionov, Porous carbon materials for Li–S batteries based on resorcinol–formaldehyde resin with inverse opal structure, J. Power Sources. 261 (2014) 363–370.

[160] T. Saha, S. Choudhury, K. Naskar, M. Stamm, G. Heinrich, A. Das, A highly stretchable gel-polymer electrolyte for lithium-sulfur batteries, Polymer (Guildf). 112 (2017) 447–456. doi:10.1016/j.polymer.2017.02.021.

[161] J. Song, B. Sun, H. Liu, Z. Ma, Z. Chen, G. Shao, G. Wang, Enhancement of the rate capability of LiFePO4 by a new highly graphitic carbon-coating method, ACS Appl. Mater. Interfaces. 8 (2016) 15225–15231. doi:10.1021/acsami.6b02567.

[162] M. Liu, D. Zhou, Y.B. He, Y. Fu, X. Qin, C. Miao, H. Du, B. Li, Q.H. Yang, Z. Lin, T.S. Zhao, F. Kang, Novel gel polymer electrolyte for high-performance lithium-sulfur batteries, Nano Energy. 22 (2016) 278–289. doi:10.1016/j.nanoen.2016.02.008.

[163] C. Barchasz, J.C. Leprêtre, F. Alloin, S. Patoux, New insights into the limiting parameters of the Li/S rechargeable cell, J. Power Sources. 199 (2012) 322–330. doi:10.1016/j.jpowsour.2011.07.021.

[164] A.R. Baboukani, E. Sharifi, S. Akhavan, A. Saatchi, Co Complexes as a Corrosion Inhibitor for 316 L Stainless Steel in H2SO4 Solution, J. Mater. Sci. Chem. Eng. 4 (2016) 28.

[165] J.-B. Jorcin, M.E. Orazem, N. Pébère, B. Tribollet, CPE analysis by local electrochemical impedance spectroscopy, Electrochim. Acta. 51 (2006) 1473–1479.

[166] H. Hassannejad, M. Moghaddasi, E. Saebnoori, A.R. Baboukani, Microstructure, deposition mechanism and corrosion behavior of nanostructured cerium oxide conversion coating modified with chitosan on AA2024 aluminum alloy, J. Alloys Compd. 725 (2017) 968–975.

[167] Z. Deng, Z. Zhang, Y. Lai, J. Liu, J. Li, Y. Liu, Electrochemical Impedance Spectroscopy Study of a Lithium/Sulfur Battery: Modeling and Analysis of Capacity Fading, J. Electrochem. Soc. 160 (2013) A553–A558. doi:10.1149/2.026304jes.

[168] V.S. Kolosnitsyn, E. V. Kuzmina, E. V. Karaseva, S.E. Mochalov, A study of the electrochemical processes in lithium-sulphur cells by impedance spectroscopy, J. Power Sources. 196 (2011) 1478–1482. doi:10.1016/j.jpowsour.2010.08.105.

[169] M. Liu, Y. Ren, D. Zhou, H. Jiang, F. Kang, T. Zhao, A Lithium/Polysulfide Battery with Dual-Working Mode Enabled by Liquid Fuel and Acrylate-Based Gel Polymer Electrolyte, ACS Appl. Mater. Interfaces. 9 (2017) 2526–2534.

[170] R. Chen, T. Zhao, J. Lu, F. Wu, L. Li, J. Chen, G. Tan, Y. Ye, K. Amine, Graphene-based three-dimensional hierarchical sandwich-type architecture for high-performance Li/S batteries, Nano Lett. 13 (2013) 4642–4649. doi:10.1021/nl4016683.

[171] L. Yuan, X. Qiu, L. Chen, W. Zhu, New insight into the discharge process of sulfur cathode by electrochemical impedance spectroscopy, J. Power Sources. 189 (2009) 127–132. doi:10.1016/j.jpowsour.2008.10.033.

[172] Y.-J. Choi, Y.-D. Chung, C.-Y. Baek, K.-W. Kim, H.-J. Ahn, J.-H. Ahn, Effects of carbon coating on the electrochemical properties of sulfur cathode for lithium/sulfur cell, J. Power Sources. 184 (2008) 548–552.

[173] Z. Jin, K. Xie, X. Hong, Z. Hu, Capacity fading mechanism in lithium sulfur cells using poly (ethylene glycol)-borate ester as plasticizer for polymer electrolytes, J. Power Sources. 242 (2013) 478–485.

[174] J. Cao, L. Wang, M. Fang, Y. Shang, L. Deng, J. Yang, J. Li, H. Chen, X. He, Interfacial compatibility of gel polymer electrolyte and electrode on performance of Li-ion battery, Electrochim. Acta. 114 (2013) 527–532. doi:10.1016/j.electacta.2013.10.052.

[175] K.H. Kim, Y.-S. Jun, J.A. Gerbec, K.A. See, G.D. Stucky, H.-T. Jung, Sulfur infiltrated mesoporous graphene–silica composite as a polysulfide retaining cathode material for lithium–sulfur batteries, Carbon N. Y. 69 (2014) 543–551.

[176] A. Chamaani, N. Chawla, M. Safa, B. El-Zahab, One-Dimensional Glass Micro-Fillers in Gel Polymer Electrolytes for Li-O 2 Battery Applications, Electrochim. Acta. 235 (2017) 56–63. doi:10.1016/j.electacta.2017.03.064.

[177] J. Jaguemont, L. Boulon, Y. Dubé, A comprehensive review of lithium-ion batteries used in hybrid and electric vehicles at cold temperatures, Appl. Energy. 164 (2016) 99–114.

[178] O.K. Park, Y. Cho, S. Lee, H.-C. Yoo, H.-K. Song, J. Cho, Who will drive electric vehicles, olivine or spinel?, Energy Environ. Sci. 4 (2011) 1621–1633. doi:10.1039/C0EE00559B.

[179] C. Capasso, O. Veneri, Experimental analysis on the performance of lithium based batteries for road full electric and hybrid vehicles, Appl. Energy. 136 (2014) 921–930.

[180] D. Linden, T.B. Reddy, Handbook of Batteries. 3rd, (2002).

[181] S. Abada, G. Marlair, A. Lecocq, M. Petit, V. Sauvant-Moynot, F. Huet, Safety focused modeling of lithium-ion batteries: A review, J. Power Sources. 306 (2016) 178–192.

[182] C. Julien, A. Mauger, A. Vijh, K. Zaghib, Lithium batteries, in: Lithium Batter., Springer, 2016: pp. 29–68. doi:10.1002/9781118615515.

[183] T.F. Miller III, Z.-G. Wang, G.W. Coates, N.P. Balsara, Designing Polymer Electrolytes for Safe and High Capacity Rechargeable Lithium Batteries, Acc. Chem. Res. 50 (2017) 590–593.

[184] J. Muldoon, C.B. Bucur, N. Boaretto, T. Gregory, V. Di Noto, Polymers: opening doors to future batteries, Polym. Rev. 55 (2015) 208–246.

[185] A. Balducci, Ionic Liquids in Lithium-Ion Batteries, Top. Curr. Chem. 375 (2017) 20.

[186] L. Balo, H. Gupta, V.K. Singh, R.K. Singh, Flexible gel polymer electrolyte based on ionic liquid EMIMTFSI for rechargeable battery application, Electrochim. Acta. 230 (2017) 123–131.

[187] N. Sugihara, K. Nishimura, H. Nishino, S. Kanehashi, K. Mayumi, Y. Tominaga, T. Shimomura, K. Ito, Ion-Conductive and Elastic Slide-Ring Gel Li Electrolytes Swollen with Ionic Liquid, Electrochim. Acta. 229 (2017) 166–172.

[188] S. Ferrari, E. Quartarone, P. Mustarelli, A. Magistris, M. Fagnoni, S. Protti, C. Gerbaldi, A. Spinella, Lithium ion conducting PVdF-HFP composite gel electrolytes based on N-methoxyethyl-N-methylpyrrolidinium bis (trifluoromethanesulfonyl)-imide ionic liquid, J. Power Sources. 195 (2010) 559–566.

[189] Y. Ma, L.B.B. Li, G.X.X. Gao, X.Y.Y. Yang, J. You, P.X.X. Yang, Ionic conductivity enhancement in gel polymer electrolyte membrane with N-methyl-N-butyl-piperidine-bis (trifluoromethylsulfonyl) imide ionic liquid for lithium ion battery, Colloids Surfaces A Physicochem. Eng. Asp. 502 (2016) 130–138. doi:10.1016/j.colsurfa.2016.05.011.

[190] A. Eftekhari, T. Saito, Synthesis and Properties of Polymerized Ionic Liquids, Eur. Polym. J. 90 (2017) 245–272. doi:10.1016/j.eurpolymj.2017.03.033.

[191] M. Li, L. Yang, S. Fang, S. Dong, S.I. Hirano, K. Tachibana, Polymer electrolytes containing guanidinium-based polymeric ionic liquids for rechargeable lithium batteries, J. Power Sources. 196 (2011) 8662–8668. doi:10.1016/j.jpowsour.2011.06.059.

[192] K. Yin, Z. Zhang, L. Yang, S. Hirano, An imidazolium-based polymerized ionic liquid via novel synthetic strategy as polymer electrolytes for lithium ion batteries, J. Power Sources. 258 (2014) 150–154. doi:10.1016/j.jpowsour.2014.02.057.

[193] F. Croce, G.B. Appetecchi, L. Persi, Nanocomposite polymer electrolytes for lithium batteries, Nature. 394 (1998) 456–458. doi:10.1038/28818.

[194] W. Zhai, Y.W. Zhang, L. Wang, F. Cai, X.M. Liu, Y.J. Shi, H. Yang, Study of nano-TiO2 composite polymer electrolyte incorporating ionic liquid PP12O1TFSI for lithium battery, Solid State Ionics. 286 (2016) 111–116. doi:10.1016/j.ssi.2016.01.019.

[195] D. Di Girolamo, S. Panero, M.A. Navarra, J. Hassoun, Quaternary polyethylene oxide electrolytes containing ionic liquid for lithium polymer battery, J. Electrochem. Soc. 163 (2016) A1175–A1180.

[196] S. Wang, Q.X. Shi, Y.S. Ye, Y. Wang, H.Y. Peng, Z.G. Xue, X.L. Xie, Y.W. Mai, Polymeric ionic liquid-functionalized mesoporous silica nanoplates: a new high-performance composite polymer electrolyte for lithium batteries, Electrochim. Acta. (2017).

[197] X. Li, C. Wang, Engineering nanostructured anodes via electrostatic spray deposition for high performance lithium ion battery application, J. Mater. Chem. A. 1 (2013) 165–182.

[198] J. Ma, Q.-Z. Qin, Electrochemical performance of nanocrystalline LiMPO 4 thin-films prepared by electrostatic spray deposition, J. Power Sources. 148 (2005) 66–71.

[199] H. Aydın, A. Bozkurt, Synthesis, characterization, and ionic conductivity of novel crosslinked polymer electrolytes for Li-ion batteries, J. Appl. Polym. Sci. 124 (2012) 1193–1199.

[200] C. Ma, J. Zhang, M. Xu, Q. Xia, J. Liu, S. Zhao, L. Chen, A. Pan, D.G. Ivey, W. Wei, Cross-linked branching nanohybrid polymer electrolyte with monodispersed TiO2 nanoparticles for high performance lithium-ion batteries, J. Power Sources. 317 (2016) 103–111. doi:10.1016/j.jpowsour.2016.03.097.

[201] L.J. Hardwick, M. Holzapfel, A. Wokaun, P. Novák, Raman study of lithium coordination in EMI-TFSI additive systems as lithium-ion battery ionic liquid electrolytes, J. Raman Spectrosc. 38 (2007) 110–112.

[202] J.-C. Lassègues, J. Grondin, D. Talaga, Lithium solvation in bis (trifluoromethanesulfonyl) imide-based ionic liquids, Phys. Chem. Chem. Phys. 8 (2006) 5629–5632.

[203] D.M. Seo, P.D. Boyle, R.D. Sommer, J.S. Daubert, O. Borodin, W.A. Henderson, Solvate structures and spectroscopic characterization of LiTFSI electrolytes, J. Phys. Chem. B. 118 (2014) 13601–13608.

[204] L. Suo, F. Zheng, Y.-S. Hu, L. Chen, FT-Raman spectroscopy study of solvent-in-salt electrolytes, Chinese Phys. B. 25 (2015) 16101.

[205] A. Chamaani, M. Safa, N. Chawla, M. Herndon, B. El-Zahab, Stabilizing effect of ion complex formation in lithium–oxygen battery electrolytes, J. Electroanal. Chem. 818 (2018) 143–150. doi:10.1016/j.jelechem.2018.03.012.

[206] X.Q. Shi, Q. Xia, X. Xiang, Y.S. Ye, Y.H. Peng, G.Z. Xue, L.X. Xie, Y.-W. Mai, Self-Assembled Polymeric Ionic Liquid-Functionalized Cellulose Nano-crystals: Constructing 3D Ion-conducting Channels Within Ionic Liquid-based Composite Polymer Electrolytes, Chem. Eur. J. (2017).

[207] I. Gunasekara, S. Mukerjee, E.J. Plichta, M.A. Hendrickson, K.M. Abraham, A study of the influence of lithium salt anions on oxygen reduction reactions in Li-air batteries, J. Electrochem. Soc. 162 (2015) A1055–A1066.

[208] S.K. Singh, L. Balo, H. Gupta, V.K. Singh, A.K. Tripathi, Y.L. Verma, R.K. Singh, Improved electrochemical performance of EMIMFSI ionic liquid based gel polymer electrolyte with temperature for rechargeable lithium battery, Energy. 150 (2018) 890–900.

[209] M. Safa, Y. Hao, A. Chamaani, E. Adelowo, N. Chawla, C. Wang, B. El-Zahab, Capacity Fading Mechanism in Lithium-Sulfur Battery using Poly(ionic liquid) Gel Electrolyte, Electrochim. Acta. 258 (2017) 1284–1292. doi:10.1016/j.electacta.2017.11.185.

[210] R. Xu, X. Zhang, X. Cheng, H. Peng, C. Zhao, C. Yan, J. Huang, Artificial Soft–Rigid Protective Layer for Dendrite-Free Lithium Metal Anode, Adv. Funct. Mater. (2018).

[211] D. Aurbach, K. Gamolsky, B. Markovsky, Y. Gofer, M. Schmidt, U. Heider, On the use of vinylene carbonate (VC) as an additive to electrolyte solutions for Li-ion batteries, Electrochim. Acta. 47 (2002) 1423–1439. doi:10.1016/S0013-4686(01)00858-1.

[212] R. Elazari, G. Salitra, Y. Talyosef, J. Grinblat, C. Scordilis-Kelley, A. Xiao, J. Affinito, D. Aurbach, Morphological and Structural Studies of Composite Sulfur Electrodes upon Cycling by HRTEM, AFM and Raman Spectroscopy, J. Electrochem. Soc. . 157 (2010) A1131–A1138. doi:10.1149/1.3479828.

[213] W.-K. Shin, J. Cho, A.G. Kannan, Y.-S. Lee, D.-W. Kim, Cross-linked composite gel polymer electrolyte using mesoporous methacrylate-functionalized SiO 2 nanoparticles for lithium-ion polymer batteries, Sci. Rep. 6 (2016) 26332.

VITA

MEER N SAFA

2002-2007	B.Sc., Materials and Metallurgical Engineering Bangladesh University of Engineering & Technology (BUET) Dhaka, Bangladesh
2008-2011	M.Sc., Materials Science and Engineering Royal Institute of Technology (KTH) Stockholm, Sweden
2012-2018	Ph.D., Materials Science and Engineering Florida International University Miami, FL, USA

PUBLICATIONS

1. Safa, M., Chamaani, A., Chawla, N., & El-Zahab, B. (2016). Polymeric ionic liquid gel electrolyte for room temperature lithium battery applications. *Electrochimica Acta*, *213*, 587-593.
2. Safa, M., Hao, Y., Chamaani, A., Adelowo, E., Chawla, N., Wang, C., & El-Zahab, B. (2017). Capacity Fading Mechanism in Lithium-Sulfur Battery using Poly (ionic liquid) Gel Electrolyte. *Electrochimica Acta*, *258*, 1284-1292.
3. Chamaani, A., Safa, M., Chawla, N., & El-Zahab, B. (2017). Composite Gel Polymer Electrolyte for Improved Cyclability in Lithium–Oxygen Batteries. *ACS applied materials & interfaces*, *9*(39), 33819-33826.
4. Chamaani, A., Safa, M., Chawla, N., Herndon, M., & El-Zahab, B. (2018). Stabilizing effect of ion complex formation in lithium–oxygen battery electrolytes. *Journal of Electroanalytical Chemistry*, *815*, 143-150.
5. Chamaani, A., Chawla, N., Safa, M., & El-Zahab, B. (2017). One-Dimensional Glass Micro-Fillers in Gel Polymer Electrolytes for Li-O2 Battery Applications. *Electrochimica Acta*, *235*, 56-63.
6. Chawla, N., Chamaani, A., Safa, M., & El-Zahab, B. (2017). Palladium-filled carbon nanotubes cathode for improved electrolyte stability and cyclability performance of Li-O2 batteries. *Journal of The Electrochemical Society*, *164*(1), A6303-A6307.
7. Safa, M., Adelowo, E.,Chamaani, A., Chawla, N., Baboukani, A., Wang, C., & El-Zahab, B. " Poly (ionic liquid) based Composite Gel Electrolyte for Lithium Battery Application. (Under Preparation).
8. Safa, M., Chamaani, A., Chawla, N., & El-Zahab, B. (2017, April). Role of Filler Additives in Ionic Liquid Based Gel Polymer Electrolyte for Room Temperature Lithium Battery Application. In *Meeting Abstracts* (No. 3, pp. 225-225). The Electrochemical Society.

9. Safa, M. N., Chamaani, A., & El-Zahab, B. (2015, April). Polymeric Ionic Liquid Electrolytes: Effect of Inorganic Fillers. In *Meeting Abstracts* (No. 1, pp. 106-106). The Electrochemical Society.
10. Chawla, N., Chamaani, A., Safa, M., & El-Zahab, B. (2017, April). Investigation of Electrochemical Performance of Li-O2 Batteries Using Catalyst Containing Carbon Nanotube Cathodes. In *Meeting Abstracts* (No. 5, pp. 455-455). The Electrochemical Society.
11. Chamaani, A., Safa, M., Chawla, N., & El-Zahab, B. (2016, June). Electrochemical Investigation of the Effect of Inorganic Fillers in Gel Polymer Electrolytes for Li-O2 Batteries. In *Meeting Abstracts* (No. 2, pp. 390-390). The Electrochemical Society.
12. Chamaani, A., Chawla, N., Safa, M., & El-Zahab, B. (2017, April). The Effect of Li Ion Dissociation Level in Gel Polymer Electrolytes on Electrochemical Performance of Li-O2 Batteries. In *Meeting Abstracts* (No. 5, pp. 459-459). The Electrochemical Society.
13. Chamaani, A., Safa, M., Chawla, N., and El-Zahab, Bilal., Hybrid Gel Polymer Electrolyte for Li-O2 Batteries. MRS Fall 2016 Meeting, Boston, MA, Nov 2016
14. Chamaani, A., Safa, M., Chawla, N., and El-Zahab, B., Electrochemical Investigation of the Effect of Inorganic Fillers in Gel Polymer Electrolytes for Li-O2 Batteries, 18th International Meeting on Lithium Batteries, Chicago, IL, Jun 2016
15. Chawla, N., Chamaani, A., Safa, M., and El-Zahab, B., Nanocatalysts for improved capacity retention in lithium-air batteries, MRS Spring Meeting 2016, March 2016
16. Chamaani, A., Safa, M., Chawla, N., and El-Zahab, B., Electrochemical Behavior of Flexible Gel Polymer Electrolyte with Fiber Fillers, 2nd Florida Statewide Graduate Student Research Symposium, Orlando, Florida, May 2015
17. Chamaani, A., Safa, M., and El-Zahab, B., Free-standing Flexible Polymer Composite Electrolyte for Li-ion Batteries, TMS 2015, Orlando, FL, March 2015
18. Safa, M., Chamaani, A., and El-Zahab, B.,Organic-Inorganic Hybrid Materials as Novel Solid-State Electrolytes for Li-ion Batteries, TMS 2015, Orlando, FL, March 2015